AD-A007 975

IR WINDOW STUDIES

Ferdinand A. Kroger, et al

University of Southern California

Prepared for:

Air Force Cambridge Research Laboratories
Defense Advanced Research Projects Agency

15 September 1974

DISTRIBUTED BY:

NTIS

National Technical Information Service
U. S. DEPARTMENT OF COMMERCE

UNCLASSIFIED

SECURITY CLASSIFICATION OF THIS PAGE (When Data Entered)

REPORT DOCUMENTATION PAGE		READ INSTRUCTIONS BEFORE COMPLETING FORM
1. REPORT NUMBER AFCRL-TR-74-0557	2. GOVT ACCESSION NO.	3. RECIPIENT'S CATALOG NUMBER AD A007 975
4. TITLE (and Subtitle) IR WINDOW STUDIES		5. TYPE OF REPORT & PERIOD COVERED Scientific - Final for Period 1 June '72-31 Aug. '74 6. PERFORMING ORG. REPORT NUMBER
7. AUTHOR(s) Ferdinand A. Kroger John H. Marburger		8. CONTRACT OR GRANT NUMBER(s) F19628-72-C-0275
9. PERFORMING ORGANIZATION NAME AND ADDRESS University of Southern California Electronic Sciences Laboratory Los Angeles, California 90007		10. PROGRAM ELEMENT, PROJECT, TASK AREA & WORK UNIT NUMBERS Project #2055 DoD Element 61101D
11. CONTROLLING OFFICE NAME AND ADDRESS Air Force Cambridge Research Laboratories (LQ) Hanscom AFB, Massachusetts 01731 Contract Monitor: A. Kahan/ LQS		12. REPORT DATE 15 September 1974 13. NUMBER OF PAGES 112
14. MONITORING AGENCY NAME & ADDRESS(if different from Controlling Office)		15. SECURITY CLASS. (of this report) UNCLASSIFIED 15a. DECLASSIFICATION/DOWNGRADING SCHEDULE

16. DISTRIBUTION STATEMENT (of this Report)

A--Approved for public release; distribution unlimited.

17. DISTRIBUTION STATEMENT (of the abstract entered in Block 20, if different from Report)

18. SUPPLEMENTARY NOTES

This Research was sponsored by Defense Advanced Research Projects Agency
ARPA Order No. 2055

19. KEY WORDS (Continue on reverse side if necessary and identify by block number)

IR Windows
Alkali Halides
III-V Semiconductors
II-VI Semiconductors
Thermal Lensing
IR Absorption

20. ABSTRACT (Continue on reverse side if necessary and identify by block number)

An apparatus for the measurement of low infrared absorption by calorimetry was set up. Absorption of seven samples of GaAs grown by different methods from the melt all show similar infrared absorption with $\alpha_{10.6} \approx 8 \times 10^{-3} cm^{-1}$ which probably represents the lowest absorption that can be achieved. Samples of 0.65 mm thick were grown at lower temperatures from molten gallium, but still have a low resistivity. Stabilized zirconia was used to remove and monitor oxygen. KCl crystals with $\alpha_{10.6\ \mu m} = 10^{-4} cm^{-1}$ were grown. For

DD FORM 1 JAN 73 1473 EDITION OF 1 NOV 65 IS OBSOLETE
S/N 0102-014-6601

UNCLASSIFIED
SECURITY CLASSIFICATION OF THIS PAGE (When Data Entered)

Reproduced by
NATIONAL TECHNICAL INFORMATION SERVICE
US Department of Commerce
Springfield, VA. 22151

PRICES SUBJECT TO CHANGE

KBr purification did not cause improvement beyond $\alpha_{10.6\ \mu m} = 2 \times 10^{-3} cm^{-1}$. The residual absorption is attributed to Br-O complexes. Deformation studies in pure and doped GaAs showed the active slip system to be {111}, <1$\bar{1}$0>. An increase of the yield strength of GaAs by Si was attributed to $Si_{Ga} - V_{Ga}$ pairs, the existence of which was indicated by local mode studies. Anomalous diffraction streaks and spots are shown to be due to diffuse scattering of electrons at phonons. Dense CdTe could be made by hot-pressing with $CdCl_2$ as a liquid sintering aid. However, removal of the last $CdCl_2$ caused some porosity. Cd and Te did not wet sufficiently. The defect structure of CdTe + In was determined by a combined study of selfdiffusion and the Hall effect. High-resistivity material with $\alpha_{10.6\ \mu m} = 9 \times 10^{-4} cm^{-1}$ can be made by quenching after annealing at 700°C. Thick pieces show stronger absorption as a result of slower cooling. Local mode studies were begun on CdTe-Al, Al + Cu, Li and P and on ZnSe-Al. A method to measure surface absorption using surface waves was developed and tested on KCl. A CO_2 TEA laser for damage studies was built and tested, and used to study damage in ZnSe and KCl. Multi-phonon absorption occurs by two mechanisms. One is based on anharmonicity of intermolecular forces, the other on non-linear dependence of electric dipole moments on lattice coordinates. An experimental method to determine the contribution by each was devised. The problem of thermal lensing was reviewed in detail.

Dielectric constants and their temperature dependents were determined at 290°K for GaS $\varepsilon = 13.08$, for CdTe $\varepsilon = 11.00$ and for ZnSe $\varepsilon = 9.25$.

CONTENTS

		Page
ABSTRACT		i
1.	INTRODUCTION	1
2.	PROGRESS BY PROJECT	
a.1	Epitaxial Growth of Semi-Insulating GaAs from Ga Solutions	2
a.2	Optimization of Alkali Halide Window Materials	4
a.3	Growth of Crystals for Infra Red Window Research	20
b.1	Fabrication of Polycrystalline IR Window Materials	26
c.1	Mechanical Behavior of III-V and II-VI Compounds	33
d.1	Dielectric Constant Measurements	44
d.2	Study of Defects in II-VI Compounds	45
e.1	Theoretical Studies of Absorption Mechanisms in IR Window Materials	49
f.1	Investigation of Infrared Loss Mechanisms in High Resitivity GaAs	57
f.2	Alakali Halide Surface Studies with Acoustic Probe Techniques	58
f.3	Absorption Studies of CdTe and ZnSe	65
g.1	Characterization of Optical Performance of IR Window Systems	75
h.1	Laser Damage Studies	86
3.	DISCUSSION	101
4.	LIST OF PUBLICATIONS AND PRESENTATIONS	105

INTRODUCTION

This is the final report for two years work carried out under contract F 19628-72-C-0275. It gives a final summing up for the programs that are not continued under the new contract. For programs that are continued both a summary of completed work and an outline of work to be done is given.

The format of this report follows:

a) Crystal growth
b) Polycrystalline window fabrication
c) Mechanical properties of window materials
d) Window material defect characterization
e) Theory of residual IR optical absorption
f) Absorption measurement techniques
g) Theoretical evaluation of optical performances of windows

a.1 Epitaxial Growth of Semi-Insulating GaAs from Ga Solutions

P. S. Vijaykumar and J. M. Whelan and Ed Miller

a.1.1 Growth of Thick GaAs Films:

There is a convincing body of information that GaAs grown from Ga solutions at low temperatures can be made with higher purities than that grown at the melting point. The initial goals were to grow thick films below the melting point which would be semi-insulating and to measure their absorption coefficients. This goal was to be completed in one year. The task was a difficult one. Layers of suitable thickness, ~1 mm have not been grown from solutions previously and secondly, no one has reported the preparation of epitaxial grown films with suitably low carrier concentrations. Since it was considered feasible to dope relatively high purity films (by diffusion if necessary) to make them semi-insulating the prime emphasis was placed on the growth of thick films.

A sliding type all-quartz epitaxial apparatus was constructed which has provisions for introducing a vertical temperature gradient. This has been used in two modes: film growth over a temperature range and isothermal growth. Films up to 0.65 mm have been grown by cooling over a temperature range of 910 to 840°C, and up to 0.35 mm by isothermal growth at 835°C. Modifications suggested by these experiments to extend the thickness to 1mm are evident. One unexpected result was the observation that tapering in the thickness occurs in the presence of small horizontal temperature gradients; such gradients are entirely unimportant in growing films ~10μm or less in thickness. These thick films are free of Ga occlusions as indicated by IR transmission but are not semi-insulating.

A tipping liquid epitaxy system suitable for growing GaAs thick films at temperatures between 900 and the melting point, 1238°C, has been built. Growths with this system will be continued as part of another program and absorption data will be included in future reports.

a.1.2 Use of Stabilized Zirconia in the Growth of GaAs:

Progress with the use of zirconia tubes as containers for the melts in the growth of GaAs films from solutions was mixed. The goal was to bias the zirconia so as to pump oxygen from the Ga melts and thus increase its ability to dissolve residual oxides from GaAs substrates. Success at this was expected to lead to lower permissible growth temperatures. Growth at

these lower temperatures, 600-725°C, was only partially successful. There appears to be at least two rate limiting steps which determine the texture of the grown films at these temperatures. The first yields a thin smooth film on the substrate and is followed by a second which yields an unacceptably rough overgrowth. We have been unable to eliminate the latter.

A side benefit to semiconductor processing has been a long term experience with the use of stabilized zirconia as gages and pumps. As gages they are far superior to any other detector for monitoring water concentrations in H_2 streams over the tested range of 0.06 to 10^4 ppm. Using carefully prepared H_2O/H_2 gas mixtures as standards we have shown that variations as small as 4% are detectable at concentrations of a few ppm. Its use as a pump to remove trace amounts of H_2O from H_2 was gratifying. It was possible to reduce the H_2O content in H_2 from a Pd diffuser which contained 6pp H_2O upon delivery to a gage, to 0.06 ppm by installing a pump between the gage and diffuser. This was so for flow rates of 200-500 std cc min^{-1}. The lower measured H_2O content was most likely due to outgassing of the glass/quartz lines separating the gage and pump.

The use of compressed O ring seals is common to prevent excluding air leaks in sliding epitaxy systems when a round sliding shaft is used to insert the melt into the furnace. These were found to introduce leaks during sliding which can temporaily raise the H_2O content to 50-100 ppm. Such seals are adequate under static conditions.

a.2 Optimization of Alkali Halide Window Materials

P. J. Shlichta, R. E. Chaney* and James Yee

a.2.1 Objectives:

As originally proposed, the USC infrared laser window program included the growth of highly pure and impurity-doped KCl crystals and the study of their optical and mechanical properties. Early in the program, as a result of the proliferation of KCl research in other laboratories, we were advised to concentrate on attempting to grow KCl crystals with a minimum (i.e., intrinsic) 10.6μm absorptivity and to identify the impurities responsible for excess absorption in commercial crystals. After numerous experimental difficulties we did succeed, as did several other laboratories, in growing KCl crystals with a near-intrinsic absorptivity of less than $10^{-4}cm^{-1}$.

Late in 1973, we were asked to redirect our research toward resolving the thousandfold discrepancy between the extremely low 10.6 μm absorptivity predicted for KBr (10^{-6} to 10^{-7} cm^{-1}) and the experimentally realized value of $10^{-3}cm^{-1}$. In this case, our purification techniques which had been successful with KCl were either ineffective or infeasible. We are therefore attempting to identify the impurities responsible for the 10.6 μm absorption in KBr and to develop special techniques for their removal.

a.2.2 Approach:

Just as with KCl (ref. 1), it is probable that there are several polyatomic anion impurities which when dissolved in KBr give rise to absorption at 10.6 μm. Therefore, the observed absorption may be due to any one of these impurities or to a combination of them. Ideally, our program should include determination of the absorption spectra of purified KBr in the 10.6 μm region so that the impurities causing absorption can be identified. Since such measurements are well beyond the sensitivity of conventional spectrophotometers, and since molecular IR spectra are seldom resolvable much above 77°K, such an effort would entail laser calorimetry or emissivity measurements at liquid nitrogen temperatures. Since we have no access to such apparatus, we are confined to determining the absorption spectra of

---

*present address: Motorola Corporation, Phoenix, Arizona.

impurity-doped crystals, inferring which impurities are most likely to be the cause of excess 10.6 μm absorption in undoped crystals, and devising purification techniques accordingly.

Our present research program is shown schematically in Figure 1. Our procedures and techniques have been described in previous quarterly technical reports and are briefly summarized in the following paragraphs.

a.2.3 Techniques:

Solution Purification: The ion exchange procedures are substantially the same as those used by Fredericks et al. (ref. 2). KBr solution is passed successively through columns of cation- and anion- exchange resins, filtered and concentrated by evaporation in a vacuum dessicator, and fractionally crystallized, (Qtr. #1, p. 8 and Figure 1, and Qtr. #2, pp. 7-8). All steps are carried out in a sealed plastic system, so that even without a clean room, atmospheric contamination can be avoided, (Qtr. #2, p. 8 and Qtr. #3, pp. 5-6).

Atomic absorption analyses for calcium, magnesium and sodium in a solution after each step of the process indicate that divalent cation concentrations are reduced to one molar part per million or less and that monovalent impurities such as sodium are reduced by a factor of about two (Qtr. #8). It is presumed but not proven that reductions of anionic impurities are effected to a similar degree.

Halogenation: The moist crystals are packed into vitreous carbon or silica crucibles, inserted into the crystal-pulling chamber, baked out under vacuum to remove moisture and then heated to the melting point of KBr under an atmosphere of flowing HBr and/or Br_2 + He. HBr and/or Br_2 + He are then bubbled through the melt for 16 to 48 hours. This procedure effectively removes hydroxide and all other anions with volatile anhydrides, such as $SO_4^=$, NO_3^-, $CO_3^=$, etc. (ref. 2, 3). The inlet tube is then replaced by a pull rod and the crystal pulling chamber is then transferred to the pulling apparatus.

Crystal Pulling: The stringent purity requirements and the use of corrosive gases forced us to develop a crystal pulling chamber constructed, insofar as possible, of non-corrosive and noncontaminating materials such as silica and vitreous carbon. At present our chambers are 64 mm diameter

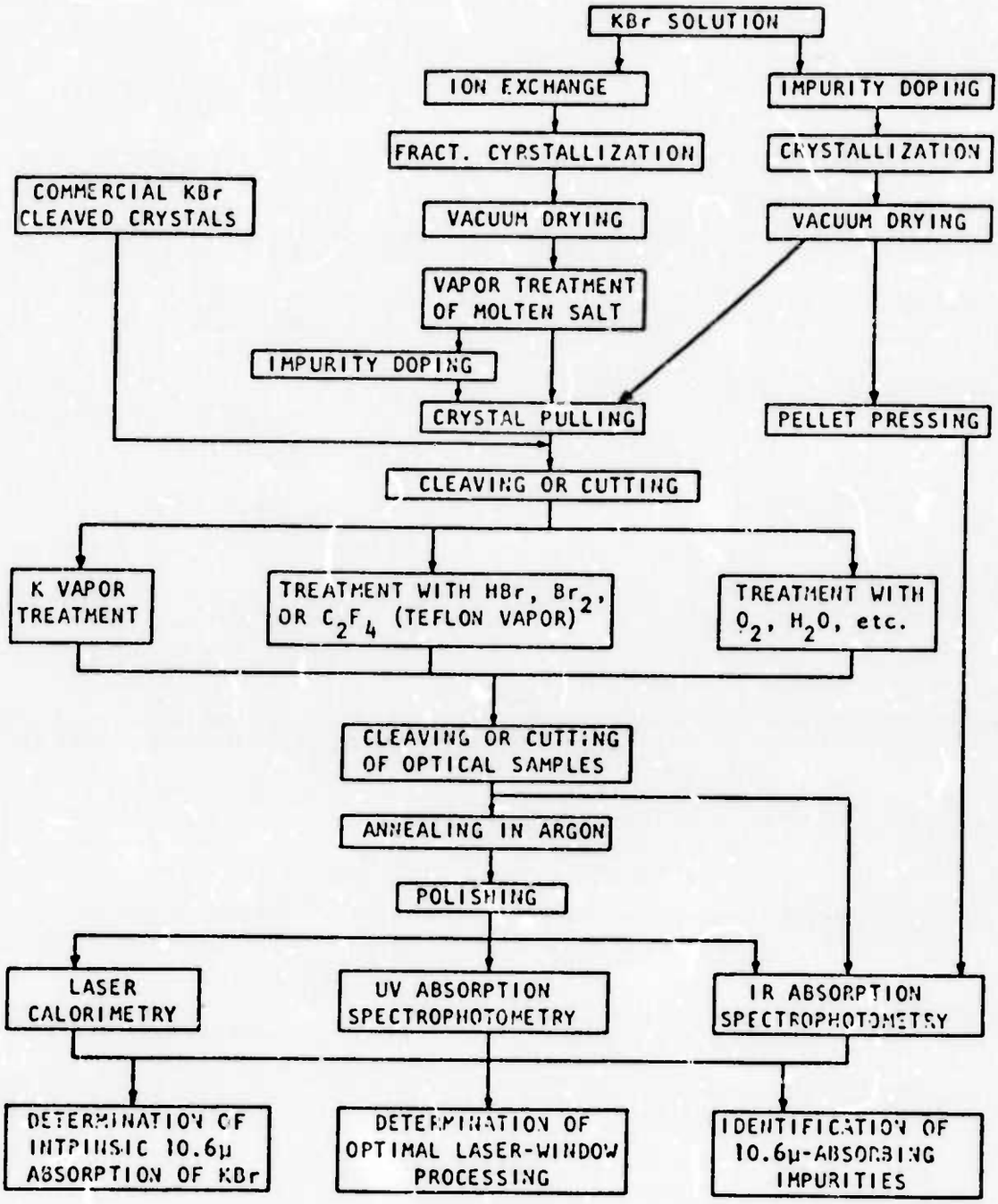


FIGURE 1 - Schematic Diagram of KBr Research Program

silica tubes sealed off at the bottom and capped by water-cooled aluminum pull-rod housings lined with teflon or impregnated graphite, (Qtr. #2, pp. 8 & 10). A 12 mm gas-cooled silica tube is used for a pull rod.

Maximum visibility for accurate seeding and diameter control is achieved by using a modification of the transparent gold-mirror furnace developed by Reed, (ref. 4) with a hairpin heating-element configuration.

The chief problem with this apparatus was inadequate heat flow, causing prohibitively slow pull rates. This difficulty was finally overcome by placing the crucible on a level with the top of the heating element; the resultant thermal gradient was high enough to permit pulling rates of over 5 cm/hr for 1 cm diameter crystals.

Impurity Doping: Doping is in most cases achieved by precipitating the KBr from a doped solution and then eliminating the halogenation step from the preparation of the molten salt. Because of matrix stabilization, this is more effective than adding the solid dopant to the KBr immediately before or during melting.

In some cases, anion doping can be accomplished by bubbling gases such as O_2, CO_2 or H_2O through the melt instead of or after the halogenation treatment. Alternatively, crystals are treated with these gases at temperatures approaching their melting point.

All of these procedures have the disadvantage that, because of possible thermal decomposition or evaporation, the exact species and concentration of the resultant impurity is not known. Identification of impurities is therefore best accomplished by measuring the IR absorption spectra of polycrystalline disks pressed from solution-precipitated powder. Our first attempts at pressing such disks convinced us of the need for vacuum evacuation, (ref. 5) and an evacuatable die assembly has been ordered.

Vapor Treatment: Molten KBr is treated with volatile liquid reagents, such as CCl_4, C_2Cl_4 or ethyl bromide, by bubbling a carrier gas (helium or argon) through the liquid and then following the same procedure as for halogenation with HBr. Similarly, crystals are treated with reagent-saturated carrier gas using the apparatus shown in Figure 2.

Treatment with potassium vapor is carried out in the apparatus shown in Figure 3. The temperature of the crystals and the vapor pressure of the potassium metal are independently regulated by adjusting the position of the tube inside the furnace and of the container inside the tube.

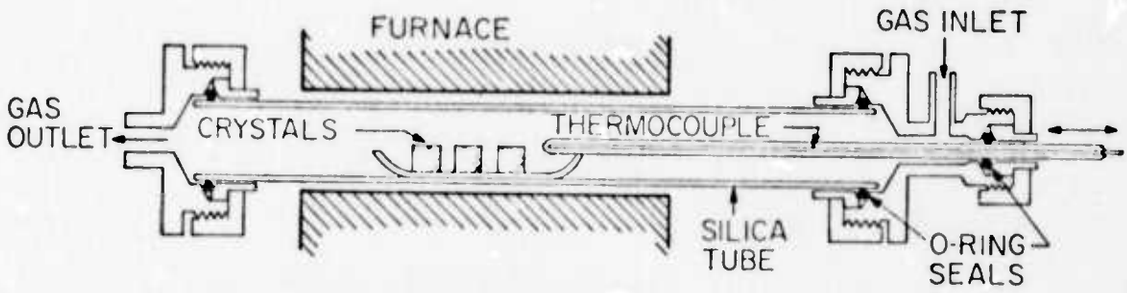


Fig. 2 Apparatus for annealing crystals in reactive gases.

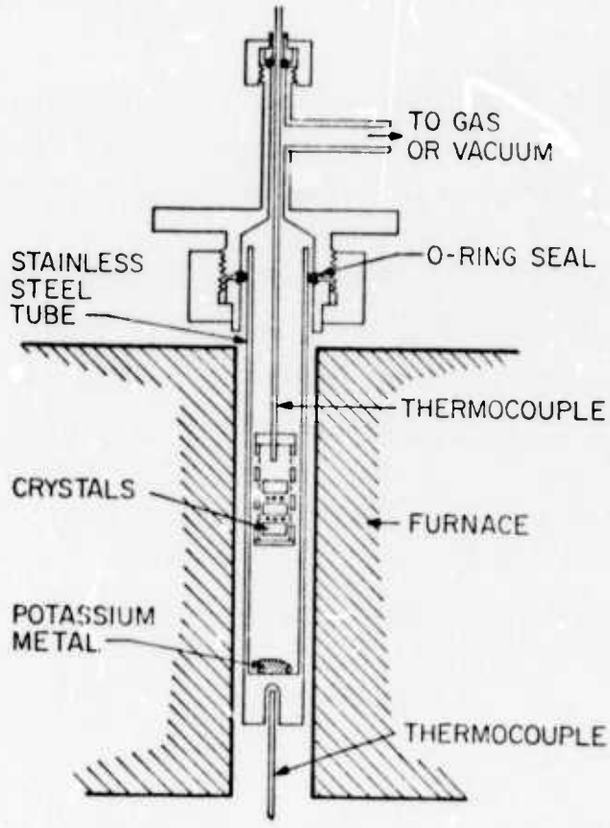


Fig. 3 Apparatus for annealing crystals in potassium vapor.

Cutting and Polishing: Samples used for laser calorimetry require extremely smooth and flat faces to prevent the scattering of part of the laser beam to the thermocouple. Initially, cleaved samples of KCl were prepared by abrasive polishing followed by chemical polishing in diluted hydrochloric acid or ethanol, (Qtr. #5, p. 9). This resulted in an unsatisfactory "orange peel" texture, presumably because the samples were not annealed before chemical polishing, (ref. 6). Selected as-cleaved samples appeared to give satisfactory laser calorimetry measurements of KCl but were not satisfactory for KBr, presumably because of excessive scattering of the laser beam by slip-band birefringence. Alternatively, annealing cleaved KBr in argon at 600°C causes dulling of the faces due to thermal etching. Therefore, some form of controlled contour solvent polishing appears to be necessary.

One procedure, developed during a NSF Summer Science Training Program project by Miss April Faagau, consists of rubbing or rotating the crystal against a porous polyethylene plate through which solvent is exuded at a constant rate,(Qtr. # 5, p. 13 and Fig. a .2.4.). This produces marginally adequate surfaces. Another apparatus, involving a modification of Dyer's apparatus, (ref. 7) in which the sample is advanced against a centrifugally spreading film of solvent on a rotating disc, is now being constructed and will soon be tested.

Absorption Spectrophotometry: Ultraviolet spectra, to identify anion impurities, are measured at room temperature by means of a Cary Model 14 double-beam spectrophotometer, using the best available purified crystal as a reference standard. Infrared spectra are measured at liquid nitrogen temperature with a Perkin-Elmer Model 210-B single-beam grating spectrophotometer. Arrangements are now being made, through the courtesy of Prof. C. Rossman of Caltech, to make at least some of our measurements with a Perkin-Elmer Model 54 double-beam far infrared spectrophotometer.

Laser Calorimetry: For these measurements at 10.6 μm the procedure of Deutsch and Rudko, (ref. 8) is used, in which the sample is heated by a constant-power CO_2 laser and then allowed to cool. The true heating rate is assumed to be the algebraic sum of the heating rate and cooling rate, and is measured by a thermocouple attached to the crystal. Calculation of the absorptivity is done by comparing the heating rate and heat capacity of the crystal with those of a reference black body, (i.e. a total-absorption

cone), and by making allowance for multiple paths due to internal reflections, (Qtr. #5, pp. 10-13 and Figure 1).

a.2.4 Results:

KCl crystals were pulled from melts of purified salt pretreated with HCl and Cl_2. Cleaved and polished samples of these were compared with cleaved samples of commercial material, (Optovac, Inc.), by CO_2 laser calorimetry. The results are summarized in Table 1.

The bulk 10.6 μm absorptivity (α) was estimated according to the method of Horrigan et. al., (ref. 9) by measuring the apparent absorptivities (β) of specimens of varying path lengths (L), and by assuming that $\beta = \alpha L + 2\sigma$ where σ is assumed to be an invariant "surface absorptivity". Therefore, when βL is plotted against L, the slope of the line corresponds to α and the βL-axis intercept to 2σ, (Fig. 4). Pastor et. al., (ref. 10) have pointed out that, when unannealed cleared samples are used, σ may be due to light scattering or absorption from birefringent slip bands or vacancy clusters caused by cleavage. However, since such damage is usually confined to the subsurface region near the cleavage, it may be considered equivalent to surface absorption so that, if a linear fit of the data is feasible, the extrapolation is probably valid.

As shown in Figure 4, the data for both commercial and USC-grown KCl appear within measuring error, to fit straight lines fairly well. From this we infer that α is about .0007 cm^{-1} for Optovac material, .00025 cm^{-1} for polished pure crystals and less than .0001 cm^{-1} for cleaved crystals. Meager as these data may be, they suggest that our purification and halogenation procedures effectively reduce the 10.6 μm absorptivity of KCl to near-intrinsic values.

Our impurity studies were confined to the growth of a hydroxide-doped crystal from a melt containing 0.5 mole % KOH. The ultraviolet absorption spectrum of this crystal indicated an OH^- concentration of .0002 mole % with no observable concentrations of oxide or peroxide, (Qtr. #5, p. 10,12 and 18). The tenfold increase of β in this crystal suggests that OH is a significantly absorptive impurity.

KBr: Just as with KCl, crystals were grown from purified melts pretreated with halogen compounds, (in this case HBr and/or Br_2), and then compared with commercial material by laser calorimetry. The results, (Table 2 and Figure 5), are disturbingly different in that the scatter is too great to permit a linear extrapolation and in that the absorptivities

SUMMARY OF LASER CALORIMETRY MEASUREMENTS

OF 10.6 μm ABSORPTIVITY OF KCl

-TABLE 1-

SOURCE	HISTORY	SURFACE PREPARATION	PATH LENGTH L (cm)	AVERAGE MEASURED βL	EXTRAPOLATION	
					α (Bulk) (cm^{-1})	σ (Surface)
USC 3-7-A	purefied undoped KCl melt treated with HCl	mech. and chem. polished	0.677	.0015		
" " " B	and Cl_2 (Qtr. #5, p. 9)	"	1.563	.00187	.0002	.0007
" " " C	" " " " "	"	0.612	.00159		
" " " D	" " " " "	as-cleaved	0.575	.00023		
" " " E	" " " " "	"	0.217	.00022	<.0001	.0001
USC 4-78-A	pulled from KOH-doped melt in silica crucible (Qtr. #5, p. 10)	as-cleaved	0.825	.00248		
" " " A`	" " " " "	"	0.471	.00283		
" " " B	" " " " "	"	0.818	.00384	~.0014	~.0010
" " " B`	" " " " "	"	0.558	.00223		
OPTOVAC 3-A	as-received (Qtr. #6, p. 14 and 18)	cleaved	5.393	.0113		
" " A`	"	"	1.090	.00513		
" 4-A	"	"	2.040	.00835	.0007	.0021
" " A`	"	"	0.712	.0055		

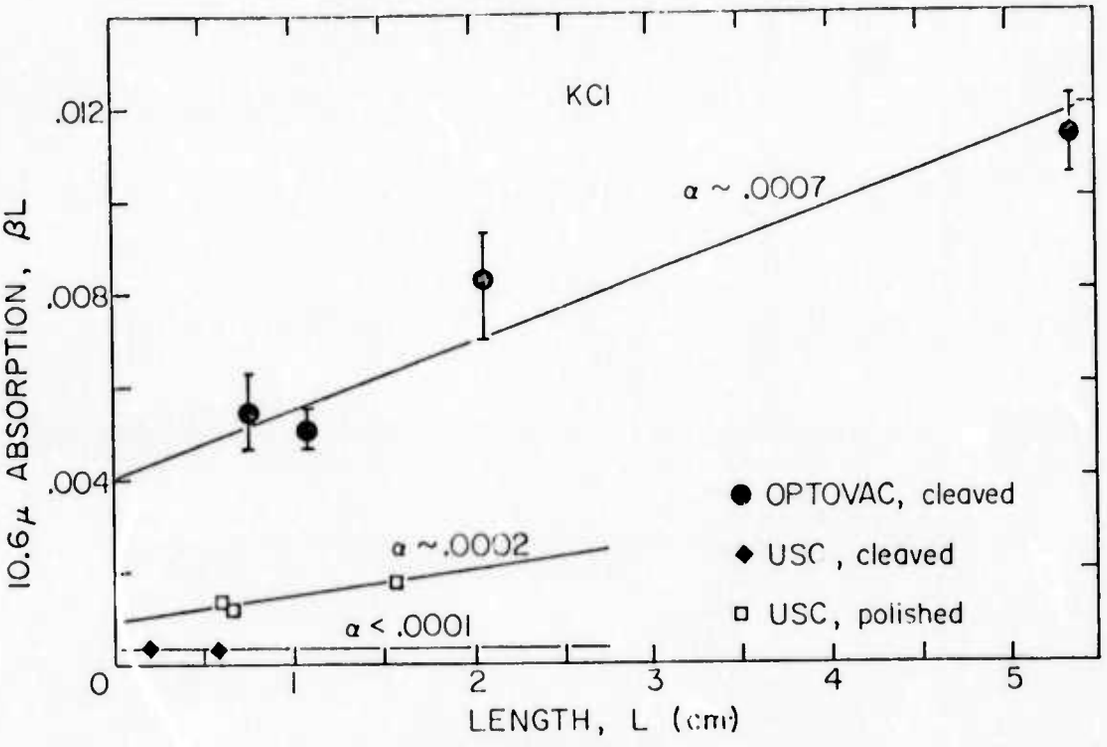


Fig. 4 10.6 μm absorptivity of KCl

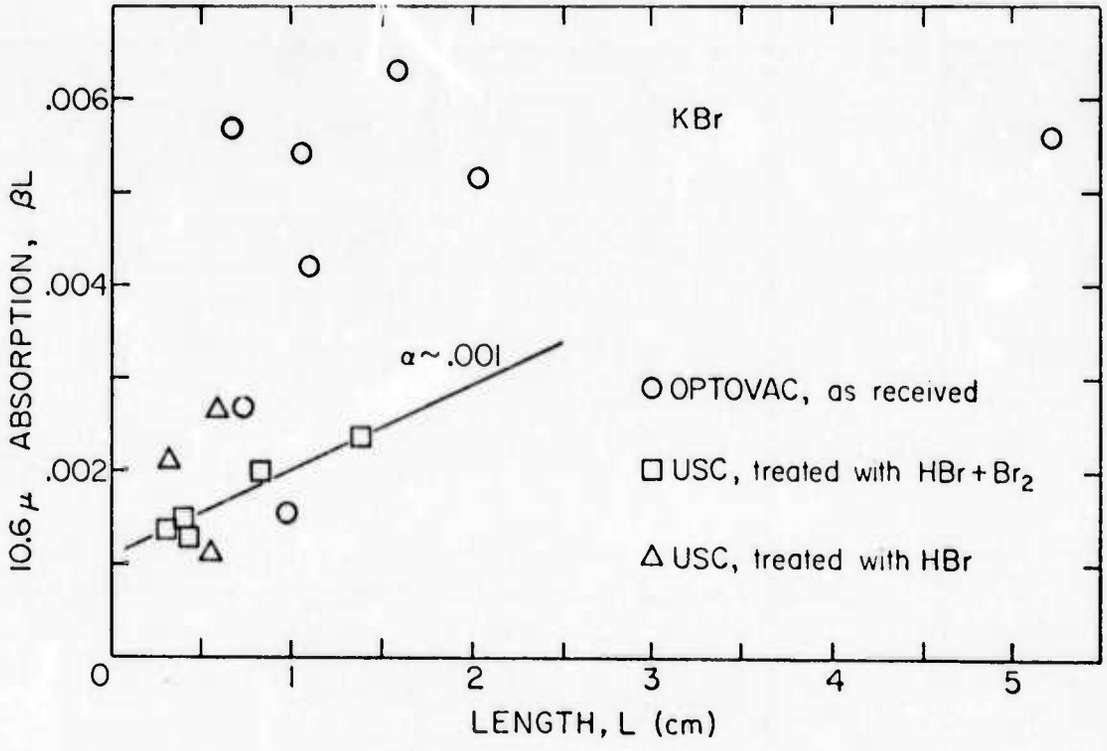


Fig. 5 10.6 μm absorptivity of KBr

TABLE 2 - SUMMARY OF LASER CALORIMETRY MEASURMENTS

OF 10.6 μm ABSORPTIVITY OF KBr

SOURCE	HISTORY	SURFACE PREPARATION	PATH LENGTH L (cm)	AVERAGE MEASURED βL	EXTRAPOLATION	
					α (Bulk)	σ (Surface)
USC 1-1-A	Pulled from melt treated with HBr and Br_2 (Qtr. #6, p. 10)	as-cleaved	0.7859	.00197	.001	.0005
" " " B	" " " "	"	1.318	.00237		
" " " C	" " " "	"	0.4486	.0013		
" " " D	" " " "	"	0.2647	.0014		
USC 3-2-A	Pulled from melt treated with HBr and Br_2 [silica crucible] (Qtr. #7, p. 9)	as-cleaved	0.389	.00148		
USC 3-3-A	Pulled from purified melt treated with HBr	as-cleaved	0.332	.00212		
" " " B	[carbon crucible] (Qtr. #7, p. 9)					
" " " B	" " " "	"	0.563	.00113		
" " " C	" " " "	"	0.613	.0027		
USC 3-6-A	Pulled from melt coprecipitated with $KBrO_3$ vacuum dried with no gas pretreatment (Qtr #7)	as-cleaved	0.565	.0390		
" " " B	" " " " pp. 5-7	"	0.561	.0166		
" " " B`	" " " "	"	0.686	.0356		
OPTOVAC 6-A	as-received	as-cleaved	5.235	.00575		
" " B		"	1.114	.00535		
OPTOVAC 7-A	as-received	as-cleaved	2.033	.00508		
" " B		"	0.7407	.0025		
OPTOVAC 8-A	as-received	as-cleaved	1.55	.00635		
" " A`		"	1.14	.0041		
" "A``		"	0.70	.00574		
OPTOVAC 9	as-received	as-cleaved	0.98	.00157		
" 91	OPTOVAC 9 after annealing in argon (Qtr. #8)	"	0.72	.00209		
" 92	OPTOVAC 9 after K vapor treatment (Qtr. #8)	"	0.38	.00846		
OPTOVAC 10	annealed in H_2O-saturated CO_2 (Qtr. #7, p.9)	as-cleaved	0.68	.00231		
" 101	OPTOVAC 10 after annealing in argon (Qtr. #8)	"	0.59	.00153		
" 102	OPTOVAC 10 after K vapor treatment (Qtr. #8)	"	0.42	.00474		
OPTOVAC 11	annealed in oxygen (Qtr. #7, p. 9)	as-cleaved	0.68	.0019		
" 111	OPTOVAC 11 after annealing in argon (Qtr. #8)	"	0.39	.00484		
" 112	OPTOVAC 11 after K vapor treatment (Qtr. #8)	"	0.49	.0110		

of the USC-grown purified crystals are not significantly lower than the commercial ones and both are far higher than theoretical prediction, (ref. 11).

KBr differs from KCl in being softer, more soluble and hence presumably more hygroscopic, and in having a more oxidizable anion. Accordingly the results might be explained by some or all of the following hypotheses:

(1) The theoretical prediction ($10^{-7}cm^{-1}$) may be erroneously low. Prof. R. Hellwarth of USC has examined this problem and is of the opinion that, even allowing for absorption mechanisms not accounted for in ref. 11, the intrinsic absorptivity of KBr cannot be much more than $10^{-6}cm^{-1}$.

(2) The scatter of data and some of the excess absorption may be due to deformation-induced absorption and/or light-scattering defects. This seems probable in view of the high degree of slip-band birefringence exhibited by as-cleaved samples. Therefore, all samples will henceforth be annealed and chemically polished before laser calorimetry.

(3) Some excess absorption may be due to the adsorption of moisture on the surfaces of the samples. This is especially likely since the ambient humidity in the calorimetry laboratory is unusually high, (Qtr. #5, p. 14). The adsorption of other atmospheric gases such as CO_2 is also a possibility. Since hygroscopicity in alkali halides is greatly enhanced by plastic deformation, this effect can presumably be reduced to a constant level by annealing. It is therefore hoped that, if annealed samples are routinely used, the contribution from adsorption can be removed by linear extrapolation of the data.

(4) Finally, it is probable that most of the excess absorption is due to an impurity or impurities not removed by our purification procedure. This is most likely to be a polyatomic anion which is either monovalent and nonvolatile, (and therefore not efficiently removed by ion exchange and halogenation) or else a product of the reaction between KBr and crucible materials or residual atmospheric contaminants or moisture. This last consideration immediately suggests bromate ion or some other oxidized bromine-oxygen complex, (Qtr. #6, p. 11; Qtr. #7, p. 6; Qtr. #8). Although $KBrO_3$ decomposes to form KBr and oxygen at 370°C, it might be supposed that isolated bromate ions in KBr might receive enough matrix stabilization to survive melting and recrystallization.

A crystal pulled from a melt of KBr coprecipitated with $KBrO_3$ showed an order of magnitude increase in 10.6 μm absorption and a complex infrared

absorption spectrum in the 9-13 μm region, (Qtr. #7, pp. 5-11). This crystal also had a strong UV absorption peak, at about 2200 Å, which seems to correspond to a shoulder in the absorption spectrum of commercial material, (Qtr. #7, pp. 9-10). However, prolonged annealing of commercial crystals in O_2 did not noticeably increase the infrared absorption.

We have therefore adopted the hypothesis that at least one of the major infrared-absorbing impurities in commercial and conventionally purified KBr is either bromate ion or some other complex of bromine and/or oxygen in an oxidized state. It has also been concluded that such an impurity would be relatively unresponsive to halogenating agents such as HBr, Br_2 or CBr_4 but might be removed by strong reducing agents such as potassium vapor or unsaturated organic compounds, (Qtr. #8).

Treatment of commercial crystals in 10 Torr potassium vapor at 650°C led to an unexpected tenfold increase in 10.6 μm absorption, (Qtr. #8). This does not necessarily mean that the absorption is due to oxide ion -- the only likely ionic reduction product of such treatment. It has already been pointed out that, whereas potassium vapor should be an efficient reducing agent in molten KBr, the reduction of bromate to oxide in the solid state requires extensive vacancy diffusion and charge disproportionation and therefore may not be feasible, (Qtr. #8). Moreover, a similar enhancement of 10 μm region absorption was reported in potassium-vapor treated sulfate-doped KCl and was attributed to ion-electron complexes such as $SO^{=}$, $SO_2^{=}$ and/or ClO_2^{-}. It is therefore believed that this effect is merely an "infrared herring" and has no bearing on the absorption in untreated crystals (ref 12). Therefore, treatment of molten KBr with potassium vapor , with or without subsequent treatment with HBr, is still a presumably valid and as-yet untried approach.

An alternative approach -- treatment with strongly reducing, (e.g. unsaturated), organic halides -- at first appeared infeasible inasmuch as all our previous attempts to treat KBr with organic bromides, such as CBr_4 and C_2H_5Br, had been unsuccessful because of carbon deposition, (Qtr. #6, pp. 11-12; Qtr. #7, p. 5). However, A. Kahan, of AFCRL, called our attention to the successful use, by various Russian laboratories, of tetrafluoroethylene (formed by the thermal decomposition of teflon) for the removal of oxygen from fluorite, (ref. 13) and even from NaCl, (ref. 14).

Acting on this suggestion, we considered the reaction of C_2F_4 with

bromate ion and concluded that it should efficiently remove bromate, and also other ions such as OH^- from both molten and solid KBr, (Qtr. #8). However, preliminary experiments, substantiated by conversations with Dupont representatives, indicated that C_2F_4 presents such formidable toxic and explosive hazards that its use at USC seemed at present infeasible (Qtr. #8). Moreover, it was observed to decompose to form carbon and CF_4 at temperatures well below the melting point of KBr. Accordingly, we considered the use of analogous reagents such as C_2Cl_4.

To determine the stability of C_2Cl_4 at high temperatures, argon was bubbled through C_2Cl_4 (whose vapor pressure is 13 Tor at 20°C) and passed through a silica tube in a furnace with a view port. No carbon deposition was observed after 30 minutes at 790°C but carbon was observed after 30 minutes at 810°C. It therefore seemed probable that C_2Cl_4 could be used for treating both molten KBr and solid crystals.

To determine the effect of the latter treatment, cleaved cubes of commercial KCl and KBr were exposed to the flowing argon + C_2Cl_4 mixture at 700°C for 72 hours. No carbon deposition was observed anywhere in the system. This treatment left the cleaved surfaces of the KCl specimen unchanged, but the KBr showed signs of etching and void formation, (Fig. 6) indicating that some exchange of halogen had probably taken place. It was also noted that this treatment removed most but not all of the cleavage-induced strain birefringence in these specimens; although slip bands were no longer resolvable, diffuse birefringence was still observable, especially in the KBr. These specimens are now awaiting polishing and laser calorimetry.

Treatment of molten KBr with C_2Cl_4 was first tried with the melt at 750 to 775°C. First HBr was bubbled through for 24 hours, then helium for 24 hours and finally (to remove chloride and possibly chlorocarbonate ions) HBr for an additional 24 hours. At the end of this treatment, carbon was observed to have deposited on the silica tube and was also dispersed throughout the melt. In another run, using the same procedure except that the melt was maintained first above the melting point, carbon was again observed on the walls of the chamber but the melt was apparently free of it. Attempts are now being made to pull a crystal from this material.

Future experiments will include the processing of melts with potassium vapor (and subsequently with HBr to remove the excess potassium) and with various combinations of C_2Cl_4 and HBr. We are also considering the possibility

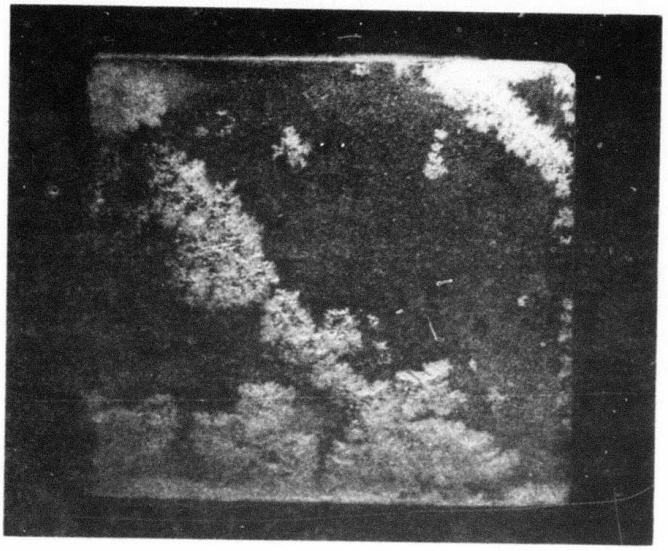


Fig. 6 Erosion and bubble formation on the surface of KBr Crystal treated with C_2Cl_4. (7.6x)

of combining C_2Cl_4 treatment with zone melting or fractional distillation. C_2Cl_4 will also be used to treat both pure and bromate-doped crystals.

References:

1. C. J. Duthler, J. Applied Physics 45 (1974) p. 2668-71.
2. W. J. Fredericks, L. W. Schuerman and L. C. Lewis, An Investigation of Crystal Growth Processes, (Dept. of Chemistry, Oregon State University, 1966) report AF-AFOSR-217-63 and -66.
3. For a comprehensive review, see F. Rosenberger in Ultrapurity, ed. by M. Zief and B. Speights (Marcel Dekker, 1972).
4. T. B. Reed, Solid State Research Report, (Lincoln Laboratory, M.I.T.) (1973) p. 1.
5. K. Ridgway and M. E. Aulton, J. Pharm. and Pharmacol, 26 (1974) pp. 46-53.
6. J. W. Davisson in Conference on High Power Infrared Laser Window Materials October 30, 31 and November 1, 1972, Vol. II, [AFCRL-TR-73-0372(11)] (19 June 1973) pp. 525-34.
7. L. D. Dyer, Rev. Sci. Instr. 34 (1963) pp. 1114-6.
8. T. F. Deutsch and R.I. Rudko, Conference on High Power Infrared Laser Window Materials: October 30, 31 and November 1, 1972, Vol. 1 [AFCRL-TR-73-0372(1)] (19 June 1973) pp. 201-222.
9. F. Horrigan, C. Klein, R. Rudko and D. Wilson, Microwaves (Jan 1969) p. 68.
10. R. C. Pastor, A. C. Pastor and J. E. Kiefer, in Conference on High Power Infrared Laser Window Materials, October 30, 31 and November 1, 1972, Vol. 2 [AFCRL-TR-73-0372(11)] (19 June 1973) pp. 535-48.
11. T. F. Deutsch, J. Phys. Chem. Solids Vol. 34, p. 2091, 1973.
12. G. Lehmann, E. H. Coker and A. B. Scott, J. Solid State Chem. 4 (1972) pp. 243-9.
13. For a review see, A. Kahan, Alkaline Earth Fluoride Windows and Domes, AFCRL Technical Memorandum LQ-21 (9 July 1974); see also references in Qtr. #8.
14. V. F. Pissarenko and S. V. Vonopaeva, Physica Status Solidi 15 (1966) p. K95-6.

a.3 Chemical Vapor Deposition of Bulk GaAs Crystals

W. R. Wilcox and E. A. Miller

a.3.1 Introduction:

We wish to summarize the effort of 18 months which was directed toward growth of bulk GaAs by the open tube CVD method, since the project has now ended. Particular emphasis will be on the last quarter's work, wherein we obtained smooth deposits 1 to 2 mm thick on GaAs substrates.

a.3.2 Experimental Procedure:

An open tube epitaxial reactor was constructed, which used the $AsCl_3$-Ga-H_2 deposition system. This system is most often used in the semiconductor process industry for growth of high purity GaAs growth of thin films, but found that these conditions were not suitable for experimentally determining the optimum conditions for substrate temperature, $AsCl_3$ mole fraction in the gas substrate orientation, and growth time.

a.3.3 Results and Discussion:

Several long runs were completed which resulted in severe substrate etching. This was accompanied by dendritic overgrowths which apparently consumed reactants from the gas stream directly above the substrates. By reducing the $AsCl_3$ supersaturation (lower $AsCl_3$ mole fraction in the gas) we were able to minimize dendritic growth. It seems, however, that given enough time dendritic overgrowth occurs regardless and acts as a factor limiting deposit thickness. For example, a 9 day run (CVD #21) gave smooth deposits, while a 27 day run under the same conditions (CVD #22) resulted in severe etching and dendritic overgrowths (see Table I).

From results of previous runs, we selected operating conditions that yielded deposits 1 to 2 mm thick in 7 days. The substrate orientation was {100}, which reportedly has a slower growth rate than other orientations tested, but more uniform deposits usually occur. Figure 1 shows the results of this run (CVD #26); note the clusters of GaAs deposits on the substrate holder, and the blade-like dendritic growths on substrate #1 located at the tip of the holder. Also see Figure 2 for a close-up view of substrate #1. The blades on substrate #2 (2nd from the tip of holder) are shown in Figure 3.

Substrate #3 was further examined. Note the appearance of large individual grains, Figure 1, the boundaries of which were revealed by inclusions and voids after lapping and chemical polishing. The orientation of these grains

remained in the {100} direction, however. All deposits in this run had many small voids and inclusions, possibly due to small air leaks in the system. See Figure 2 for example.

Table I summarizes some of the operating conditions and results obtained during this program.

a.3.4 Optical and Electrical Properties:

Some IR absorption and Hall data were taken on the deposited films. From run CVD #21, we were able to obtain a sample 4 mils thick after lapping away the substrate. Results from this sample, see Table II, show that the material obtained is approximately of the same quality as typical melt grown GaAs. These rather poor results could have been caused by the small voids and inclusions observed in the sample. Perhaps if our system had been cleaner, much better results would have been obtained. Other determinations were made on samples with many small ($\approx 0.5 mm^2$) polycrystalline inclusions in them; results in these cases were even worse. An absorption measurement at 10.6 μm was made on one of the blades grown in run CVD #26. The absorbance was so high that a hole was burned through the sample at 5 watts incident power. In addition, operation at the lower $AsCl_3$ mole fractions (necessary to produce thick films) increases the tendency for impurity incorporation (mainly Si)[1], thus further degrading the electrical properties.

References

1. J.V. DiLorenzo, J. Crystal Growth 17, 189 (1972).

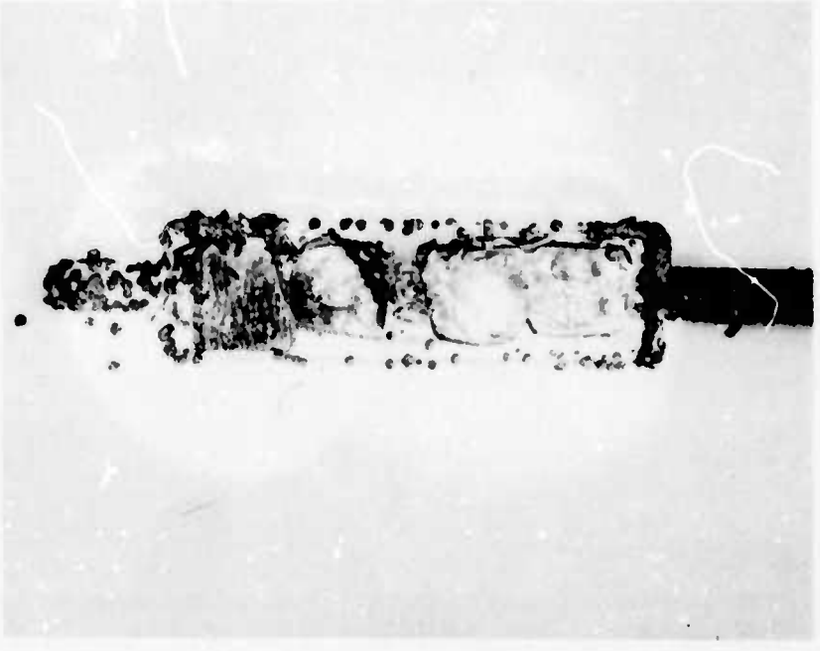


Figure 1 CVD #26 0.7X



Figure 2 CVD #26 Substrate #1 4X



Figure 3 CVD #26, Stustrate #2 10X

TABLE I

SUMMARY OF RUNS 3/1/73 - 11/30/73

Run #	$AsCl_3$ Mole Fraction	Length of Run	Substrate Orientation	Substrate Temp.	Results
CVD #13	6×10^{-3}	1 Day	{100}	750°C*	Growth with many hillocks
CVD #16	5.6×10^{-3}	1 Day	{111} A & B {100}	770°C	Smooth growth on {100}, uniformly rough deposit on {111} A
CVD #17	5.6×10^{-3}	5 Days	{111}A	750°C	Severe dendritic growth, slight substrate etching
CVD #19	2.8×10^{-3}	3 Days	{111}A 4 pcs	735 - 765°C	Deposit uniform, but rough, few dendrites
CVD #21	2.3×10^{-3}	9 Days	{111}A 2 pcs {100}2 pcs	735 - 765°C	Growth pits {111}A; specular, hillock growth {100}
CVD #22	2.2×10^{-3}	27 Days	{111}A 2 pcs {100} 2 pcs	735 - 765°C	Severe etching on all substrates
CVD #24	5.6×10^{-3}	5 Days	{111}A 2 pcs {110} 2 pcs	775 - 795°C	Rough polycrystalline deposits, some specular areas
CVD #25	3.5×10^{-3}	7 Days	{111}A 2 pcs {110} 2 pcs	765 - 785°C	Rough polycrystalline deposit {110}, specular polycrystalline depost {111}A
CVD #26	4.5×10^{-3}	7 Days	{100} 4 pcs	745 - 775°C	Smooth, specular, 1 - 2 mm thick deposits, many small voids, blades grew in high temperature regions

*Temperature profile as reported by C.M. Wolfe, A. G. Foyt, Electrochem Tech., 6, 208 (1968)

TABLE II

SUMMARY OF ELECTRICAL AND OPTICAL MEASUREMENTS

Run #	Orientation	Thickness	Resistivity	Hall Mobility	Carrier Concentration	Absorption Coefficient (10.6μ)
CVD #21 Wafer #2	{100}	5 mils	0.16Ω-cm	$3400 \frac{cm^2}{v \cdot sec}$	$5 \times 10^{15}_{cc^{-1}}$	
CVD #21 Wafer #4	{100}	4 mils				$0.046 cm^{-1}$
CVD #24 Wafer #2	{111}A Polycrystalline inclusions	5 mils	0.35Ω-cm	$280 \frac{cm^2}{v \cdot sec}$	$7 \times 10^{16}_{cc^{-1}}$	$2.1 cm^{-1}$
CVD #26 Wafer #3	{100}	0.7mm	0.06Ω-cm	$980 \frac{cm^2}{v \cdot sec}$	$1 \times 10^{17}_{cc^{-1}}$	$0.9 cm^{-1}$

b.1 Fabrication of Polycrystalline IR Window Material

S. M. Copley, J. M. Whelan, and V. Rana

The goal of this part of the program has been to produce IR Window materials in polycrystalline form by hot pressing a semiconductor powder with the help of a volatile sintering aid. The sintering aid is present as a liquid phase at the hot pressing temperature, enhancing the compaction of the powder to near theoretical density by liquid phase sintering processes. The sintering aid which is still present in the compact after the hot pressing operation is evaporated from the compact by a post-annealing treatment.

With the help of a volatile sintering aid, it should be possible to obtain a highly dense window material at lower temperatures than is possible by conventional hot pressing. The final product should be a polycrystalline window of extremely high density and small grain size and should have a high fracture strength.

Initially it was planned to hot press GaAs powder using excess As as a sintering aid, and CdTe powder using either Cd or Te as a sintering aid. Only a component of the semiconducting compound was chosen as a sintering aid so that no impurities would be intentionally introduced into the window material. It was also thought that impurities in and on the surface of the powder introduced during the powder preparation and handling might be preferentially dissolved by the liquid phase due to solvent extraction process, and then preferentially evaporated during the post annealing treatment.

A hot press was designed and constructed for this work, as described in detail earlier.[1]

Since it was realized during the course of this work that a CdTe window could be produced having a lower absorption than a GaAs window, interest in GaAs diminished. Therefore, hot pressing runs were carried out only on CdTe.

The details of the hot pressing operations have been described in an earlier report.[2]

Starting Material: Most of the CdTe used in this work, was synthesized from high purity elements in our laboratory. The synthesis of CdTe and its reduction into powder form was described in detail in the earlier report.[3]

As reported earlier[4] hot pressings done using an excess of liquid Cd were not successful. In order to successfully sinter a powder with a liquid phase, the liquid must wet the surfaces of the solid powder. Preliminary experiments[5] showed that both Te and Cd liquids do not wet CdTe below 700°C in vacuum. The contact angle is greater than 90°. This may be due to the presence of an oxide layer on CdTe. In order that wetting of a solid surface by a liquid takes place, it is required that

$$\gamma_{SV} > \gamma_{LV}$$

where γ_{SV} = surface free energy of the solid-vapor interface
γ_{LV} = surface free energy of the liquid vapor interface.

Usually metal oxides have lower surface energy than the corresponding metal. This reduces γ_{SV} and hence reduces wetting. We observed a reduction of the temperature of wetting of CdTe (solid) by Cd (liquid) to 600°C in a H_2 atmosphere, which substantiates this view.

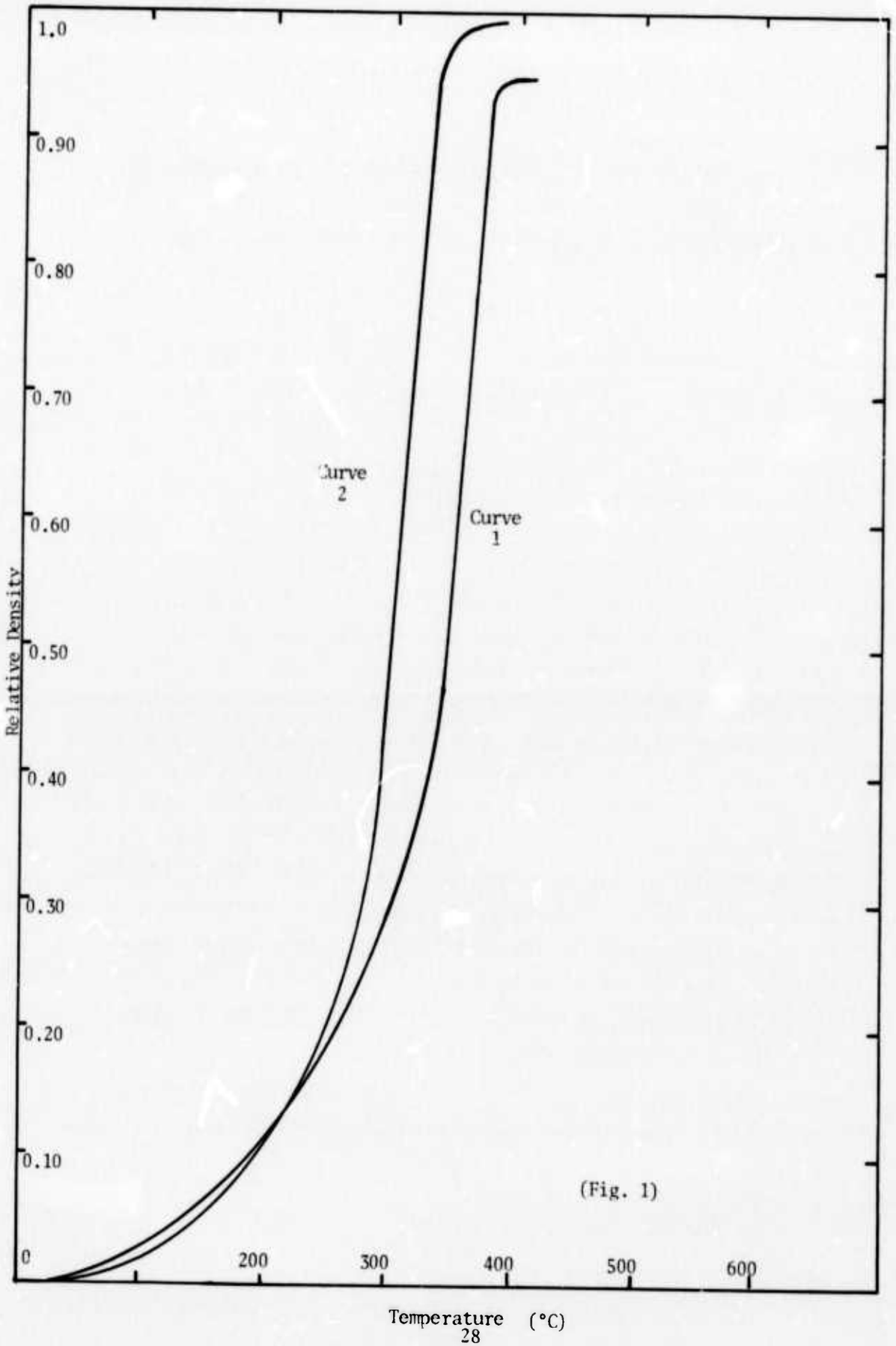
$CdCl_2$ as a sintering aid: It was decided to investigate $CdCl_2$ as a volatile sintering aid for CdTe. Molten $CdCl_2$ is known to wet CdTe so that capillarity should distribute it throughout the compact. It was hoped that sintering would be rapid enough and take place at a low enough temperature so that doping of the bulk grains by Cl would not occur.

Hot Pressing with $CdCl_2$: The procedure for hot pressing with $CdCl_2$ as a sintering aid was reported earlier.[6]

Densification: In the temperature range 250°C - 400°C, which is well below the melting point of $CdCl_2$, the CdTe - $CdCl_2$ compacts were observed to sinter rapidly, Fig. 1. The final density appears to depend on the particle size as shown in Table 1.

Table 1: Effect of Particle Size on Final Sintered Density of CdTe with 5wt % $CdCl_2$.

Average Particle Size	% Relative Density after Hot Pressing
1μ (Curve 1, Fig. 1)	94.95
< 1μ (Curve 2, Fig. 1)	98.99


1.0
0.90
0.80
0.70
0.60
0.50
0.40
0.30
0.20
0.10
0
Relative Density
Curve 2
Curve 1
200
300
400
500
600
Temperature (°C)

(Fig. 1)

These values of relative densities are based on the density of pure CdTe, 5.853 gms/c.c. Since there is $CdCl_2$ present in the hot-pressed compacts, the actual density of the compacts without pores would be less than this value. Hence, the compacts are less porous than is suggested by the relative values given in the Table.

S.E.M. photomicrographs,(Fig. 2),of a hot-pressed compact suggest the presence of a liquid phase at grain boundaries. During the hot pressing operation the liquid seems to get squeezed out of the compact, as there was more of this phase present in areas near the outside of the compact, (Fig. 3), than near the center of the compact, (Fig. 2).

The origin of the liquid that is believed to form in the compact below the melting point of $CdCl_2$ was not determined. $CdCl_2$ has been reported to dissolve CdO film present on Cd[7], so it is possible that a low melting alloy in the Cd-O-Cl system may be involved. It is also possible that water may be an important component in the liquid forming reaction in view of the hygroscopic tendencies of $CdCl_2$. The formation of such a low melting liquid and the observed enhancement of sintering suggests that a dense compact without significant Cl doping due to volume diffusion, might be obtained.

Post-Annealing Treatments on Hot Pressed Compacts: Highly dense, hot pressed CdTe compacts were given a post annealing treatment under varying experimental conditions to give different rates of evaporation of the liquid from the compact. A loss in density of up to 12% was noted in the different annealing treatments carried out as shown in Table 2.

Table 2: Effect of Post - Annealing Treatments on the Hot Pressed CdTe Compacts.

Annealing Treatments	Total Time	Starting Relative Density	Final Relative Density
1. Starting from room temp. we heated the compact to 500°C in a vacuum at the rate of 2° to 3°C/min.	3 hrs.	98.47%	86.33%
2. We sealed the compact in an evacuated quartz tube and annealed at 400°C; the other end of the tube was 340°C.	8 hrs.	98.47%	96.33%

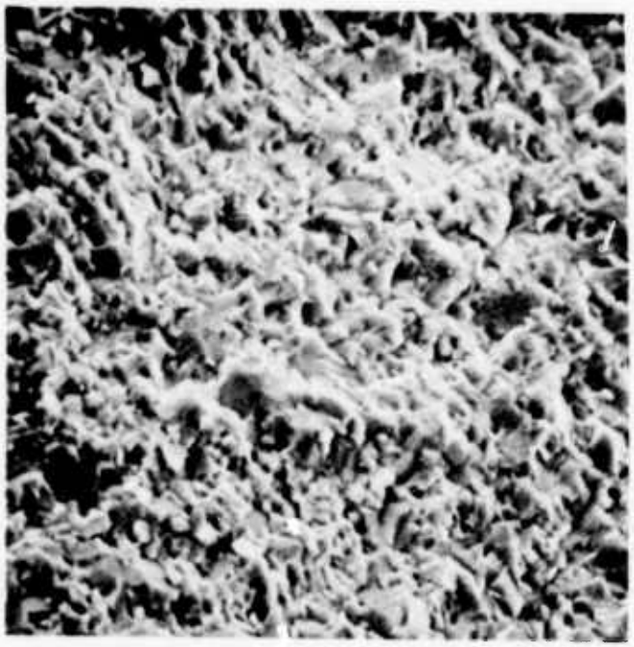


Fig. 2a

Fig. 2: Hot pressed CdTe-$CdCl_2$ compact
(a) near center
(b) near surface

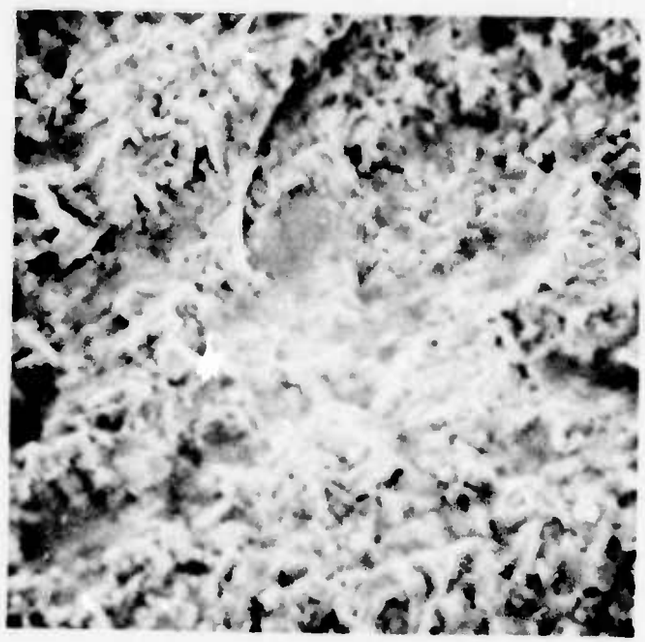


Fig. 2 b

Annealing Treatments	Total Time	Starting Relative Density	Final Relative Density
3. Annealed at 425°C in an evacuated tube containing $CdCl_2$ at 525°C.	10 hrs.	98.47%	94.74%

Fig. 3 shows photomicrographs of a hot pressed compact before and after the post-annealing treatment respectively. These photomicrographs verify that an increase in porosity upon annealing does indeed occur.

The behavior of the CdTe-$CdCl_2$ compacts during hot pressing is similar to that of MgO-LiF compacts. In both cases, rapid densification is observed at temperatures well below the melting point of the sintering aid. In the case of MgO-LiF, post annealing of the highly dense compacts produces a transparent pore free window.[8] In case of CdTe the amount of porosity increases during post annealing. The reason for this difference in behavior is not understood. The interpretation of our observation is complicated because of uncertainties regarding the composition and properties of the Cd-O-Cl-(H_2O) liquid phase.

References:

1. Quarterly Technical Report #2.
2. Quarterly Technical Report #5.
3. Quarterly Technical Report #7.
4. ibid.
5. ibid.
6. Quarterly Technical Report #8.
7. Menter, J. W. and Hall, E. O., "Surface Effects in the Creep of Cd Single Crystal" Nature vol. 165, p. 611 (1950).
8. Benecke, M. W. et al, "Effect of LiF on the Lot pressing of MgO" J. Am. Ceram. Soc. vol. 50 No. 7 p. 365 (1967).

Students Supported

Virendra Rana- This contract supported Mr. Rana's PhD. thesis research which he will be continuing under another grant.



Fig. 3 a

Fig. 3: Hot pressed CdTe-$CdCl_2$ compact
(a) before post annealing treatment
(b) after post annealing treatment



Fig. 3 b

c.1 Mechanical Behavior of III-V and II-VI Compounds - Final Report
S. M. Copley and V. Swaminathan

In our first proposal (November 1971), we proposed a basic investigation of the mechanical behavior of III-V and II-VI compounds. One objective of this investigation was to increase the understanding of plastic deformation and fracture in GaAs, thereby enabling the prediction of its mechanical behavior under various conditions. Another objective was to enhance the knowledge of defect structure and interaction between defects in the III-V and II-VI compounds. In what follows, we first review work completed prior to December 1973 (Phase I). We then review work completed after December 1973 (Phase II).

Phase I:

Stress-Strain Experiments: Since the initial emphasis of the ARPA/USC program was on GaAs, we chose this compound to begin our investigation. Crystals of window quality were available only in very limited amounts. Thus, we decided to carry out most of our measurements on Si-doped GaAs (n-type), which was readily available, but to include some measurements on Cr-doped (high resistivity), nominally undoped (high resistivity) and Zn-doped (p-type) GaAs to determine the effect of doping.
The specific objectives of our investigation were:

-- To determine the active slip systems in GaAs.
-- To determine the critical resolved shear stress (CRSS) for slip on these systems.
-- To determine the effect of loading rate on stress-strain behavior.
-- To determine the effect of temperature on stress-strain behavior.
-- To determine the effect of unloading and reloading on the flow stress.
-- To determine the microstructure of deformed material by transmission electron microscope (T.E.M.) in order to elucidate the mechanisms of deformation and fracture.

All this work was completed by December 1973. A presentation of part of the work was made at the 1973 Fall Meeting of the Basic Science Division of the American Ceramic Society (September 1973) by V. Swaminathan. A more complete presentation of this work was made at the Third Conference on High-Power Infrared Laser Window Materials (November 1973) by S. M. Copley and a paper by V. Swaminathan and S. M. Copley was published in the conference proceedings. A paper describing this work titled "The Temperature and

Orientation Dependence of Plastic Deformation in GaAs Single Crystals", by V. Swaminathan and S. M. Copley was submitted to the Journal of the American Ceramic Society on August 19, 1974. The results of this work are summarized below:

(1) Stress-strain curves were obtained for Si-doped GaAs single crystals deformed in compression parallel to <100> and <111> at temperatures ranging from 250 to 550°C.

(2) In both orientations, slip was shown to occur only on {111} $\langle 1\bar{1}0 \rangle$.

(3) Repeated yielding experiments on GaAs crystals, both undoped and doped with Si, Cr or Zn indicate that Si-doped crystals (n-type) have a greater yield stress than undoped crystals, undoped crystals have a greater yield stress than Zn doped crystals (p-type) and that Cr doping does not significantly affect the yield stress.

(4) Extensive crack formation due to deformation was not observed. Compression specimens normally failed by breaking into several columnar fragments parallel to the stress axis.

Microstructural Characterization: During Phase I, the scope of the microstructural characterization work involving transmission electron microscopy studies of deformed GaAs specimens was broadened to include:

-- the characterization of the microstructures of several of the high resistivity, low absorption GaAs crystals investigated by Steier and co-workers as part of this program (Qtr. # 4).
-- an investigation of the origin of anomalous streaks and spots in the electron diffraction patterns of GaAs
-- a determination of the conditions for recrystallizing GaAs by cold working and process annealing

While developing our technique of preparing thin foils of GaAs, we observed anomalous streaks and spots in electron diffraction pattern from GaAs (Qtr. #2). At about the same time, Haggerty and Peters had reported observing similar streaks (Second Conference on High Power Laser Window Materials, Oct. - Nov. 1972). They had concluded that the streaks were due to the presence of rod-like precipitates lying parallel to <110> and had developed a model explaining the magnitude of the observed optical absorptivity of GaAs at 10.6 μm based on this conclusion. Since the principal goal of the ARPA/USC program, Phase I, was to assess the potential of GaAs as a window material, we initiated a study of the streaks. Clearly, if such

precipitates were present as an inherent source of absorption, then this factor should be considered in our assessment of GaAs. Our investigation of the streaks was completed by December 1973. Our major conclusion was that the streaks were not due to precipitates but instead to the thermal diffuse scattering of electrons by phonons. This work was presented at the Third Conference on High Power Laser Window Materials (November 1973) by S. M. Copley and was published in the conference proceedings. A paper describing this work titled, "Anomalous Diffraction Effects in Gallium Arsenide Single Crystals", by G. H. Narayanan and S. M. Copley was published in the May 1974 issue of Physica Status Solidi.

As an outgrowth of the transmission electron microscopy studies of deformed specimens, it was decided to determine the conditions for recrystallizing single crystals by cold working and process annealing. It was thought that the recrystallization process might rearrange impurities and defects within the crystal (e.g. an impurity might be transferred from a lattice site to a lower symmetry grain boundary site) and, thereby, bring about a decrease in optical absorptivity. This work, including a determination of the optical absorptivity of recrystallized materials, was not completed prior to December 1973 and, thus will be reported as Phase II work.

Phase II:

During Phase II of the ARPA/USC program we have:

-- Completed an investigation of impurity hardening in GaAs.
-- Investigated the possibility that GaAs might twin at room temperature.
-- Completed a study of the effect of recrystallization on optical absorptivity.
-- Written a short note and another paper on anomalous streaks and spots in diffraction patterns from compound semiconductors.
-- Carried out a brief study of the microstructure and mechanical properties of CdTe equilibrated with various partial pressures of Cd at various temperatures.

Impurity Hardening in GaAs: A major conclusion of the Phase I investigation of the mechanical behavior of GaAs was that hardening by donor impurities may be due to the interaction of the glide dislocations with vacancy-donor impurity $(Si_{Ga}V_{Ga})^{x}$ pairs. During Phase II, we have studied the effect of aging in the range 400-700°C on the CRSS of a

Si-doped GaAs crystal in collaboration with Dr. G. H. Narayanan and Dr. W. G. Spitzer* Dr. Narayanan has studied the effect of the aging treatments on microstructure. Dr. Spitzer has studied the effect of the aging treatments on point defect populations employing a variety of techniques including local mode infrared spectroscopy. The current status of this work is summarized below:

(1) Wafers adjacent to each other were cut from the bulk crystal. These wafers will be identified as #4, #5 and #6.

(2) Compression specimens with stress axis parallel to [111] were obtained from these wafers. Specimens were annealed in sealed quartz tubes The temperatures and durations of annealing were determined from previous studies. (Qtr. # 7) Compression experiments were carried out either at a constant stress rate of 20 psi/sec or at a constant strain rate of 9×10^{-4}/sec. The temperature of deformation was maintained at 400°C and experiments were carried out either in air or in argon. The different atmospheres employed during the experiments did not give rise to any detectable change in the yield stress.

(3) Fig. 1 shows the aging curves for two different temperatures. The yield stress increases with time for both the temperatures. For the same time of aging the yield stress at 400°C is greater than that at 700°C. It should be noted that the concentration of the asymmetrical defects like $(Si_{Ga}V_{Ga})^{x}$ would be expected to decrease with increasing temperature.

(4) Fig. 2 shows the yield stress as a function of annealing treatment. Transmission Electron Microscopic Studies on GaAs single crystals by Narayanan and Kachare (submitted to Phys. Stat. Solidi 1974) indicated the presence of a high density of dislocation loops in samples annealed at 700 and 800°C. The loops also will act as hardening centers because of an elastic interaction between the glide dislocations and the loops. Therefore the contribution by the loops to the yield stress must be subtracted from the total yield stress in order to estimate the hardening by the defect complexes.

(5) Presently the following calculations are being carried out:
a) Estimation of the dislocation loop strengthening from the theories of Saada and Washburn (J. Phys. Soc. Japan, Suppl. I, 18, 43, 1962) and Kroupa and Hirsch (Disc. Faraday Soc. 38 49, 1964). Both theories estimate the

*Supported in part by JSEP

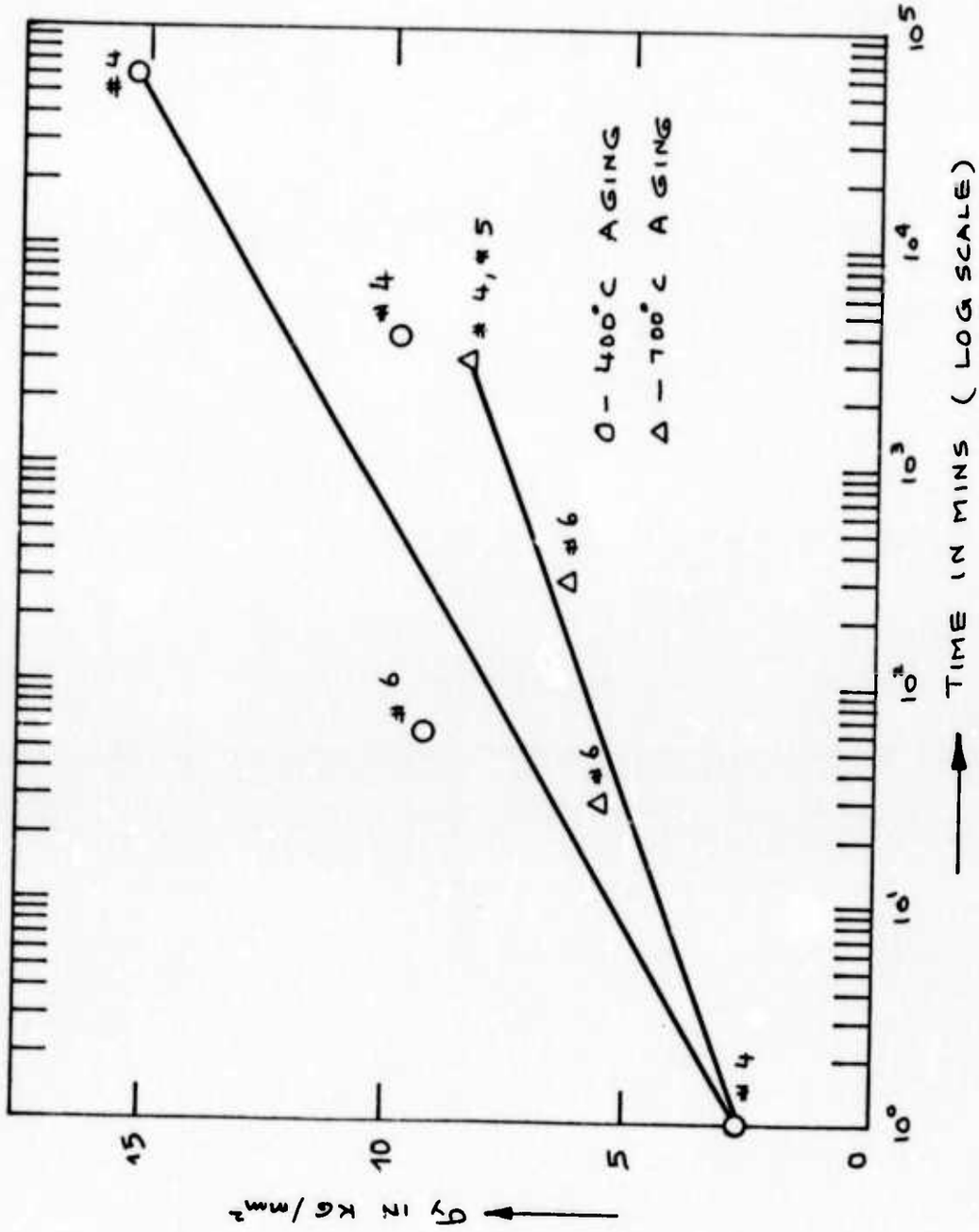


Figure 1: Yield stress vs time curves for samples annealed at 1100°C for 15 minutes and subsequently aged at 400°C and 700°C. The yield stress was measured in compression at 400°C.

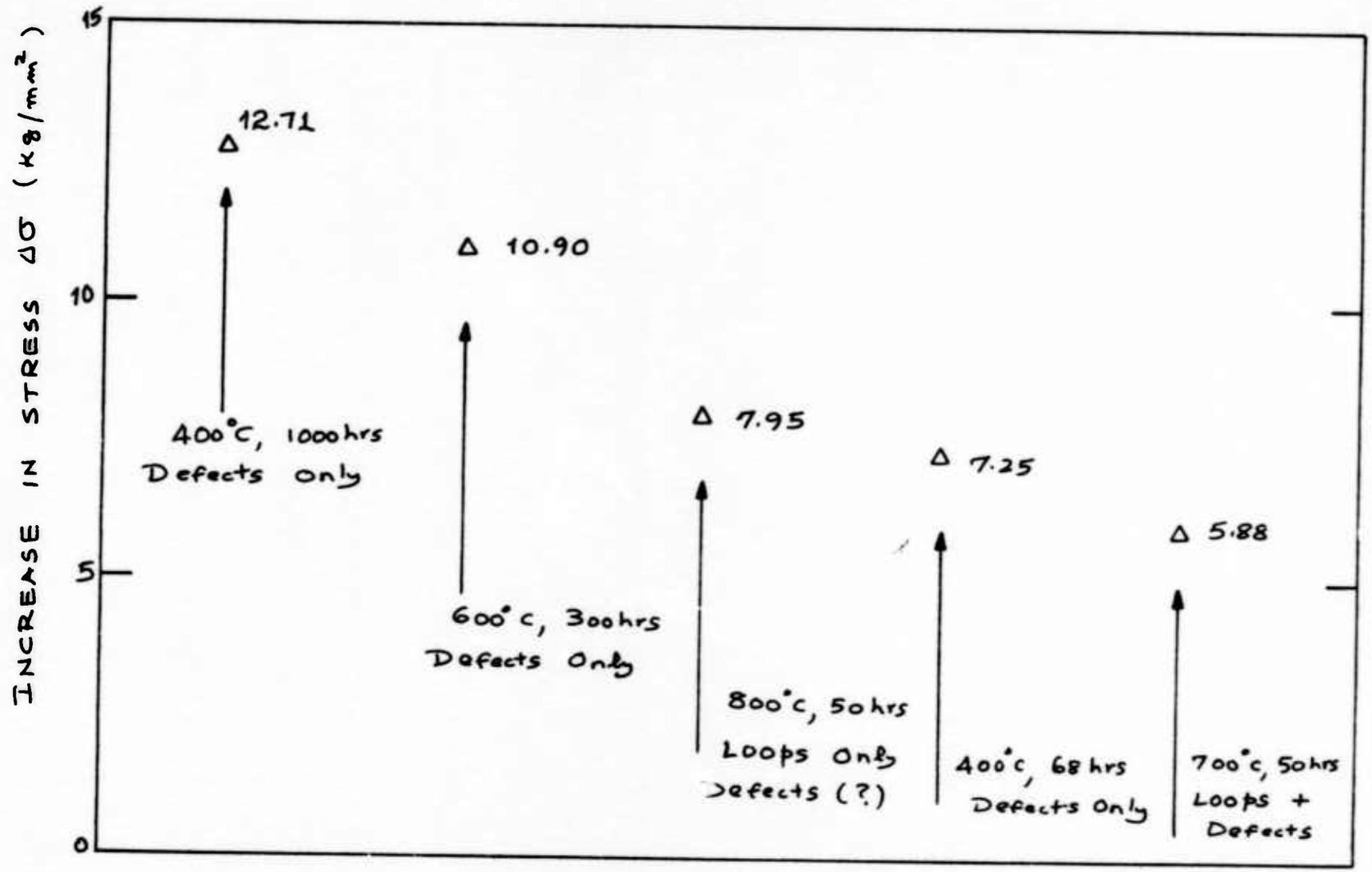


Figure 2: Increase in the yield stress ($\sigma y_o - \sigma y$) as a function of annealing treatment. σy_o is the yield stress of a sample annealed at 1100°C for 15 minutes. Note: the abscissa does not correspond to any parameter.

loop hardening by considering the elastic interaction of glide dislocations with the loops.

b) Estimation of the concentration of asymmetrical defects. Defects like ($Si_{Ga}V_{Ga}$) and ($Si_{Ga}Si_{As}$) are being considered.

c) To show that vacancies themselves are not effective hardening centers in GaAs.

Twinning in GaAs at Room Temperature:

GaAs like other semiconductors becomes brittle at low temperatures, i.e., at temperatures lower than 250°C. However, the possibility of twinning as a low temperature deformation mechanism has not been investigated before. With this in mind, we carried out compression tests on Si-doped GaAs single crystals at room temperature. To avoid any problem of misalignment during testing a spherically aligned loading head was used. No twinning or slip was observed and the samples were found to break into several columnar fragments with their long dimensions parallel to the stress axis. On examining the fracture surface, cleavage facets were observed. The orientation of several of these facets was determined by electron channeling technique. In all cases the cleavage facet was found to be within $\pm$ 5° of {110}.

Effect of Recrystallization on Optical Absorptivity:

To determine the effects of thermal and thermo mechanical treatments on optical absorption, experiments were carried out on Bell-Howell Cr-doped GaAs samples, (Sample #6013T). By using the technique of laser calorimetry the absorption coefficient as a function of wavelength was measured for three test samples. The results are summarized in Fig. 3. In Fig. 3 curve A corresponds to a as grown sample. Curve B corresponds to a sample which was deformed to a strain of 20% at 550°C and which after deformation was annealed at 1100°C for 20 minutes. This treatment of cold working and process annealing was shown to give rise to recrystallization, (Qtr. # 4). Curve C corresponds to a sample annealed at 1100°C for 15 minutes. it can be seen that at all wave lengths the sample that was treated for recrystallization has higher absorption than the annealed and the as grown samples. The annealed sample, on the other,hand has lower absorption than the as grown sample. This is in agreement with our previous observation where the same annealing treatment on Cr-doped GaAs (Sample #6050T) produced a decrease in absorption coefficient as compared to the as grown sample. In the present case, for example at 10.6 μm, the recrystallized sample has an absorption coefficient

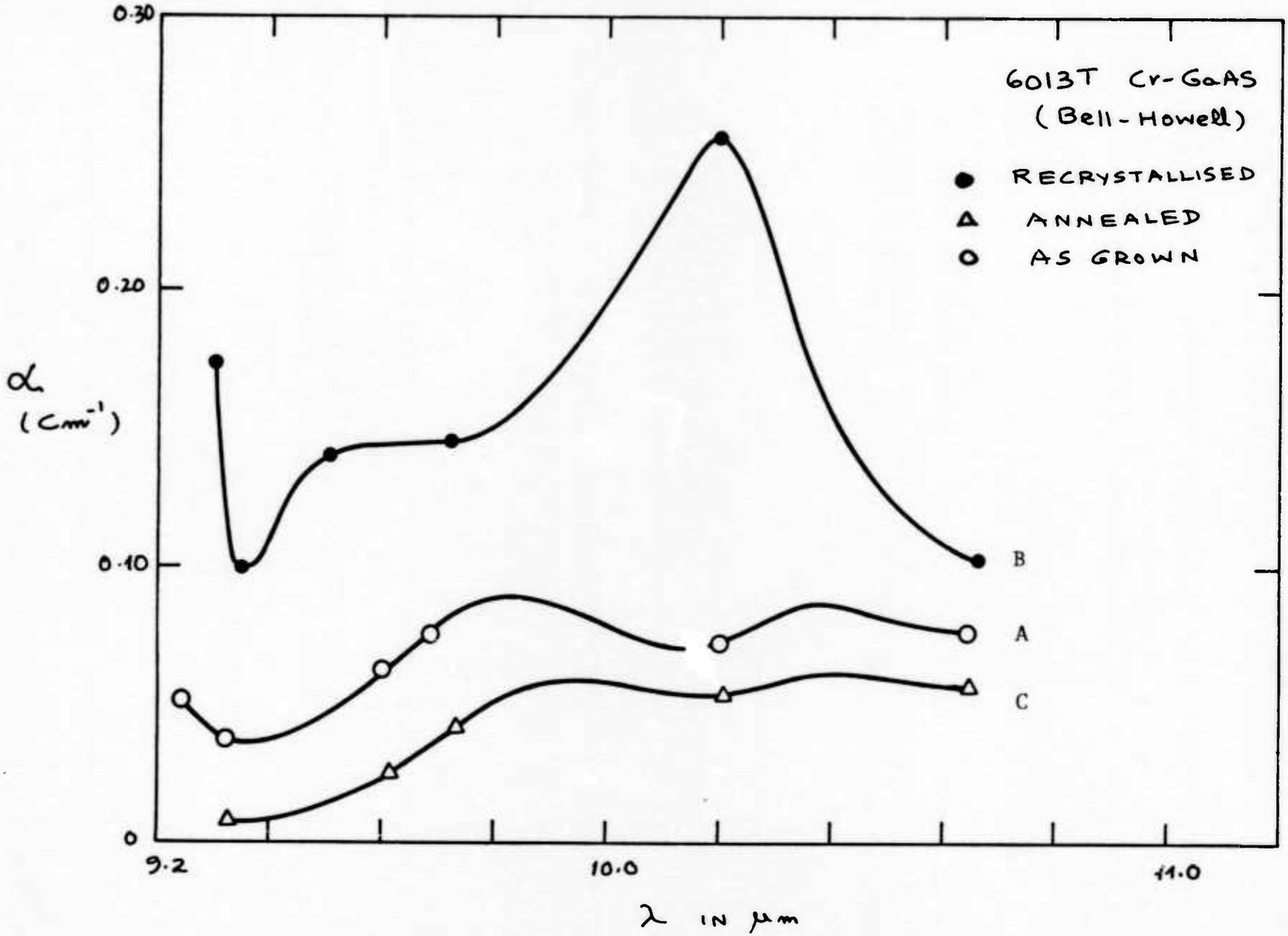


Figure 3: Absorption coefficient as a function of wave length for three different Cr-doped GaAs samples. See text for explanation.

of 0.104 cm^{-1} compared to the as grown and annealed samples which have absorption coefficients of 0.08 cm^{-1} and 0.062 cm^{-1} respectively. These results indicate that the 1100°C annealing treatment if employed separately lowers the absorption. But the same thermal treatment if employed as a process annealing treatment after a cold working state is not effective in reducing the absorption coefficient. This may be due to the fact that during recrystallization the cold working treatment in itself might have increased the absorption coefficient by many orders of magnitude and therefore the thermal treatment when employed after cold working is not effective in reducing the absorption. It should also be pointed out that dislocations which have not taken part in recrystallization and therefore are remaining within the grain may act as scattering centers and increase the absorption coefficient.

Anomalous Streaks: A copy of the paper titled "Anomalous Diffraction Effects in GaAs Single Crystals", by G. H. Narayanan and S. M. Copley was sent to Dr. J. B. VanderSande at M.I.T. on January 22, 1974, thereby informing him of our disagreement with the Haggerty and Peters work. Nevertheless, a paper based on this work by J. B. VanderSande and E. T. Peters was published in the April 1974 issue of the Journal of Applied Physics which proposed that the streaks in diffraction patterns from GaAs were due to precipitates and which made no mention of disagreement with the Narayanan and Copley work. Thus we submitted a note titled "Comment on the Evidence of a Precipitate-Like Zone in As-Grown GaAs and its Influence on Optical Absorptivity", by V. Swaminathan, G. H. Narayanan and S. M. Copley to the Journal of Applied Physics on August 19, 1974. A copy of this note is included at the end of this report. A short paper titled "Diffuse Streaks in Electron Diffraction Patterns from CdTe Single Crystals", by V. Swaminathan and G. H. Narayanan has also been submitted to the Journal of Applied Physics. This paper shows that similar diffuse streaks occur in diffraction patterns from CdTe crystals with extremely low optical absorptivity and that the intensity of these streaks decreases markedly with decreasing temperature, thereby, confirming that they are of thermal origin. A copy of this paper is also included in Appendix A.

Microstructural Characterization of CdTe:

The results of the microstructural characterization of CdTe single crystals annealed at different temperatures were reported in Quarterly Technical Report #8. It was concluded that cadmium interstitials were

the dominant native defects at 700°C and 800°C and that upon cooling after annealing at 900°C cadmium precipitated as a separate phase.

Mechanical Measurements:

The objective of this investigation, in the beginning, was to study the effect of annealing treatments on the mechanical behavior of CdTe. Due to the fact that all the annealing experiments were carried out on thin samples to facilitate quenching and that big single crystals were not available, only hardness measurements were attempted. Although the microhardness of a semiconductor is not directly related to its yield stress it serves as a measure of the resistance to deformation. Samples were annealed at different temperatures and for each temperature at different partial pressures of cadmium (P_{Cd}). Following the annealing,the samples were quenched to room temperature and their carrier concentrations were measured. (Qtr. # 8, Section by Kroger & Selim). The samples were mechanically ground and then were polished chemically in HNO_3-H_2O-$K_2Cr_2O_7$ (20cc - 30cc-12gms). The orientation of all samples was approximately [110]. Hardness was measured in the Leitz microhardness tester under a load of 50 gms. From the length of the diagonal of the indentation, hardness was obtained from standard tables. Fig. 4 shows the hardness vs P_{Cd} for In-doped CdTe crystal for three different temperatures. It can be seen that the hardness value increases with partial pressure of Cd at all temperatures. It should be noted that the carrier concentration also increases with P_{Cd} (see section by Kroger and Selim). This suggests that dislocation motion is governed by the position of the Fermi level with respect to the dislocation level in the forbidden energy gap.

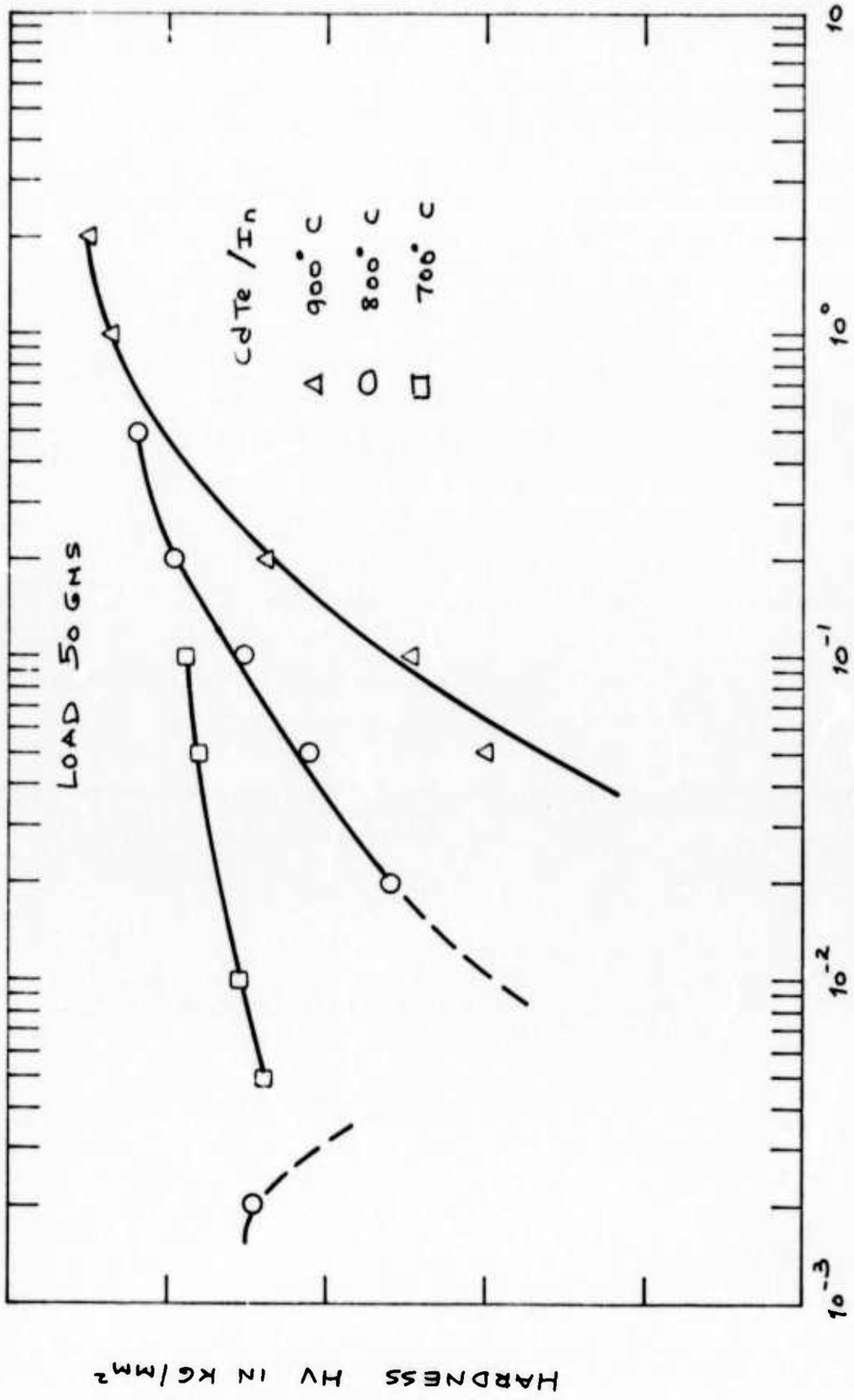


Figure 4: Microhardness vs partial pressure of cadmium for In-doped CdTe single crystals annealed at 700°C, 800°C and 900°C.

d.1 Dielectric Constant Measurements

C. R. Crowell and S. Joshi

During the contract period, accurate measurements of the dielectric constants of GaAs, CdTe and ZnSe as function of temperature were carried out. The results are summarized in a paper by Strzalkowski, Joshi and Crowell, to be published in Applied Physics Letters. The manuscript of this paper is attached. In addition to the dielectric constant measurements, the group made high impedance Hall effect measurements that determined carrier concentrations and mobilities in the high ρ materials used in absorption studies by Dr. Steier et al. Attempts to study correlation between surface losses and electrical measurements of interface charge states were unsuccessful due to lack of time and personnel.

Values of the dielectic constants of GaAs, CdTe and ZnSe found were $\varepsilon = 13.08$ for GaS; $\varepsilon = 11.00$ for CdTe; $\varepsilon = 9.25$ for ZnSe. All values were determined at 290°K.

For a detailed description of the experimental procedure see the manuscript of the publication (#15) attached at the end of this report.

d.2 Study of Defects in II-VI Compounds

F. A. Kroger, S. S. Chern, H. R. Vydyanath and F. A. Selim

A combined study of the high-temperature Hall effect of pure and donor-doped CdTe crystals in equilibrium with atmospheres of well defined cadmium pressure, and of Cd and Te tracer self diffusion as a function of cadmium pressure and temperature was carried out. The former gives information about the concentrations of electrons, the latter gives information about the concentrations of atomic point defects. Analysis of these data, combined with results on cooled crystals by de Nobel led to a complete defect model and the thermodynamic parameters of defect formation. Five papers were written, two of which have so far been accepted for publication by the Journal of Solid State Chemistry and one by Physica Status Solidi. In order to remove possible errors resulting from the use of data obtained by different workers, we have started work on the comparison of high-temperature properties of the same crystal after cooling. Properties measured after cooling included the carrier density (from the Hall effect), and the absorption at 10.6 μm (measured by calorimetry). In addition Copley and Swaminathan studied the occurrence and nature of precipitates in the cooled crystals. Results on two batches of crystals purchased from the II-VI Company, one doped with 5×10^{16} Cl, the other with 10^{17} In cm^{-3} and one batch of crystals with 10^{18} In cm^{-3} grown by B. V. Dutt show that:

(a) absorption at 10.6 μm is largely due to free carriers. Absorption cross sections for electrons and holes are respectively:

$$\beta_e = (1.4 \pm 0.1)\ 10^{-16} cm^2$$

and

$$\beta_h = (1.98 \pm 0.21)\ 10^{-16} cm^2$$

(b) in rapidly quenched thin crystals ($d \approx 1mm$) low absorption coefficients can be obtained by annealing of donor-doped crystals under appropriate conditions. Best results so far yield $\alpha_{10.6} = 9 \times 10^{-4} cm^{-1}$ after annealing at 700°C at $P_{Cd} = 5 \times 10^{-3}$ atm.

(c) crystals of ≈1cm thickness cannot be quenched as fast. For annealing at 700°C, $P_{Cd} = 5 \times 20^{-3}$ atm, these show higher absorption mainly due to free carriers remaining in the material as a result of the precipitation of electron traps (V'_{Cd}). However, annealing at lower does not give much better results (Fig. 1).

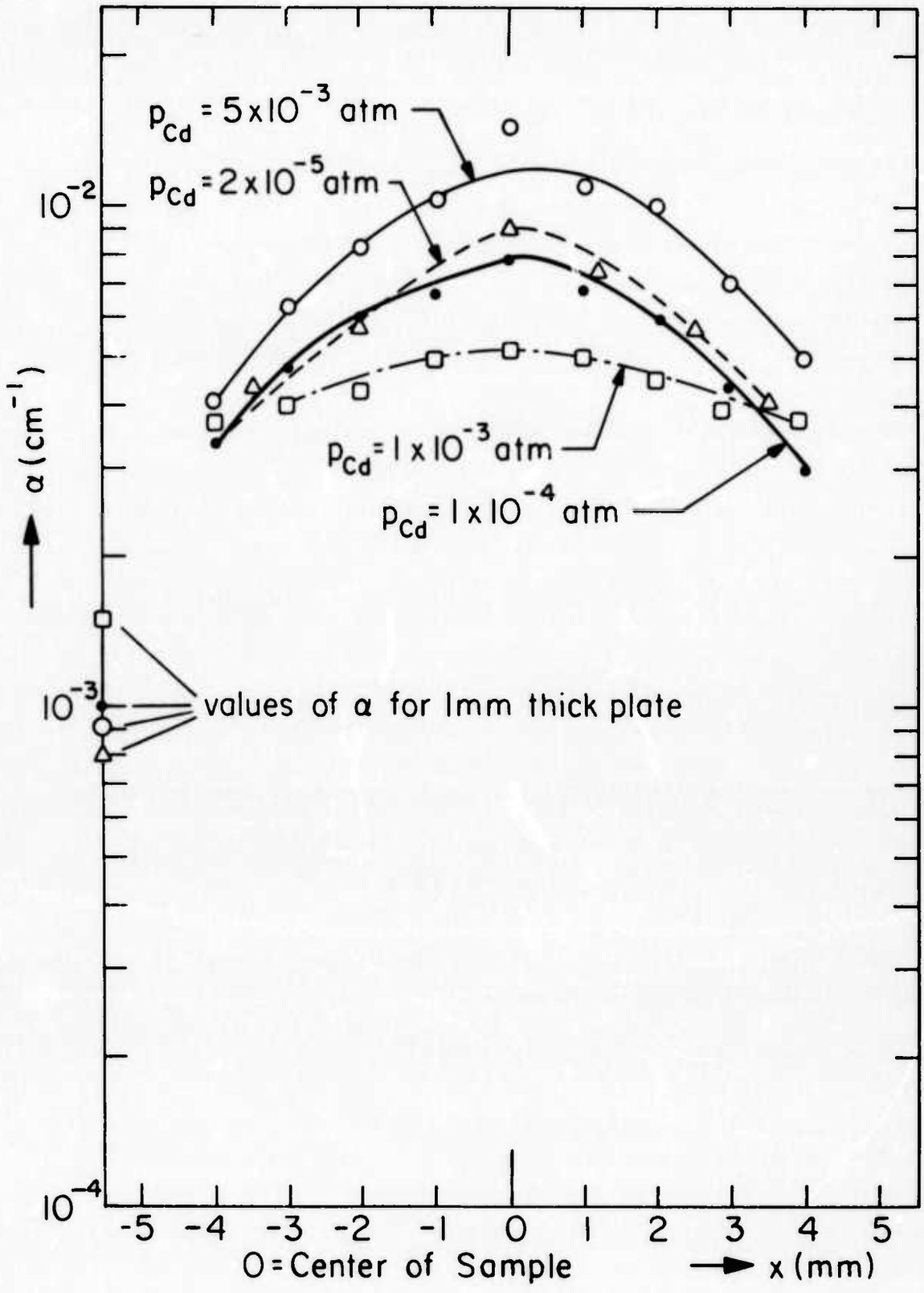


Fig. 1 The absorption coefficient α at 10.6 μm along a line through the center connecting the center of opposite faces for a cube of CeTe + 10^{17} In cm^{-3} quenched after 95 hour anneal at 700°C and different p_{Cd}.

(d) Excess cadmium present as a result of annealing CdTe at high P_{Cd} at 700-1000°C, precipitates upon cooling. Investigation of Swaminathan on crystals with a small concentration of excess Cd shows dislocation loops of the type formed by agglomeration of interstitial cadmium. This indicates that excess Cd is present mainly as interstitials rather than as tellurium vacancies. At larger excess concentrations metallic precipitates are found.

(e) Quenching of indium doped crystals, after annealing at high P_{Cd} by decreasing the temperature of the crystal before reducing the temperature of the Cd reservoir, leads to crystals with concentrations of free electrons 5-10 times smaller than the dopant concentration. This effect must be due to precipitation of the donor in one form or another. The result is unexpected in that:

(1) the final electron concentration is a function of the amount of indium present (which is unusual for a solubility limit).

(2) The result is different from that reported by de Nobel, who found electron concentrations equal to the amount of indium.

Preliminary results indicate that the difference arises from a different way of cooling: cooling in such a way that the Cd-pressure is reduced before the crystal is quenched leads to crystals in which the final electron concentration is equal to the total indium concentration (as found by de Nobel). No indium is precipitated. Cooling the crystal without reducing the cadmium pressure leads to precipitation of In and reduction of the electron concentration. This suggests that indium precipitates only if Cd precipitates forming a Cd-In alloy. If the Cd excess is removed, no Cd-precipitate is formed and no Cd-In alloy is formed. The Cd precipitate, probably molten at the time during quenching when the indium content is reduced, acts as a sink for the indium, partially extracting the indium from the solid solution in the crystal. This also explains why, if extraction occurs, the final electron concentration (and thus the final concentration of un-precipitated In) is a function of the total amount of indium present in the crystal. For a large indium content, the Cd-In alloy formed is In-rich and therefore the concentration of In remaining in the crystal in equilibrium with the alloy is also larger than at lower total indium concentrations. The situation is similar to that reported for CdS-Ag, when at higher P_{Cd} silver precipitates as a Cd-Ag alloy, the amount of Ag in the crystal increasing with the amount of

Ag in the alloy. We do not expect the effect in CdTe-In to be of importance for the fabrication of crystals with low free carrier absorption: these are annealed at lower P_{Cd} where the concentration of interstitial Cd is reduced to the extent that no Cd-precipitation is to be expected. There is in fact some V_{Cd} (≡ excess Te) precipitation (see c).

(f) CdTe + 2 x 10^{18}Ge cm^{-3}, quenched after annealing at 700°C at various P_{Cd} shows an absorption at 10.6 μm of α 2 to 4 x $10^{-2}cm^{-1}$, independent of cadmium pressure. The material has a resistivity of 7 x $10^{5}\Omega$ cm. The absorption is probably due to precipitates observed in an infrared microscope. We are checking this by making a crystal with less Ge. High resistivities for Ge doped CdTe were previously reported by V. V. Matlak, E. S. Nikonyuk, A. V. Savitskii and K. D. Tolstyuk, Sov. Phys. Semicond. 6 (1973) 1760.

e.1 Theoretical Studies of Absorption Mechanisms in IR Window Materials

R. W. Hellwarth and M. Mangir

In order to assess the potential performance of various candidate materials for high-power laser windows, we made calculations of the lower limit placed on the infrared and optical absorption coefficient at "window" wavelengths by various fundamental absorption mechanisms. At frequencies below the electronic band edge, the universal exponential dropoff in absorption (Urbach tail) seems to be fairly well understood. However, at frequencies between 2 and 50 times the fundamental lattice absorption frequency (the lattice absorption tail) the limiting absorption was not understood. It is in this lattice absorption tail where high power operation is currently of most interest and where the measured absorption in candidate materials is generally unacceptably high.

In a perfectly insulating lattice with no vacancies, interstitial ions, or impurities, two mechanisms give rise to the lattice absorption tail: (a) the small anharmonicity in inter-nuclear forces permits the decay of a virtual phonon, created by a photon, into several (n) phonons whose energy adds to that of the absorbed photon; and (b) the (slightly) nonlinear dependence of the electric dipole moment on the lattice coordinates permits the direct decay of a photon into several phonons. Of course vacancies and interstitials always exist at finite temperatures, but our present feeling is that their main effect on the lattice absorption tail appears via altered anharmonicity and nonlinearity parameters in the "anharmonic lattice" and "anharmonic moment" mechanisms of (a) and (b) above. Therefore we have concentrated our efforts in calculating the absorption from these latter mechanisms for various models.[1] Our major achievements in this were:

A. We achieved the first exact calculation of the multiphonon absorption coefficient $\beta(\omega)cm^{-1}$ for any of the widely used, but approximate, independent-molecule models of diatomic lattices. This was a quantum-mechanical calcula-

tion performed for a) Born-Mayer potential and b) Morse potential for frequencies up to 6 to 8 times the transverse optical mode frequency ω_{TO}.[1] Results of both were similar and agreed well with experimental β for alkali halides, employing adjustable effective-charge and anharmonicity parameters.

B. We achieved first exact calculation of $\beta(\omega)$ for Morse potential with quadratic nonlinear moment function.[1] Re-adjusting the previously used parameters, we could still obtain a good fit to experimental β over the range of physically possible nonlinear moments. The arbitrariness of the models became evident and led to the following two projects.

C. We made first checks on the accuracy of models used to calculate multi-phonon absorption, using exact but calculable expressions derived for various frequency moments of $\beta(\omega)$.[2] Marked failures in standard theories were found, although their qualitative correctness was verified.

D. We developed two experimental methods to measure the relative contribution to multiphonon absorption of the two mechanisms: a) anharmonic forces, and b) nonlinear dipole moment. We applied the first method, requiring measurement of $\varepsilon_2(\omega)$ (the imaginary part of the dielectric function), to data on LiF, finding mechanism (a) dominates, while determining magnitude and sign of coefficient for (b).[3] We are presently applying a second method, requiring measurement of IR dispersion in refractive index, to determine the multi-phonon absorption mechanism in ZnSe.

An expanded summary of these results follows:

A. Multiphonon Absorption from Anharmonic Forces

We have calculated the frequency and temperature dependence of the absorption coefficient β for simple lattice models derived from approximations that appear not inappropriate to ionic insulators. The n-phonon matrix elements appearing in the absorption formulae for these simple models are equivalent to those for a lattice of non-interacting diatomic molecules each

bound by an effective, slightly anharmonic, potential v(r).

1) Using the Born-Mayer potential for v(r) we found that the form of $\beta(\omega)$ in the n-phonon region is well-approximated by the exponential fall-off that has been established experimentally for alkali halides by Deutsch:[4]

$$\beta(\omega) \cong A \exp(-\gamma\omega/\omega_o), \tag{1}$$

where ω_o is the transverse optical frequency. We calculated that the parameters are given by

$$A = \frac{2\pi^2 e^{*2} N_o}{\mu c n \lambda^2 g^2} \tag{2}$$

and

$$\gamma = [\ell n\, \lambda^2 g^2 (\bar{n}+1)] . \tag{3}$$

Here e^* is the effective charge per ion, N_o is the number of molecules per unit volume, μ is the reduced mass of the molecule, c the speed of light, n index of refraction, $\bar{n} \equiv (e^{h\omega_o/kT}-1)^{-1}$ λ is the anharmonicity parameter in the Born-Mayer potential, and g is a measure of the effect of dispersion and matrix element variations. Using reasonable values of λ and e^* derived from bulk modulus and dielectric constant data we obtained good fit to experimental $\beta(\omega)$ as shown in the figures of reference 1.

2) The temperature dependence of $\beta(\omega)$ is given qualitatively by (1) when the temperature dependence of the parameters is also taken into account, as well as the explicit dependence of $\bar{n}$ on T.

3) Recalculating β, using a Morse potential instead of the Born-Mayer potential, we found essentially the same form as (1).

B. Effects of Nonlinear Moment on Multiphonon Absorption

In (A) above we assumed the electric moment per ion M, to be e^*r, where r is the ionic displacement from equilibrium. However, it is possible that terms in M that are higher order in r may cause significant multiphonon absorption. Therefore we recalculated $\beta(\omega)$, but with a nonlinear moment $M=e^*(r+\frac{1}{2}fr^2)$ coupling the field to ions bound by a Morse potential, for several values of the nonlinear moment parameter f.

As described in Section D and ref. 3, we know that $f=0.9\pm0.3\text{Å}^{-1}$ for LiF. Using values of f in this range we could still obtain a good fit to experimental $\beta(\omega)$ with a new set of e^* and λ. Also the predicted temperature dependence is not altered appreciably. These calculations showed that the terms of β arising from $\frac{1}{2}fe^*r^2$ tend to cancel these from e^*r, and for the above range of f values, the quadratic terms in r dominates the linear term at frequencies above the cross-over frequency that is around $3\omega_o$. However, at this point it became clear that this sort of modelling could not give a clue as to the actual mechanism of the observed multiphonon absorption in window materials.

C. Checks of Multiphonon Absorption Theory.

The nature of the approximations used in the above, and other, calculations of $\beta(\omega)$ left considerable uncertainty as to the accuracy of these calculations. Therefore we developed exact "sum rules" that enabled us to calculate exactly various moments defined as $S^{(n)} \equiv \int_o^\infty d\omega \omega^n \chi''(\omega)$, of the imaginary part $\chi''(\omega)$ of the electrical susceptibility (to which $\beta(\omega)$ is related). For example evaluating the contribution of the 2-phonon absorption to the fifth moment $S_{2ph}^{(5)}$ we obtained for a diatomic cubic lattice having nearest-neighbor forces

$$S_{2ph}^{(5)} = \frac{2c_3^2 e^2 \hbar I(\gamma)}{\mu^4 a^3 \omega_o} \tag{4}$$

where a is the lattice parameter, c_3 is the coefficient of third order term in the anharmonic potential, and

$$I(\gamma) \equiv \int_o^1 duu(1-u^2)^{\frac{1}{2}} \coth \gamma u. \tag{5}$$

The temperature parameter γ is

$$\gamma \equiv \frac{\hbar\omega_o}{2kT}. \tag{6}$$

At high temperatures

$$I(\gamma) \to \frac{\pi}{4\gamma}, \quad \gamma \to 0, \tag{7}$$

and at low temperatures $I(\gamma) \to \frac{1}{3}, \quad \gamma \to \infty$. (8)

For fixed ω_o, c_3, e, and a, the independent-anharmonic-molecule models predicted for this or any other type of lattice, a

2-phonon temperature factor $2\bar{n}+1$, where $\bar{n}$ is the Planck function $(e^{2\gamma}-1)^{-1}$. These approximate theories predict for example

$$\frac{S_{2ph}^{(5)}(T=0)}{S_{2ph}^{(5)}(T\to\infty)} = \gamma \qquad (9)$$

rather than the exact result for this lattice model of $4\gamma/3\pi$. At least part of this error is due to the neglect of the difference bands in independent-molecule models. The numerical comparison of $I(\gamma)$ with $2\bar{n}+1$ in ref. 2 shows that this inaccuracy is most evident at low temperature. Further examination of these points is to be found in ref. 2.

D. Methods for Determining the Mechanism of Multiphonon Absorption

The parameters governing multiphonon absorption in IR window materials, especially in zincblende structure crystals, such as ZnSe, GaAs and CdTe, are unknown. This limiting multiphonon absorption can be due to either (a) anharmonic interatomic forces, or (b) to a "nonlinear Moment", i.e., a nonlinear dependence of the electric dipole moment $M_i(i=x,y,z)$ in any small volume V, about a position $\vec{r}$ in the crystal, on displacements $r_{i\alpha}(i=x,y,z)$ of the N ions (labeled by α) in V. We have proved that, irregardless of the nature of the anharmonic forces, the first frequency moment of the imaginary part $\varepsilon_2(\omega)$ of the dielectric constant of the crystal is given by[3]

$$\int_0^\infty \omega\varepsilon_2(\omega)\,d\omega = \frac{2\pi^2}{V}\Sigma_{\alpha,i}\left\langle\left(\frac{\partial M_x}{\partial r_{i\alpha}}\right)^2\right\rangle/m_\alpha \qquad (10)$$

where m_α is the mass of the ion α.

1) When the nonlinear moment can be neglected, the sum in (10) reduces in the case of a diatomic cubic crystal to $\frac{1}{2}Ne^2/\mu$, where e is the "Born" effective of an ion and μ is the reduced mass of a molecule, both parameters being invariant to temperature change. When the nonlinear moment can't be neglected, the form of M_x must be modelled and an average of an expression quadratic in ionic displacements must be performed in the harmonic lattice approximation. When the calculated value of the right hand side is compared with the

experimental measurement of the left hand side at two temperatures, both the effective charge e and a nonlinear moment coefficient f are determined uniquely.

2) We applied this method to LiF using reported values of $\varepsilon_2(\omega)$ obtained from reflection and transmission measurements at several temperatures.[3] The data was accurate enough to conclude that LiF has the positive quadratic moment given in (B) above, and that anharmonic forces give a larger contribution to the integral of $\omega\varepsilon_2(\omega)$ than does the nonlinear moment. We established the meaningful nature of our definition of the parameter f by comparing its value both in an approximate and a nearly exact nonlinear moment model. The reader is referred to ref. 3 for details.

3) Because measurements of $\varepsilon_2(\omega)$ which are accurate enough for the foregoing analysis are difficult to obtain, we have developed the following new method of measuring the desired integral in (10). This method employs refractive index measurements, which are inherently more accurate than absorption and transmission measurements.

It is well known that causality leads to the relation for the real part ε_1 of the dielectric constant in terms of the imaginary part ε_2:

$$\varepsilon_1(\omega) = \varepsilon_{e\ell}(\omega) - \frac{2}{\pi}\int_0^\infty \frac{\nu d\nu \varepsilon_2(\nu)}{\omega^2 - \nu^2} \tag{11}$$

at frequencies ω below the electronic band gap, where the electronic contribution $\varepsilon_{e\ell}$ is real. For ω in the range 3 to 10 times the reststrahl frequency, the expansion

$$\varepsilon_1 \tilde{=} \varepsilon_\infty + A\omega^2 - B\omega^{-2} + C\omega^{-4} \tag{12}$$

is accurate to at least a part in 10^4. Comparing (3) with (2) shows immediately that B equals the integral needed in (1) $(x2/\pi)$. Therefore by measuring the refractive index in the above frequency range for ZnSe at two temperatures we can determine the change in the dispersion coefficient B, and thereby the size of the nonlinear moment through (1).

4) To prepare for using the new method above to determine the mechanism for multiphonon absorption in ZnSe, we have made numerical calculations to determine the frequency range and accuracy needed in measuring index of refraction $n(\omega)$ to be able to obtain dispersion coefficient B to within the 1% accuracy desired. Presently, we are preparing the experimental apparatus to perform the refractive index measurements in polycrystalline ZnSe window material.

References

1. T. C. McGill, R. W. Hellwarth, M. Mangir and H. V. Winston "Infrared Absorption in Ionic Insulators due to Multiphonon Processes," J. Phys. Chem. Solids 34, 2105 (1973).

2. R. W. Hellwarth,"Checks of Multiphonon Absorption Theory", Proceedings of 1973 Symposium on Damage in Laser Materials, Boulder, Colorado, May 15,16, 1973 (N.B.S. Special Publications).

3. R. Hellwarth and M. Mangir, Proceedings of the Third Conference on High Power Infrared Laser Window Materials, Vol. I, ed. by C. A. Pitha and B. Bendow (Air Force Cambridge Research Lab. Special Report No. 174, February 1974, p. 16); "A Method for Measuring The Contribution of the Nonlinear Dipole Moment to Multiphonon Absorption", Physical Review B10, 1635, (1974).

4. T. F. Deutsch, "Absorption Coefficient of Infrared Laser Window Materials", J. Phys. Chem. Solids 34, 2091 (1973).

f.1 Investigation of Infrared Loss Mechanisms in High Resistivity GaAS

C. P. Christensen, R. Joiner, S.T.K. Nieh and W.H. Steier

The GaAs evaluation program has been completed, and the results of the investigation have been prepared for publication. The preprint of this publication is included at the end of this report.

f.2 Alkali Halide Studies with Acoustic Probe Techniques

J. H. Parks, D. A. Rockwell, T. S. Colbert

The principle effort of our research program has been to develop a new measurement process which utilizes acoustic surface waves to detect the surface depth dependence of radiative absorption. Further, a detailed theoretical analysis of this detection process was necessary to reliably relate these measurements to a quantitative model of surface absorption phenomena.

These new experimental techniques and the related theoretical analyses involved advances beyond the current state of acoustic surface wave technology. For this reason, considerable research was necessary to develop a detailed understanding of surface wave propagation in the presence of a nonuniform temperature distribution. Reliable and well studied acoustic materials were used for this purpose. During this effort, infrared window materials were involved primarily to demonstrate applicability of these techniques rather than as controlled samples for analysis. The principle accomplishment of this program has been the successful development of the surface wave measurement process and its associated theoretical description as reliable research tools. As a result, specific studies have recently been initiated to measure the depth dependence of surface radiative absorption on both polished and etched alkali halide surfaces.

This final report will briefly discuss the research accomplishments which have been presented in more detail in previous progress reports. In addition to describing the current state of the research, this report will outline the

immediate plans for further studies.

f.2.a Acoustic Surface Wave Detection of Radiative Absorption

A fundamental understanding of the physics involved in the surface wave detection process was obtained in quantitative studies on α quartz. This research has been described in a technical paper submitted to Applied Physics Letters which is appended to this report. It was found that surface wave propagation in a region heated by radiative absorption could be completely described by an induced phase change. The phase change arises from a change in propagation path length via thermoelastic strains and also a change in wave velocity through the temperature variation of the elastic coefficients. Both these effects were calculated from first principles leaving no free parameters to characterize the propagation effects. The quantitative agreement between theory and experiment was within 15%. In these experiments emphasis was placed upon the ability to describe the surface wave-thermal interaction within a depth which was uniformly heated by radiative absorption. Radiative pulse widths were much greater than times characterizing thermal diffusion within the depth of the acoustic wave energy. In this way, the need to account for propagation in the presence of an axial temperature gradient was avoided and the resulting analysis provided a clear picture of the fundamental processes contributing to the induced phase changes.

The feasability of detecting absorption in thin films was also demonstrated but not greatly emphasized. The detection of $\sim$10μJ energy deposited in a highly absorbing layer $\sim$10μ thick has indicated the utility of this technique for thin

film absorption measurement. This sensitivity indicates that the detection process may be adequate for thin film measurements of protective and high reflectivity film materials being considered in the infrared window program.

Finally, the possibility of using the induced phase change as a detector of fast infrared pulses was considered by observing the response to a 10 nsec radiative pulse. The detector risetime was limited by the surface wave traversal time across the acoustic transducer and was measured to be ∿100 nsec. This transducer limited risetime can be reduced by a factor of 20-30. In this case wave traversal of the radiative spot size will limit detector response which may approach $\lesssim$10 nsec.

f.2.b Surface Wave Propagation on Nonpiezoelectric Surfaces

The general application of the surface wave detection process requires the ability to propagate waves on the surface of arbitrary materials. In particular, it is necessary to propagate waves on nonpiezoelectrics in order to study many window materials presently under consideration. In addition, wave propagation must be generated by a technique which does not affect the surface properties under analysis. This latter condition eliminates the deposition of piezoelectric films and acoustic transducers directly on the sample surface which is a standard technique in current surface wave technology. An alternative technique relies on the excitation of a wave on a piezoleectric material and the subsequent coupling of this wave through a fluid layer to the nonpiezoelectric surface. Although this method has received relatively little development, it is of a particular advantage for our purpose.

Our research program has included an experimental study of fluid coupling techniques which has resulted in successfully coupling surface waves to KCl surfaces. Initial comparison of induced phase changes of α quartz using both direct transduction and fluid coupled waves indicate agreement within 10-20%. Several fluids have been found to be applicable of which ethylene glycol and xylene produce the smallest phase drift due to evaporation. An experimental transducer configuration has been designed which accepts arbitrary sample sizes and provides ample access to the sample surface for the infrared laser source. Analysis of the fluid coupling process has been extended to materials of interest to our program. The multi-mode behavior of fluid layer wave propagation has been considered as well as the efficiency of acoustic energy transfer to KCl surfaces. A technical paper is presently being prepared for publication which describes these research applications of fluid coupled wave propagation.

f.2.c Detection of Radiative Absorption on KCl Surfaces

Surface wave phase variations induced by the absorption of 10.6μ radiation have been measured on KCl surfaces. The surface absorption σ of these samples was also measured by calorimetry to be $\sigma \sim 2 \times 10^{-3}$. The fluid coupled surface waves produced stable, reproducible phase variations of ∿20 millirad per joule of incident radiation for a 1 sec pulse width. These phase change signals had a signal to noise ratio of ∿5 and the dominant noise source results from local fluid instabilities in the coupling process.

These results are significant since they indicate the phase change signal level which can be expected for shorter pulses. As the pulse width decreases, the effect of heat diffusion is reduced, resulting in a higher surface temperature and consequently a larger induced phase change. For example, a radiative pulse of 100 msec and 200 mjoules energy has been observed to induce a 10 mrad phase change. The importance of these results becomes more evident if we consider that approximately 50 mjoules incident energy will be necessary to generate a comparable phase change for a 1 msec pulse. For these short pulsewidths, calculations indicate the temperature gradient induced by surface absorption will be detectable with acoustic surface wave techniques. Thus the ability to detect alkali halide surface processes appears to be quite feasible with laser peak powers of $\sim$50 watts. A crude data reduction of KCl data obtained places a lower limit on a surface absorption coefficient of $\sim 10^{-2} cm^{-1}$.

f.2.d Depth Variation of Surface Absorptive Properties

A surface wave travelling in a spatially non-uniform medium experiences dispersion if the spatial inhomogeneity is comparable to the acoustic wavelength. Since the surface wave essentially samples a depth the order of an acoustic wavelength, dispersive propagation will result in the presence of a temperature variation within this depth. For this reason, an analysis of the dispersive character of the propagation yields information of the temperature variation. In turn this temperature distribution depends on the model used to represent surface absorption properties. Thus, in principle,

a model relying on parameters such as a surface absorption coefficient β_s defined over some characteristic depth d and a bulk absorption coefficient β_B will relate the surface wave dispersion to these material properties. The extension of surface wave probe techniques to measure dispersion and thereby the depth variation of material properties required experimental evidence of these predicted effects and a dispersion theory to calculate the induced phase change.

The measurement of dispersive propagation on α quartz induced by radiative absorption and detected via phase change techniques represents the first time a surface temperature gradient has been observed. For a 10 msec infrared pulse, the resulting temperature distribution falls to half the surface value in ∿135μ. For this radiative pulse, the phase change signal at an acoustic wavelength of 102μ is measured to be ∿40% lower than the signal for a wavelength of 25μ. Note that this induced phase change is not the result of a dominant surface absorption coefficient. However, such an effect is simulated experimentally by the large temperature gradient resulting from the bulk absorption coefficient of α quartz ($\beta \simeq 240 cm^{-1}$). The sensitivity of the dispersion is surprising considering the effect of heat diffusion which tends to greatly reduce axial temperature gradients over the timescale of a 10msec pulse in α quartz.

A theory has been developed to calculate the velocity variation of the surface wave in the presence of a temperature gradient. The calculation is based on a perturbative solution

of the wave equation for the case in which the elastic coefficients exhibit spatial variation through their temperature dependence. We have solved this problem for the case of propagation in an isotropic material and are presently extending the theory to describe anisotropic materials, in particular those with cubic symmetry. The utility of a perturbative treatment is the advantage gained by representing temperature analytically. This allows a precise model of surface absorption to be easily incorporated into the analysis and thus related to the dispersion and subsequent phase change.

f.2.e Research Plans for Alkali Halide Surface Studies

The current research and immediate plans for studies of the depth dependence of radiative absorption on alkali halide surfaces include the following:

(a) continuation of theoretical calculations relating material absorptive properties to dispersive phase change measurements,

(b) application of four different frequency transducer sets presently on hand to verify that dispersion effects offer adequate sensitivity to indicate the presence of a highly absorbing surface layer on KCl, and an analysis of this dispersion to reduce the surface coefficient β_s and the characteristic depth of variation d for polished and etched samples,

(c) fabrication of multiple frequency transducer configurations using higher frequency harmonics to increase the number of discrete data points and thus increase the accuracy by which the dispersion can be calculated.

f.3 Absorption Studies of CdTe and ZnSe

B. V. Dutt and W. G. Spitzer

It has been emphasized in the previous progress reports, that the long range goals of this investigation are to identify the absorption mechanisms and the spectral range in which they influence the optical properties. Native defect centers, impurities, complexes and precipitates can affect the absorption. The character and concentration of native or impurity centers, or the presence of precipitates is dependent on the conditions of growth or post growth annealing treatments. This program includes the following principal measurements:

(a) Conventional infrared measurements by using an infrared spectrometer covering the range $5000 < \nu < 250\ cm^{-1}$.

(b) Laser calorimetry near 10.6 μm in cases where the transmission measurements in (a) are near theoretical maximum, as given by $T_{max} = \frac{1-R}{1+R}$, where $R = \frac{(n-1)^2}{(n+1)^2}$ and n = refractive index.

(c) Simple electrical transport measurements to supplement the optical data in determining absorption corss sections of free carriers.

The primary emphasis is on the observation and measurement of impurity-induced localized vibrational mode absorption and any other absorption related to the defects that may occur in the 10 μm range, e.g. from the higher order harmonics of the fundamental local mode frequencies. Therefore, the measurements are generally on material that is intentionally doped with fairly high concentration of different impurities.

Work in this part of the program was started in December 1973. Progress reports No's. 7 and 8 summarized our early literature survey and some infrared measurements on CdTe and ZnSe. In this final report the results of our absorption measurements on CdTe and ZnSe and the crystal growth of CdTe with several different impurities are summarized. Some of the earlier experimental results are highlighted to avoid repeated references to the previous reports.

Sources of Material: The materials used in our earlier experiments were obtained from the following sources:

(a) Hughes Research Laboratories: undoped CdTe through the courtesy of Dr. G. Picus.

(b) II-VI Inc.: Boules of large grain polycrystalline CdTe-In, ($In=10^{17}/cc$) and CdTe-Cl, ($Cl=5x10^{16}/cc$). Two pieces of undoped polycrystalline

ZnSe were also purchased. The ZnSe was grown at Raytheon Corporation.

(c) Dr. Fahrig of Eagle Picher Labs, Miami, Oklahoma provided us with a sample of Al-doped ZnSe.

(d) Some CdTe and ZnSe (both undoped) were also obtained through the courtesy of Dr. D. C. Reynolds of Wright Patterson AFB, Ohio.

(e) At the present time we are using CdTe crystals grown with different dopants in our laboratory by the Horizontal Bridgman Technique.

A) CdTe:

(1) Our efforts were in the direction of impurity-related absorption by using conventional infrared spectrometric measurements to measure relatively strong absorption and laser calorimetry whenever the absorption in a material is relatively low.

The first experiments were started on CdTe with a view to study impurity-related effects with lithium as a dopant. We expected localized vibrational modes due to lithium present in the crystal as possible substitutional, interstitial or complex centers. From electrical transport measurements on lithium diffused samples, Desnica and Urli[1], reported on amphoteric behavior of this impurity, while from IR absorption measurements Balkanski, et. al.[2], reported a broad absorption band centered at 275 cm^{-1}, with $\Delta\nu$ = 35 cm^{-1}. This is an abnormally large width for the band to be attributed to the localized mode due to substitutional lithium. In ref.(2) the samples were doped with lithium by the addition of Li_2CO_3 to the melt during crystal growth. We tried the introduction of lithium by diffusion from a surface alloyed layer. The resulting material in most of the experiments turned out to be mechanically unstable or brittle, as reported in ref. (1). On some of the larger samples, infrared measurement indicated a strong absorption band centered at 270 cm^{-1}, so that samples of 3 mil thickness are opaque in this region. This behavior is as yet unexplained.

To characterize lithium as an impurity in CdTe and to understand its influence on absorption, we plan to diffuse lithium into donor doped material, e.g. CdTe-In and CdTe-Al at 680°C under the corresponding saturation pressure of cadmium. It was suggested in ref (1) that these conditions of diffusion yielded better mechanical and electrical performance. Depending on these results we intend to pursue the CdTe-Li system with appropriate experiments.

(2) By using the horizontal Bridgman technique we have grown ingots separately doped with Al, P, Ge, In and Si. In each case dopants are added to the starting materials, which are elemental cadmium and tellurium, sealed in a graphite-coated quartz ampoule under a pressure of 1/3 atm of He gas. In the case of Si and Al-dopants, the ampoules were evacuated to 10^{-5} - 10^{-6} mm Hg. The crystal growth is carried out in a four-zone horizontal furnace which can be moved on rails relative to the stationary growth tube. The growth was initiated in the following way: the temperature of the furnace is raised to $\sim$500°C where elemental Cd and Te start to react. The vigor of the reaction depends on the degree of mixing of the Cd and Te in the ampoule. The reaction is exothermic and as soon as we observe the reaction to start the furnace power is reduced until the reaction rate slows down. The temperature then is raised again until the reaction starts and then lowered to avoid excessive heating of the ampoule. This is repeated until all the material has completely reacted. Then the temperature of the furnace is gradually raised to 1100°C to completely melt all the CdTe. Then the material is solidified in a gradiant by moving the furnace relative to the container. The average rate of growth is about 3 to 6 mms per hour. The product obtained is a large-grain polycrystalline ingot from which single crystals of sufficient size for electrical transport measurements could be recovered. Typical single crystal section dimensions were several millimeters.

In the case of Al-doped CdTe, we found that the crystal was sticking to the ampoule and also in this initial attempt there was a crack in the ampoule when it was removed from the furnace. In the Si-doped batch we found there was some white ash-like material on the crystal and the quality of the crystal was poorer in that it was
covered by a layer with a sponge-like apperance, and the grain size was somewhat smaller than with CdTe-Al, CdTe-P, CdTe-Ge, CdTe-In.

Of the above five ingots, the phosphorus and Ge-doped ingots have been analyzed by spectroscopic analysis which showed an average phosphorus content of 500 ppm and germanium content of 30 ppm, respectively, with some other residual impurities.

(3) Silicon-doped CdTe shows practically the same behavior as the CdTe-Cl (Cl of 5×10 16/cc) obtained from II-VI Inc. previously. We have

not observed any localized vibrations that can be related to silicon as an impurity in CdTe. This makes us suspect that the silicon may have been oxidized and did not enter the crystal as dopant in sufficiently high concentrations. Efforts are underway to grow a new Si-doped ingot.

(4) CdTe-Al: Samples from one region of the Al-doped CdTe ingot, which was broken while removing from the quartz to which it was sticking, are fairly well compensated in the as-grown condition. Room temperature transmission in the range 4000 $cm^{-1} < \nu < 400\ cm^{-1}$ is frequency independent and about 65% on a 6 mil thick sample. Thicker samples are in preparation for absorption measurements in this range and if we find the absorption is low, we intend to carry out laser calorimetry at 10.6 μm. We observed localized vibrations at $\nu = 287.5\ cm^{-1}$, $299.5\ cm^{-1}$ and $326.5\ cm^{-1}$, (see fig. 1). It appears that the band at $\nu = 287.5\ cm^{-1}$ is possibly a doublet, though in the only sample examined we are unable to see the two bands of the doublet well resolved. More samples from different regions of the present ingot will be examined shortly for this and also in the broad spectral range covering 10 μm. We also plan to perform liquid helium measurements if it proves impossible to resolve the band at $\nu = 287.5\ cm^{-1}$ at higher temperatures. If this is indeed a doublet, the interpretation of the bands is possible along the following lines: the as-grown material is well-compensated indicating that native or other foreign defects are present in concentrations comparable to $[Al_{Cd}^{\cdot}]$ and that electrons are a minority species. The compensating atomic defects could be foreign acceptors (unintentionally introduced), Cd-vacancies, Te-interstitials, aluminum on Te-sites, or complexes of $Al_{Cd}^{\cdot}$ with V_{Cd}'' or of $Al_{Cd}^{\cdot}$ with Te_i''. From symmetry considerations coupled with the compensations enumerated, at present we tentatively make the following assignments:

(a) The fundamental local mode frequency of isolated Al_{Cd} is $299.5\ cm^{-1}$ and

(b) the triple degeneracy of the (Al_{Cd}) local mode can be lifted into three separate bands in addition to the local mode by a complex having a C_{2v} symmetry, i.e. the pair or complex forms along a <110> or <100> direction. There are two possible complexes that can do this: $(Al_{Cd}^{\cdot} - V_{Cd}'')$ and $(Al_{Cd}^{\cdot} - Te_i'')$. The present information does not permit a choice between them at this time.

As can be seen from fig. 1 where differential transmission of CdTe-Al compared with an undoped CdTe is shown, there is some background absorption

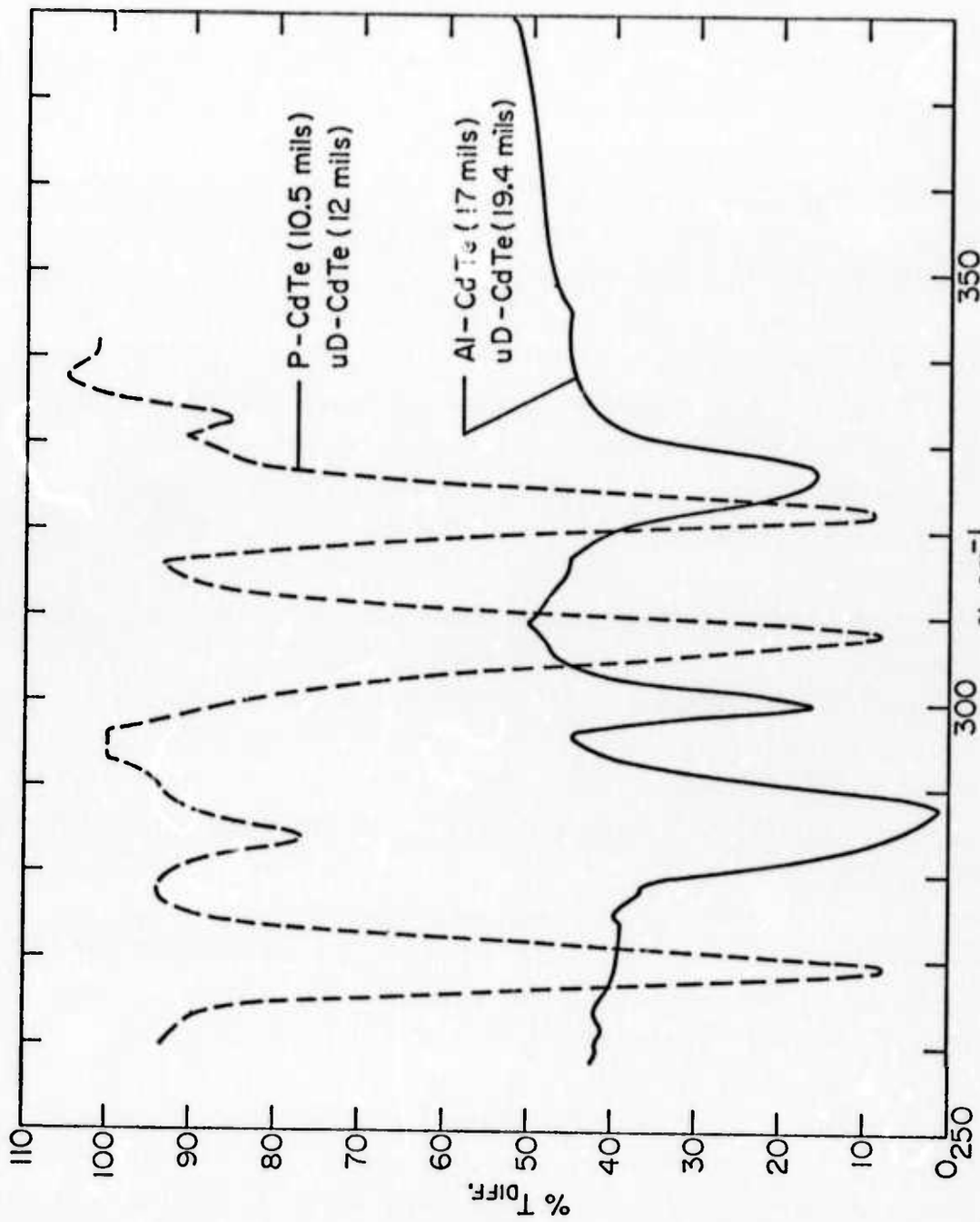


Fig. 1 Differential transmission of CdTe-Al and CdTe-P relative to undoped CdTe

in the range $400 < \nu < 250$ cm^{-1}. Whether it is absorption or scattering is not known. Also, as mentioned earlier, the ampoule containing CdTe-Al ingot was cracked when removed from the furnace and this might have led to partial oxidation of the ingot. It is not clear if this low differential transmission is related to the presence of oxide precipitates.

We plan to do the following in case of CdTe-Al:

4(a) Grow CdTe with different Al-concentrations and study two different aspects of the IR absorption.

(1) We want to determine if there is a dependence of the frequency independent absorption or scattering losses on Al Concentration. This will involve a number of 10.6 μm calorimetric measurements as well as standard transmission measurements in the 5000 cm^{-1} $< \nu <$ 500 cm^{-1} range.

(2) Examine the dependence of local mode intensity on Al Concentration.

4(b) Double doping of CdTe-Al with Cu by diffusion. Cu is expected to diffuse rapidly by an interstitial mechanism and is supposed to finally occupy the Cd-sites, thus acting as acceptor Cu'_{Cd} and compensate for $(Al^{\cdot}_{Cd})$. This will help identify the bands in CdTe-Al.

4(c) Depending on the availabilty of instrumentation we intend to carry out photoluminescence measurements on CdTe-Al, and CdTe-Al, Cu.

(5) CdTe-P: Some regions of the as-grown ingot are well-compensated as inferred from the observation of near theoretical maximum in transmission [$T_{max} = (1-R)/(1+R)$ and $R = (n-1)^2/(n+1)^2$ with $n = 2.67$, $T_{mas} = 66\%$] in a 72 milthick sample. In this case we observed the anticipated frequency independent transmission in the range $4000 < \nu < 400$ cm^{-1} since there are no measurable absorption losses, at least in a conventional transmission measurement. In addition we observed three strong local modes at ν = 269,308 and 322 cm^{-1} and two weaker modes at ν = 284 and 333 cm^{-1}. (See fig. 1). Phosphorus as an impurity in CdTe is expected to substitutionally occupy Te-site and therefore behave like an acceptor. V. Capek et. al.[6] reported infrared measurements on p-type CdTe doped with P, As and Sb, and in the case of CdTe-P, they estimated an acceptor ionization energy of $E_a = 0.07$ ev above the valence band. The samples examined by us, thus far, are well-compensated indicating that the hole concentration is small and there is the possibility of P'_{Te} association with other defects like $P^{\cdots}_{Cd}$, $Cd^{\cdot\cdot}_i$, $V^{\cdot\cdot}_{Te}$ and the like. However, with the present information, we cannot offer any explanation of the five bands seen.

We plan to carry out annealing studies on CdTe-Al and CdTe-P under Cd and Te rich conditions and study the nature of defect centers and their influence on local mode absorption as well as absorption in a broad spectral range covering 10 μm.

(6) CdTe-Ge: Room temperature absorption measurements on a sample of 48 mil thickness from the ingot grown here with ~30 ppm of Ge show only 50% transmission, which is frequency independent in the range 4000 cm^{-1} < ν < 400 cm^{-1}. Professor Kroger's group is initiating a detailed annealing study on this ingot and on CdTe-P.

B) ZnSe:

(1) Laser Calorimetry measurements gave an absorption coefficient of 4.1×10^{-4} cm^{-1} on the polycrystalline ZnSe material as obtained from II-VI Inc.

(2) As mentioned in our previous progress report (No. 8), Al-doped ZnSe obtained from Eagle Picher Co. was well-compensated. Localized vibrational bands due to aluminum are seen at ν = 339, 342, 346, 359, 388 and 393 cm^{-1} in these Eagle Picher materials. These bands were observed and reported by Mitsuishi et. al.[3] On diffusion of copper into this material under zinc-rich conditions, five out of the six bands, i.e. all except the 359 cm^{-1} band, disappear. In this double doped ZnSe-Al, Cu sample we observed the 359 cm^{-1} band and in addition three new bands at ν = 348.5, 351.5 and 377 cm^{-1}. This would seem to confirm the assignments of Mitsuishi, et. al. for the band at ν = 359 cm^{-1} in ZnSe-Al to unassociated Al_{Zn}. However, the origin of the other five bands in ZnSe-Al is not clear. From the luminescence work on this material, the presence of self-activated luminescence center or the so-called A-center, which is a (Al_{Zn} - V_{Zn}) complex, has been known for some time. (See ref. 4 and 5). The five bands we observe cannot be explained on the basis of only the Al_{Zn} - V_{Zn} complex, for the T_d-site symmetry of Al_{Zn} will be lowered to C_s if Al_{Zn} pairs with V_{Zn}. This lifts the triple degeneracy of the Al_{Zn} local mode and one expects three new bands besides the 359 cm^{-1} band. There is an observation that is worth pointing out. The five new bands are divided as a higher doublet 388, 393 cm^{-1} and a lower triplet 339, 342 and 346 cm^{-1}. The doublet and triplet are roughly separated by Δ = 390 - 340 $\simeq$50 cm^{-1}. The doublet is about 30 cm^{-1} (= 3/5 Δ) above and the triplet is 20 cm^{-1} (= 2/5 Δ) below the isolated Al_{Zn} band at 359 cm^{-1}. This situation is reminiscent of the crystal field splitting of the d states in a potential

of T_d symmetry. This analogy is being explored further to help us find the origin of these bands. Despite the fact that the six bands observed in ZnSe-Al are unidentified, the four bands in the double-doped ZnSe-Al,Cu can be explained on the basis that the local mode of Al_{Zn} is at $\nu = 359\ cm^{-1}$ and the other three bands at $\nu = 348.5$, 351.5 and 377 cm^{-1} arise from $(Al_{Zn} - Cn_{Zn})$ pairs, which have C_s symmetry.

(3) As mentioned in our previous report, (No. 8), we carried out anneals of ZnSe-Al in a two-zone furnace with the crystal at 885°C and a zinc reservior at T = 430°C, 520°C, 740°C and 800°C. Room temperature absorption measurements are shown in fig. 2 in the range 5000 $cm^{-1} < \nu <$ 1000 cm^{-1}. At all the pressures in the range 10^{-3} - 1 atm, we find the absorption coefficient proportional to ν^{-3}. Liquid N_2 measurements of the absorption show a behavior similar to the room temperature absorption in both frequency dependence and magnitude. This temperature independence and the ν^{-3} power law indicates that the absorption mechanism probably involves ionized impurity scattering.

To pursue the results obtained for ZnSe above we plan to carry out the following:

(1) To understand the nature of the complexes of Al with the native defects in ZnSe-Al, we intend to carry out electron irradiation on a series of samples annealed under various conditions. We hope to correlate the changes in the local mode absorption with the pre-irradiation carrier absorption.

(2) To perform electrical transport measurements on Zn-annealed ZnSe-Al to measure carrier concentration and determine the free electron absorption cross section.

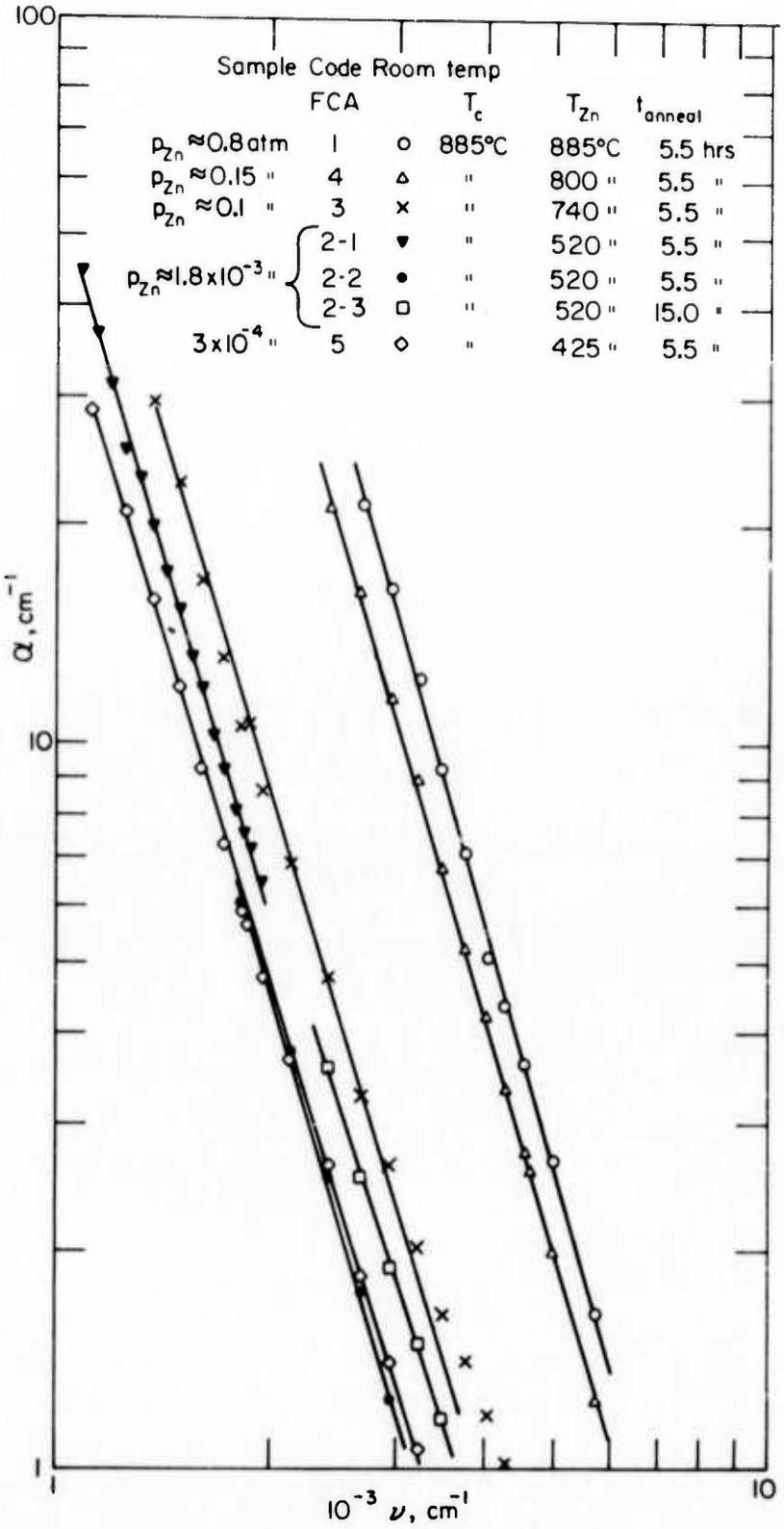


Fig. 2 Absorption as function of frequency for ZnSe-Al annealed at various zinc pressures at 885°C.

References

1. U. V. Desnica and N. B. Urli, Phys. Rev. (B), 6 (8), 1972, p. 1527.
2. M. Balkanski, et al; in Localized Excitation in Solids, Ed. R. F. Wallis, p. 154.
3. A. Mutsuiki, et al, Suppl. Prog. Theor. Phys. vol. 45, p. 21, 1970.
4. M. Aven and J. S. Prenes, The Phys. and Chem. of II-VI Compounds North-Holland Publ. Co.
5. Articles by S. Shionoza and J. Schneider in II-VI Semiconducting Compounds, Ed. D. G. Thomas, Benjamin Publishing Co.
6. V. Capek, K. Zimmerman, C. Konak, M. Popova and P. Polivka, Phys. Stat. Sol. (b) 56, 739 (1973).

g.1 Characterization of Optical Performance of IR Window Systems

M. Flannery and J. Marburger

The following material continues our narrative discussion of thermal lensing theory.

(13) THE GENERAL REFOCUSING PROBLEM:

The general problem of refocusing is to redirect an aberrated phase front to obtain the maximum power within a specified focal spot. This is a very difficult variational problem because it involves finding the refocusing parameter as a function of time and position in the aperture subject to a variational condition where the refocusing parameter appears under four integrations. If we wish to maximize the power, P, in a disk of fixed radius, ρ_o, in the focal plane, $\zeta = R$, the variational condition is,

$$\delta P = \delta \int_0^{2\pi} \int_0^{\rho_o} I(\rho,\theta)\rho\partial\rho\partial\theta = 0 \qquad (13.1)$$

where $I(\rho,\theta)$ is the beam intensity in the focal plane given by Kirchhoff's diffraction integral. The kernel of the diffraction integral, equation (1.10), Quarterly Report No. 6, can be modified to include the refocusing parameter, R_f,

$$K(\vec{\rho},\vec{\rho}',\zeta,R_f(\vec{\rho}',\tau)) = \exp i\left[\frac{\rho'^2}{2}\left(\frac{1}{\zeta} - \frac{1}{R} + \frac{1}{R_f}\right) - \frac{\vec{\rho}\cdot\vec{\rho}'}{\zeta}\right] \qquad (13.2)$$

This form of the kernel was chosen because it reduces to a simple change in the focal length of the system if R_f is a function of τ only.

On reflection it may appear that this statement of the problem is superfluous since we know what the ideal refocusing function is: the inverse of the aberration introduced by the window. For example in the case of simple lensing with no birefringence this could be accomplished with a properly profiled mirror. When birefringence is added it becomes necessary to individually refocus the two principle polarizations at each point in the window, which suggests using a composite window with compensating aberrations. In any case it is unlikely that perfect compensation can be achieved, so it will be necessary to consider approximate forms for the refocusing function and optimize them through the variational problem.

Simple Refocusing of Birefringent Beams:

The simplest compensation we can make for focal plane intensity degradation is to modify the focal length of the entire system, which means

we assume R_f is a function of τ only. Our previous experience with simply lensed Gaussian beams[1] shows that the variational condition (13.1) is equivalent to maximizing the focal point intensity. When birefringence is included we can no longer assume that to be true because this condition will only optimize the focusing of the on-axis component E_o, since the birefringent component always satisfies $E_2(\rho = 0) = 0$. Note that refocusing merely introduces the same additional phase factor into E_o and E_2 which spatially redistributes the energy in each component, but never transfers energy from one to the other. Also, the birefringent field will generally produce its most tightly focused ring structure at a different focal length than the optimum for E_o, so it will be necessary to resort to (13.1) to find the best overall function R_f. However, if the spot size considered is small compared to the dimensions of the ring structure, or the birefringence is kept small, maximizing the focal point intensity should produce nearly optimum refocusing, provided we can extend our experience with simply lensed Gaussian beams to the $\cos\Delta E_i(\rho')$ effective field for birefringent windows.

The condition for E_o (0, R) to have a maximum is,

$$\frac{\partial E_o(o,R)}{\partial R_f} \propto_o \int^1 \rho'^3 \partial\rho' e^{i\phi} \cos\Delta E_i(\rho') e^{i\rho'^2/2R_f(\tau)} = o \qquad (13.3)$$

which is the same as the expression for E_o except for the added factor of ρ'^2. Thus we have a condition which is really no more practical than examining the focal intensity as a function of R_f, and calculating the intensity itself will give us a picture of the output which can be used to estimate the sensitivity to focusing errors. While this characterizes the problem very well it has the disadvantage of requiring numerical solutions for each case considered.

To avoid the problem we attempted to fit the aberrated phase front, given for the simple window model of section 9, by

$$\zeta_a(\rho) = -\tau[e^{-2\alpha^2\rho^2} - 1] \qquad (13.4)$$

to a simple spherical phase

$$\zeta_s(\rho) = \frac{\rho^2}{2R_f} \qquad (13.5)$$

In (13.4) a constant phase, τ has been subtracted from the thermally induced phase so that $\zeta_a(0) = \zeta_s(0) = 0$. Also, after the spherical phase front is

fitted to the aberrated phase front, the resulting expression for ζ_s must have its sign changed so it compensates for the aberrations. This sign change has already been included in the sign of R_f in the kernel (13.2).

In examining fitting schemes we first notice that the aberration grows linearly with time so the dominant temporal behavior of R_f should be $R_f\alpha^1/\tau$. We considered several simple fitting schemes before trying more elaborate methods in the hope that they might give reasonable estimates of the refocusing required as well as some simple connection between the best refocusing phase front and the aberrated one. Numerical values are for $\alpha = 1.122$.

a) Expand the aberration and pick R_f to cancel the simple thermal lensing term:

$$\tau R_f = \frac{1}{4\alpha^2} = 0.198 \tag{13.6}$$

b) Let the two surfaces be equal at some off-axis point ρ':

$$\tau R_f = \frac{\rho'^2}{2(1 - \exp(-2\alpha^2\rho'^2))} \tag{13.7}$$

Two natural choices for ρ' might be the field and intensity e^{-1} points, but we chose the field e^{-1} point $\rho' = \alpha^{-1}$ because it includes most of the power in the beam, 69% in this case;

$$\tau R_f = \frac{1}{2\alpha^2(1 - e^{-2})} = 0.46 \tag{13.8}$$

c) A linear difference fit over the aperture;

$$\int_0^1 (\zeta_s - \zeta_a)\rho\partial\rho = 0 \tag{13.9}$$

which gives,

$$\tau R_f = \frac{\alpha^2}{2(2\alpha^2 - 1 + e^{-2\alpha^2})} = 0.39 \tag{13.10}$$

More complicated methods of fitting were also tried, including variations of a least squares fit over a region of the aperture, $(0,\rho)$, weighted by the effective intensity $\cos^2\Delta e^{-2\alpha^2\rho'^2}$

$$\int_0^\rho (\zeta_s - \zeta_a)^2 \cos^2\Delta e^{-2\alpha^2\rho'^2}\rho'\partial\rho = 0 \tag{13.11}$$

It was hoped this would provide an effective fit as well as including some extra time dependence from the $\cos\Delta$ factor,

$$\Delta = \frac{\sigma\tau}{2}(g(\rho) - 2f(\rho))$$

where g and f are given in Quarterly Report No. 6, equations (9.2) and (9.3). When we took $\Delta \approx 0$ so that $\cos\Delta \approx 1$, (13.11) gave very small values of R_f for any simple values of ρ. Further when $\cos^2\Delta$ was expanded to first order in $\sigma\tau$ to get the lowest order effect of birefringence on the temporal behavior of R_f, (13.11) produced divergent integrals which couldn't be evaluated.

Our final observation for birefringent beams is that we can write

$$e^{i\phi}\cos\Delta = \tfrac{1}{2}(e^{i(\phi+\Delta)} + e^{i(\phi-\Delta)}) \tag{13.13}$$

in E_o and a similar expression for $\sin\Delta e^{i\phi}$ in E_2, and then use equations (4.5) from Quarterly Report No. 6, namely

$$\begin{aligned} \phi &= \frac{k}{2}(\Phi_r + \Phi_\theta) \\ \Delta &= \frac{k}{2}(\Phi_r - \Phi_\theta) \end{aligned} \tag{13.14}$$

to give,

$$e^{i\phi}\cos\Delta = \tfrac{1}{2}(e^{ik\Phi_r} + e^{ik\Phi_\theta}) \tag{13.15}$$

This just shows that E_o and E_2 contain components that 'defocus' with different effective phases. It may be better to try to interpret birefringent refocusing in terms of these four components rather than E_o and E_2, but we have not yet investigated this point.

Comparison of Analytic and Computer Calculations:

Our first attempt at refocusing was the method of part a), merely canceling the quadratic term in the aberration. We knew that the higher order terms in the aberrations could be quite large if ρ became large, but it was thought that the most important contribution to the focal intensities would come from small ρ and reasonable compensation would result. Figure 13.1 is the original focal intensity of a Gaussian beam, $\alpha = 1.122$, focused at the Rayleigh range of the aperture for several values of the birefringence, σ. Compare this to Figure 13.2 which shows the same beam with cancellation of the quadratic aberration. In general the refocused beam is worse than the original, particularly since the half intensity degradation time, $\tau_{\frac{1}{2}}$, has decreased. Two interesting points the case illustrates are that important contributions to the focal intensity come from regions where higher order aberrations are large, and the quadratic aberration in fact partially compensates for them.

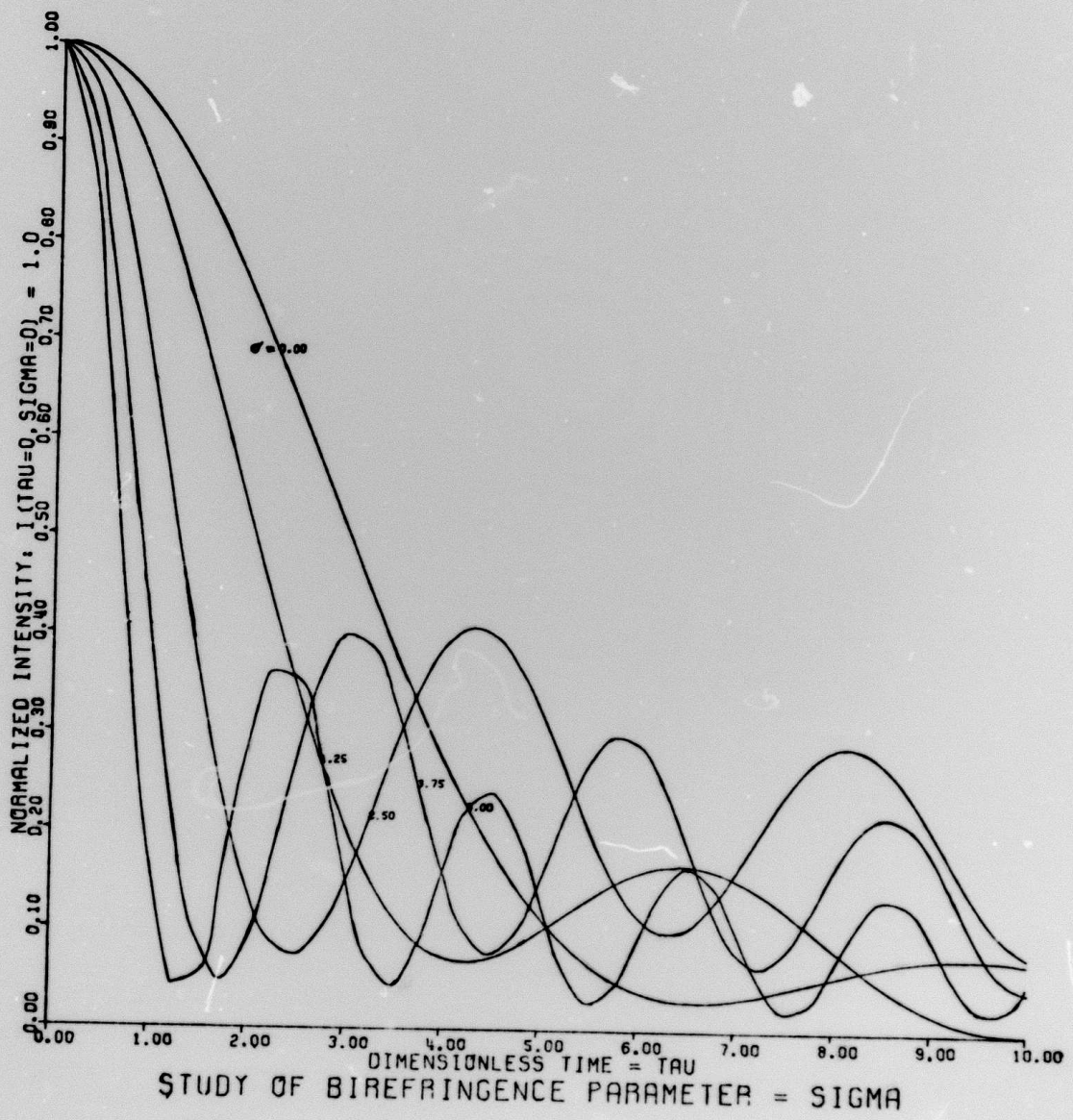


Fig. 13.1: Focal point intensity versus time for several values of σ; Gaussian beam (α=1.122), linearly polarized and focused at the Rayleigh range $Z = ka^2$. Window response is calculated using the simple window model developed in section 9.

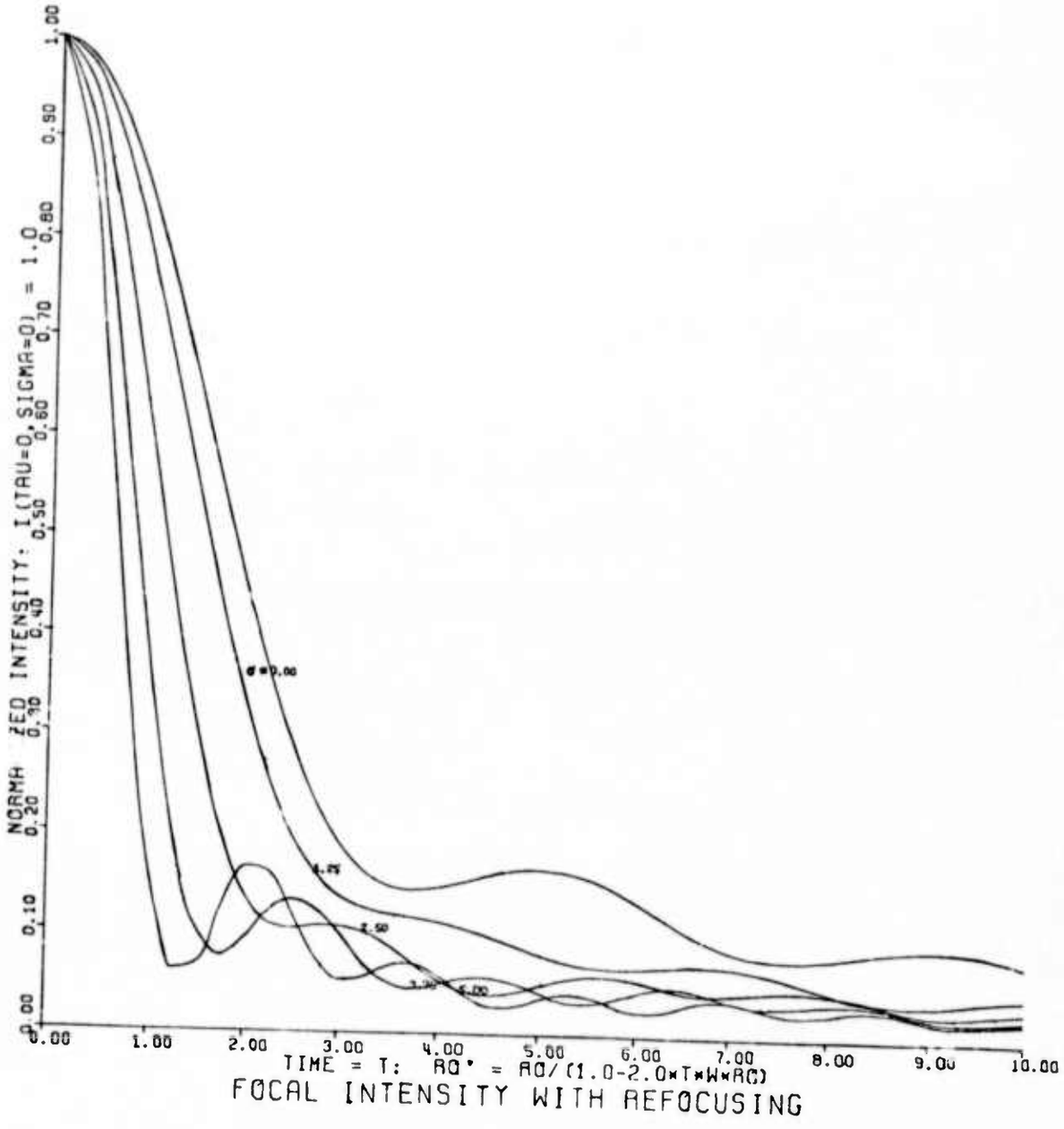


Fig. 13.2: Original focal point intensity (ζ=R) versus time for beam of Fig. 13.1, with quadratic thermal aberration removed.

The simple theories for refocusing only yielded refocusing parameters with the form τR_f = constant which we can write as $R_f^{-1} = \tau R_{er}$. Thus we chose to examine the dependence of the intensity on R_{er} rather than R_f directly because the simple theories could be indicated on these graphs as R_{er} = constant. We again used a Gaussian beam, $\alpha = 1.122$, originally focused at the Rayleigh range and plotted it for the range $0 \leq R_{er} \leq 4.0$, which corresponds to $\infty \leq \tau R_f \leq 0.25$. Figures 13.3, 13.4 and 13.5 illustrate this for $\sigma = 0, 0.5, 1.0$.

First for Figure 13.3 we find a well defined optimum refocusing parameter $R_{er} = 1.85$, which greatly improves the degradation time from $\tau_{1/2} = 3.0$ to $\tau_{1/2} = 9.5$. Further, this refocusing value isn't too sensitive since variations of 10% or so only cause about 5% intensity drop. Thus the phase front fit given by (13.8), $\tau R_f = 0.46$ or $R_{er} = 2.18$ gives a resonable estimate of the optimum refocusing parameter while most others give too high a value for R_{er}. When we shift to long times, $\tau \approx 12$, the optimum refocusing drifts off to higher values of R_{er}. Previous experience[1] with Gaussian beams shows this irregular drifting decreases as α decreases, so it is apparently due to aberrations in the wings of the Gaussian.

Figure 13.4, for $\sigma = 0.5$ shows very similar behavior, except for a decreased degradation time, $\tau_{1/2} \times 5.5$, and a time, $\tau \approx 12$ where the curves become very low and flat. In this region we can no longer effectively refocus.

Figure 13.5, for $\sigma = 1.0$, demonstrates this even more dramatically for $\tau = 6$, and gives us a hint as to what might be happening. Initially the major effect is simple thermal lensing, but then birefringence begins to interfere with it through the $\cos\Delta$ term, first causing a weakly oscillating curve and then a dramatic refocusing for smaller values of R_{er}. It was this type of behavior that suggested the decomposition of equation (13.13) and the idea that birefringence induces an interference effect between the two components of the beam.

We also looked at off-axis refocusing for $\sigma = 1.0$. For $\rho = 1.0$ the curves looked very much like Figure 13.5 with the intensities decreased by 30%, but further off-axis the curves became very erratic and could not be consistently refocused.

Our conclusion is that simple refocusing can dramatically improve results for small amounts of birefringence but as σ becomes larger, problems

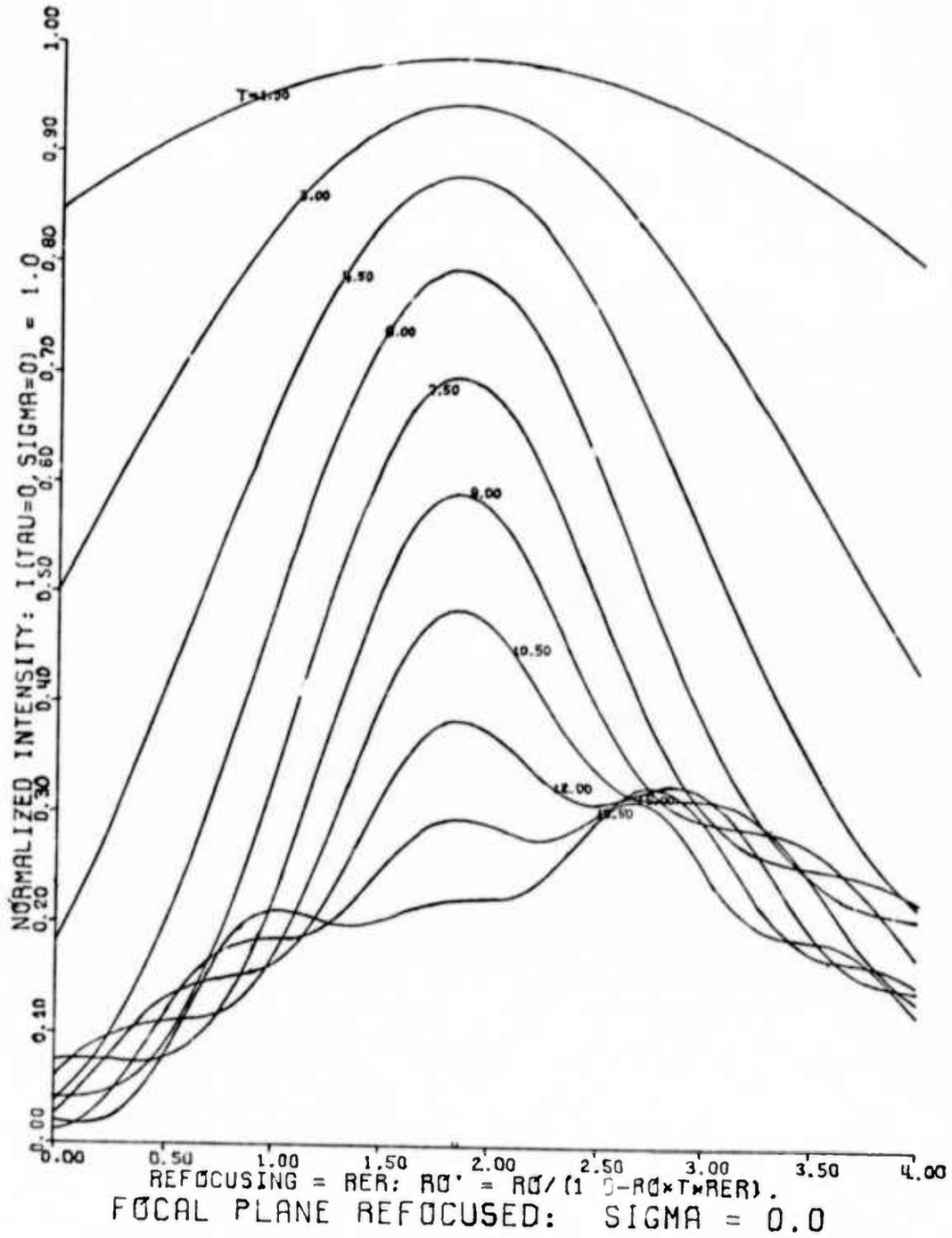


Fig. 13.3: Original focal point intensity vs. refocusing parameter R_{er} for various times. Same beam as in Fig. 13.1 for $\sigma = 0$.

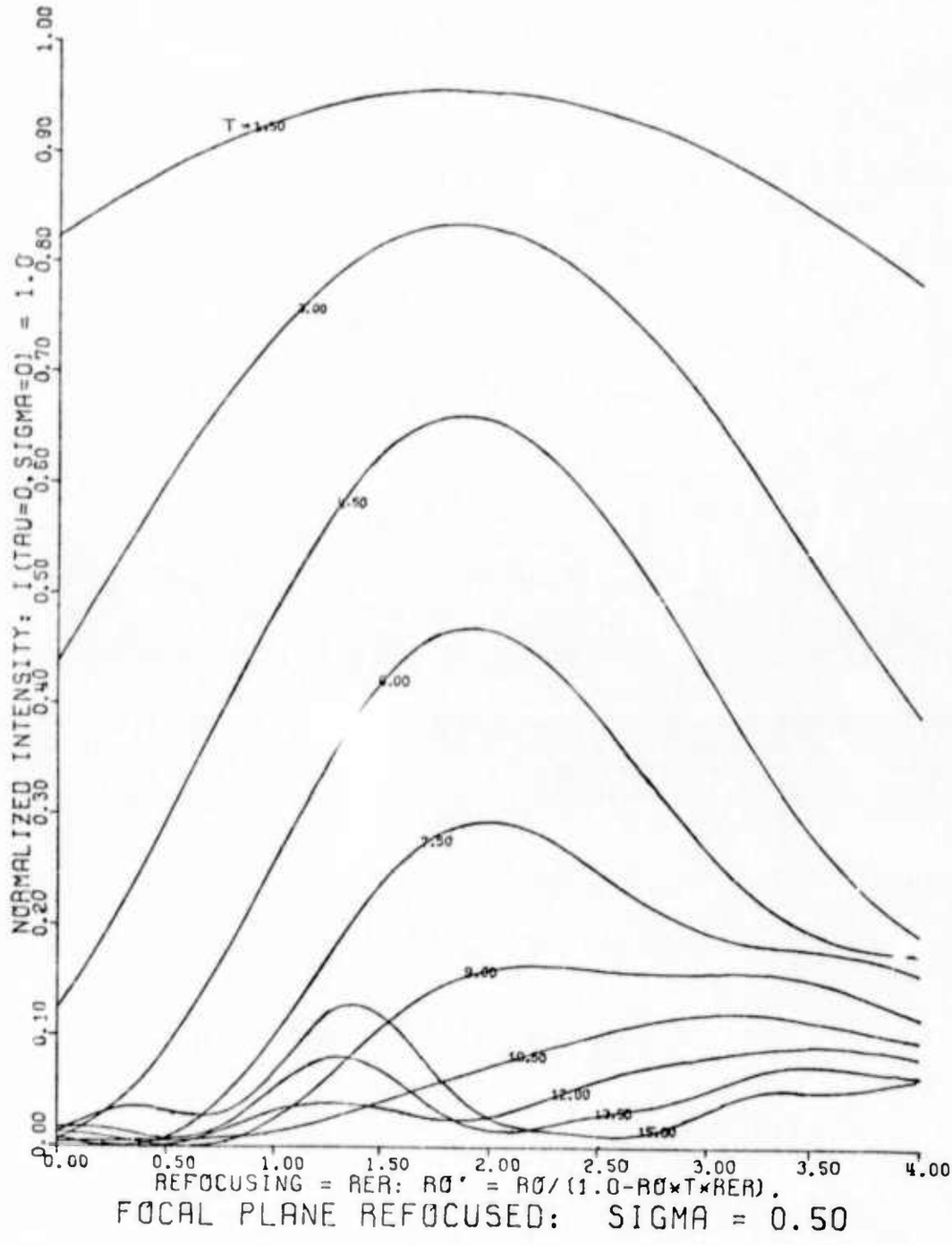


Fig. 13.4: Original focal point intensity vs. refocusing parameter R_{er} for various times. Same beam as in Fig. 13.1 for $\sigma = 0.5$.

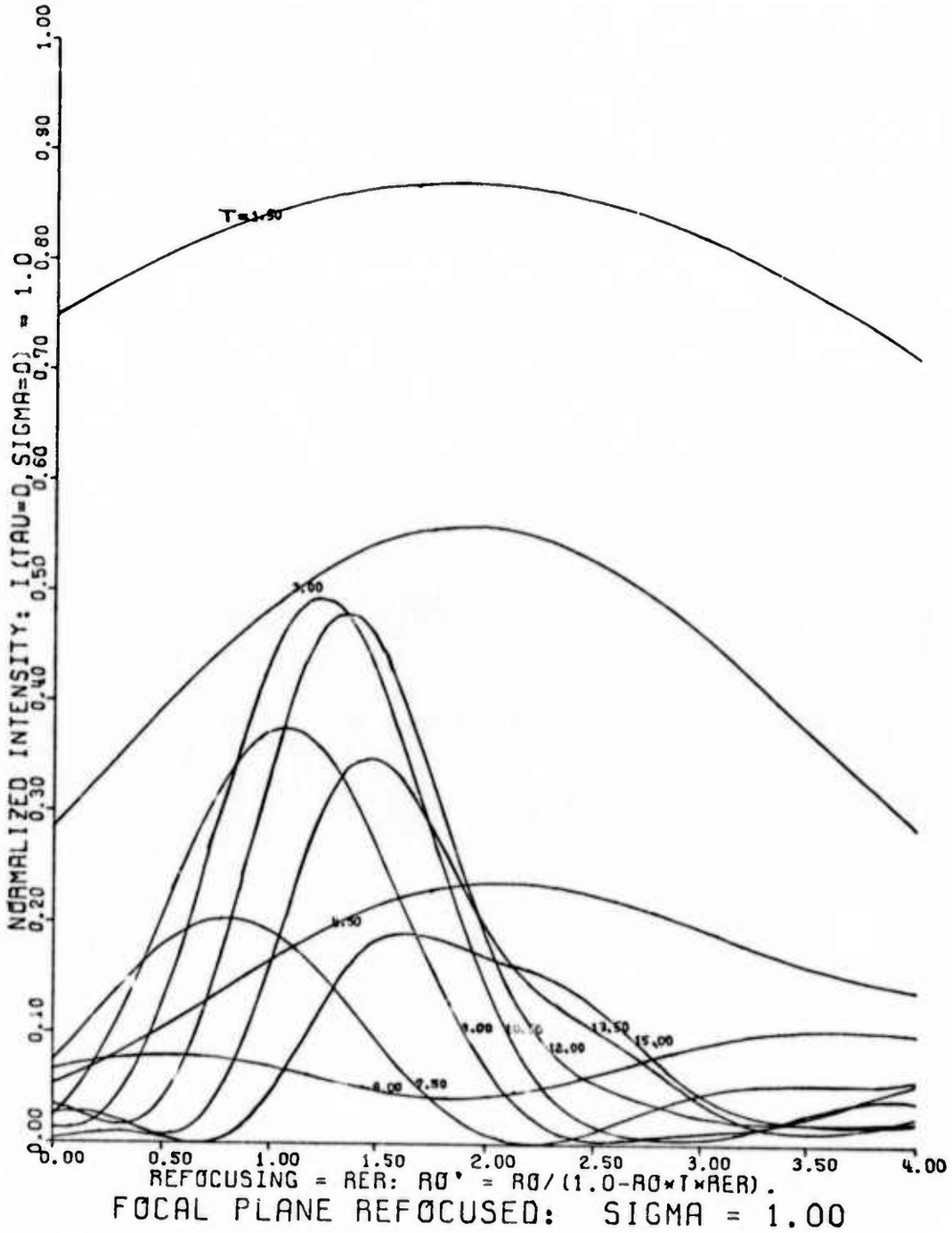


Fig. 13.5: Original focal point intensity vs. refocusing parameter R_{er} for various times. Same beam as in Fig. 13.1 for $\sigma = 1.0$

develop. It appears that some help may come from the onset of thermal equilibrium which would reduce stresses and smooth out the aberrations, but in addition it will be necessary to compensate for the birefringence as much as possible and to develop more sophisticated refocusing schemes.

References:

1. J. Marburger and M. Flannery "IR Window Criteria: 'Exact' Analysis of the Thermal Distortion Problem" in Proceedings of Conference on 'High Power IR Laser Window Materials" Air Force Cambridge Research Laboratories, p. 11 (1971).
2. IR Window Studies, USC Quarterly Technical Report No. 6, USCEE Report 469, AFCRL-TR-74-0060, F. A. Kroger and J. H. Marburger, Editors 15 Dec. 1973.

h. 1 Laser Damage Studies

M. Bass, K. M. Leung

h. 1.a. CO_2 TEA Laser

A CO_2 TEA laser was prepared for use in the laser damage experiments. This unit was built according to designs developed during previous work and is described in detail in the report of that program.[1] Table I gives some of the important laser parameters and Table II gives the performance data achieved so far in our laboratory. Figure 1-a shows the laser's output waveform when the optical cavity permits many transverse modes to oscillate. When the intracavity aperture is closed to ~9 mm diameter, TEM_{00} mode oscillation is obtained and the much smoother waveform of Figure 1-b is obtained. Figure 1-c shows the mode locked spikes of Figure 1-b more clearly. These data, which are similar to that reported in Reference 1, were obtained using a Rofin photon drag detector[2] and a Tektronix 7904 oscilloscope without the photographic image enhancing feature. The photographs, therefore, have been retouched to make reproduction in this report possible.

The laser, when restricted to TEM_{00} mode oscillation, was used to obtain the preliminary damage data described later in this report.

h. 1.b. Characterization of the Samples

In Table III, we list the three ZnSe and fifteen KCl samples obtained for this work. After hearing the description of the newly developed "scatterometer" presented at the 1974 Laser Damage Symposium in Boulder[3], we arranged to add light scattering data to our sample characterization effort. The data listed in Table III were obtained at China Lake using the facilities and techniques described in Reference 3. The data was obtained at 0.6328 μm. The quantity listed represents the part of the total scattered light measured relative to the transmitted intensity due to the surface or per cm if the scattering is produced in the bulk. These data were supplemented by Nomarski interference

Table I. CO_2 TEA Laser Parameters

Discharge Length	41 cm
Height	5 cm
Width	1.7 cm
Volume	348 cm^3
Energy Storage Capacitance	0.08 μf
Typical Operating Voltage	23 kv
Typical Input Energy	21 J
Flow Rate Ratios $He:CO_2:N_2$	8.7:2.4:2.6 (l/min)

Table II. CO_2 TEA Laser Performance Data

Cavity Length	120 cm
Mirrors:	100%R - Flat
	80%R - 10m Radius, Ge
Brewster Windows	KCl
At 21 J Input:	
Multimode Output	0.85 J
TEM_{00} Mode (9mm apperture between 100%R mirror and discharge)	0.1 J
Miltimode Efficiency	4%
Multimode Output Energy Density	2.4 J/l

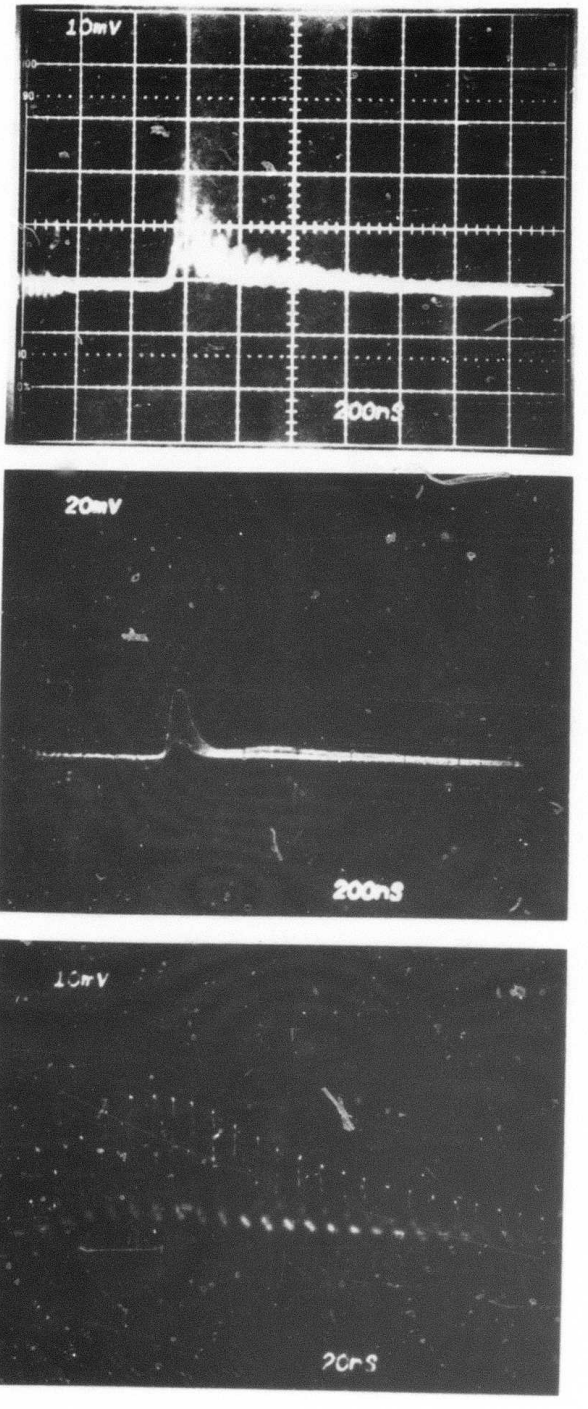


Figure 1: CO_2 TEA output pulse waveforms:
a. multimode
b. TEM_{00} mode
c. TEM_{00} mode showing mode locked spikes
The photographs were retouched for the purpose of reproduction.

Table III. Samples Studied

Material	Sample No.	Dimensions (mm) L x W x H	Index of Refraction	Absorptivity at 10.6 μm (cm^{-1})	Scattering at 0.63 μm S_t*	S_B*	S_o*	Source
ZnSe	ZRMB	68 x 45 x 3.5	2.43	- -		0.14 cm^{-1}		Raytheon/M. Bass
ZnSe	ZRG-734	27 x 25 x 7.4	2.43	0.0046		0.07 cm^{-1}		Raytheon/AFML
ZnSe	ZR-II-VI	25 dia. x 2.0	2.43	- -		too large to measure		II-VI/Raytheon
KCl	KG-10	38 dia. x 12.0	1.49	0.0008	0.0170		0.0200	International Crystal
	KIC-4a	25 x 25 x 4.0		0.0034	0.0024		0.0038	
	b			- -	0.0062		0.0035	
	c			- -	0.0190		0.003	
	d			- -	0.0220		0.0025	
	e			- -	0.0210		0.0050	
	KIC-65a	39.5 x 39.5 x 6.5		- -	0.0165		0.0270	
	b			- -	0.0290		0.0140	
	c			- -	0.0310		0.0410	
	d			- -	0.0018		0.0093	
	KH-5a	25 dia. x 5.0		0.0023				Harshaw
	b			- -	0.0076		0.0052	
	c			- -	0.0059		0.0055	
	d			- -	0.0063		0.0052	
	e			- -	(Broken)			

* Measured in this work at Naval Weapons Center at China Lake.

S_t is the part of the total scatter at 0.63 μm due to the entrance face
S_o is the part of the total scatter at 0.63 μm due to the exit face
S_B is the part of the total scatter at 0.63 μm due to the bulk in cm^{-1}

photomicrographs such as shown in Figures 2-5.

The scattering data clearly demonstrated the following:

1. The visible light scattering in ZnSe is principally caused by scattering centers in the bulk. In fact, as a comparison of the photomicrographs in Figures 2-5 indicates, the density of small diameter ($\leq 1\,\mu m$) scratches of the ZnSe sample is lower than on the KCl crystals. On the other hand, large diameter ($> 5\,\mu m$) scratches are present on all our samples with nearly the same density irrespective of material or source. Since the latter are more likely to be significant in the 10.6 μm laser induced damage process, it is clear that the finishing techniques for both materials must be improved.

2. The Harshaw samples generally were finished more uniformly than those provided by International Crystal and show generally less 0.63 μm scattering. Note too that the scattering from International Crystal's surfaces varies by nearly one order of magnitude. We suspect that this may be caused by poor packaging techniques. This again suggests the need for protective coatings and standards for packaging, shipping and storing polished infrared laser window materials.

3. No significant visible scattering was measured in the bulk of the KCl samples. By comparing the data listed in Table III for samples KG-10 and KIC-4a, we see that visible light scattering and absorption at 10.6 μm do not appear to be correlated. When scatterometry equipment is developed to measure 10.6 μm scattering, it may be possible to determine the effect of scattering on the measured infrared absorption.

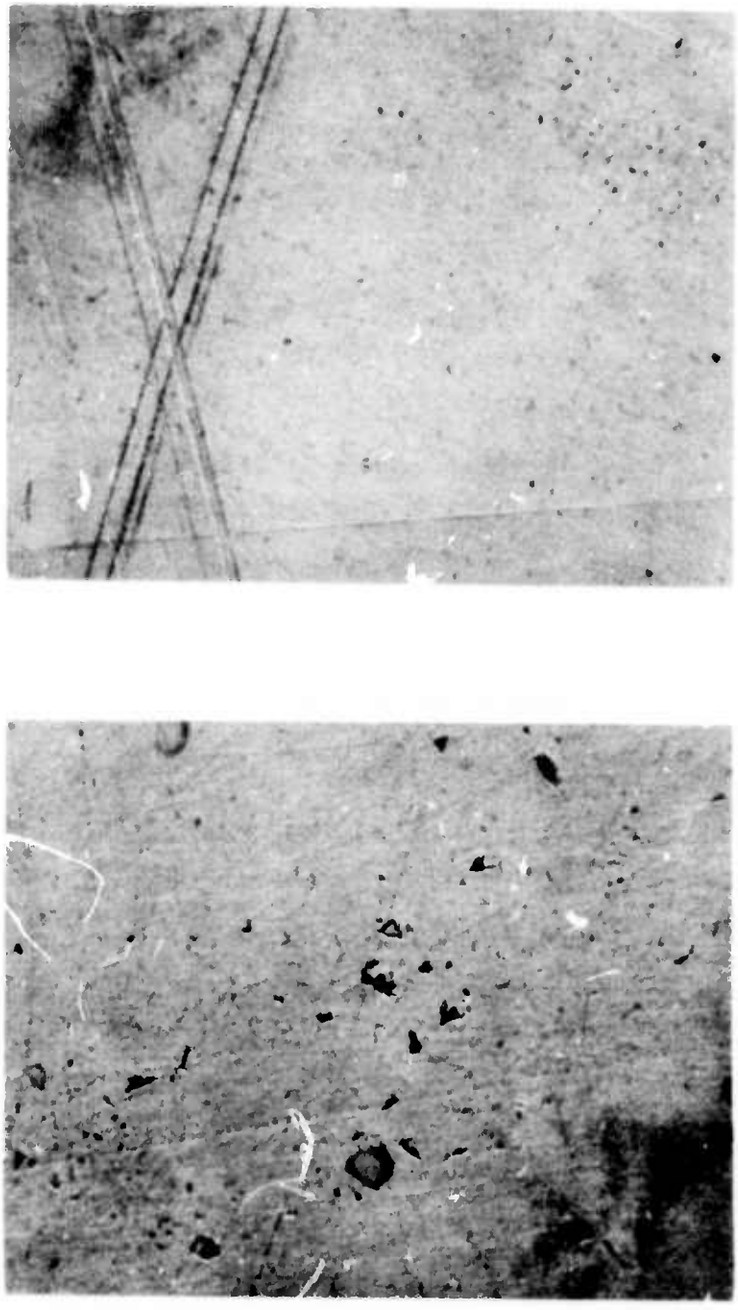


Figure 2: Nomarski micrographs of the surfaces of ZnSe sample No. ZRMB
a. entrance surface
b. exit surface

Magnification = 260

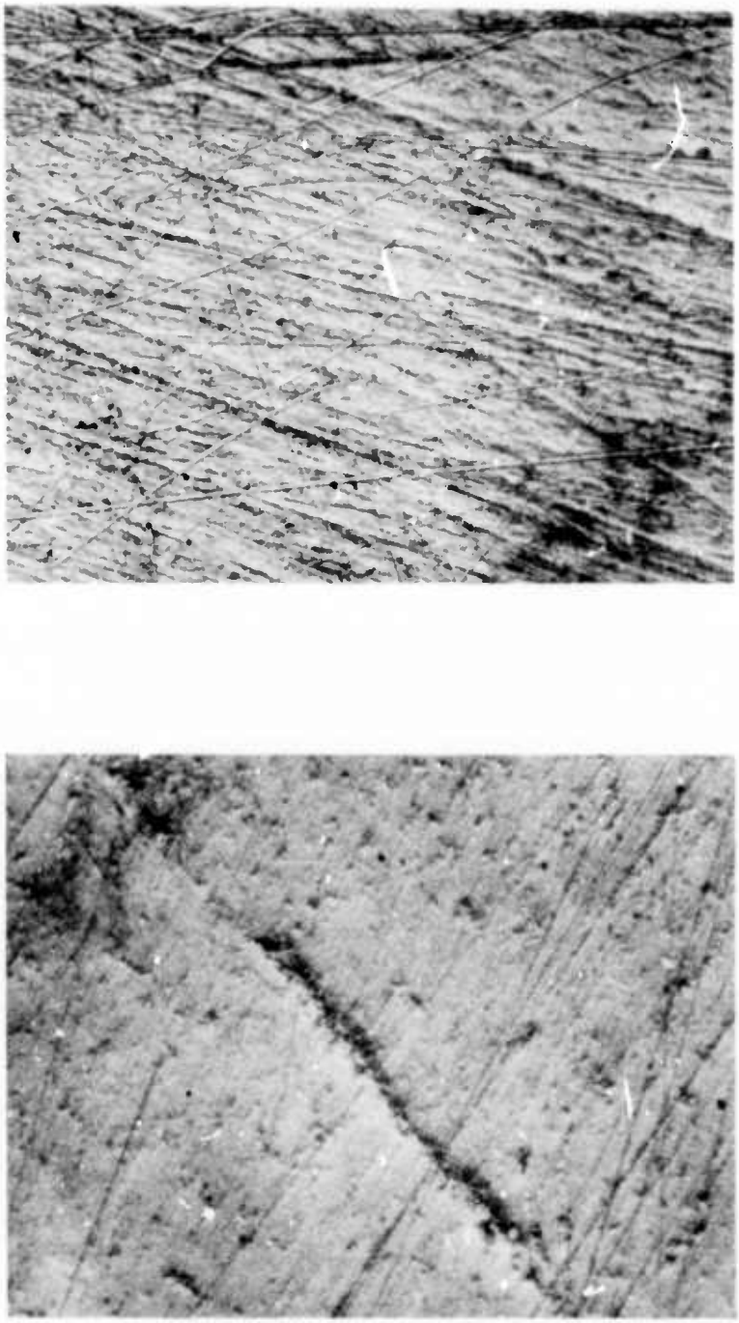


Figure 3: Nomarski micrographs of the surfaces of KCl sample No. KIC-65c
a. entrance surface
b. exit surface

Magnification = 260

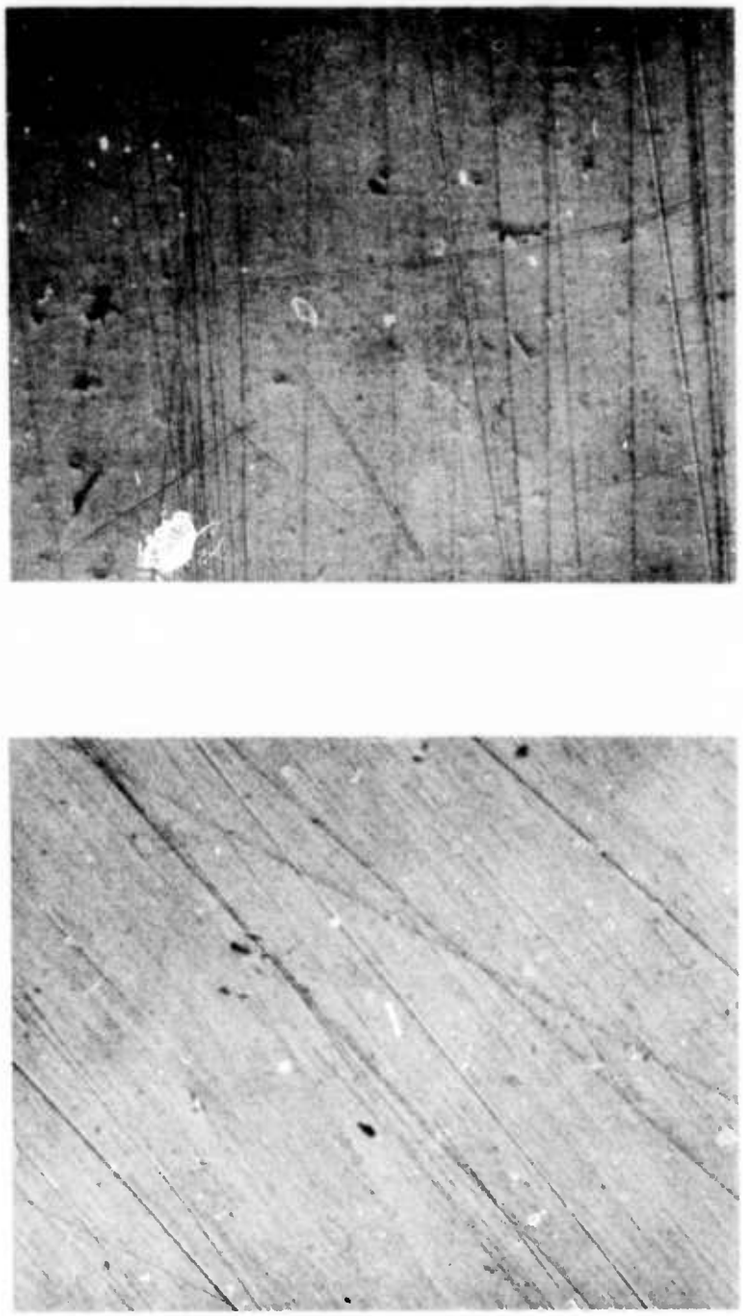


Figure 4: Nomarski micrographs of the surfaces of KCl sample No. KIC-65d
a. entrance surface
b. exit surface

Magnification = 260

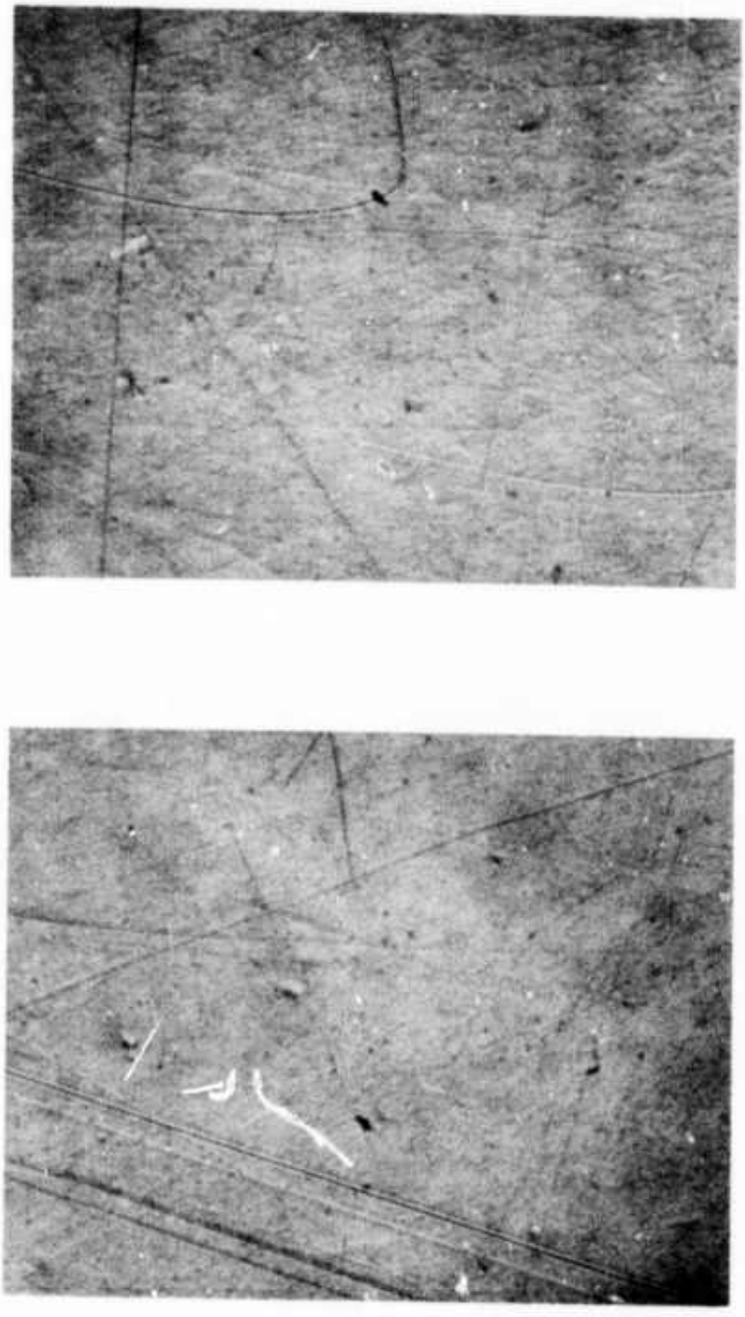


Figure 5: Nomarski micrographs of the surfaces of KCl sample No. KH-5d
a. entrance surface
b. exit surface

Magnification = 260

h. l. c. Preliminary Laser Damage Data

Since the completion of the laser for the damage measurements was delayed by the delay in ordering the power supply and by a machining error, we were only able to obtain the preliminary damage data described in this section. Again, because of the lack of the photographic image enhancing feature on our Tektronix 7904 oscilloscope, the photographs have been retouched for the purposes of reproduction.

The occurrence of a damaging interaction was monitored by observing the onset of the attenuation of the transmitted laser pulse. Figure 6 shows this type of data for a laser induced air breakdown. A 3.8 cm plano-convex lens was used to focus ~15 mJ of laser energy having the waveform shown in the lower trace in Figure 6. The laser was operating in the TEM_{00} mode. However, we have since become suspicious of the laser attenuator we used (a Si wafer near Brewsters angle) and feel that some spatial profile distortion may have occurred. Thus we present these preliminary results with some caution. Under the conditions described above, air breakdown could be observed on every pulse. The pulse energy was attenuated to obtain the laser waveform data.

Figure 7 shows the type of attenuation observed when ZnSe was irradiated. In both cases, bulk damage only was observed. This, and the morphology, suggest that the damage process is determined by the presence of absorbing inclusions in the irradiated volume. As pointed out elsewhere, even if one focuses on a surface, bulk damage is most likely to occur unless there is a specific reason for the surface to be more easily damaged than the bulk.[4] However, if inclusions cause the sample to damage, then there are many more inclusions which may be damaged in the volume irradiated than on the surface. Thus, even the higher intensity obtained when one focuses on the surface should not cause localized surface damage.

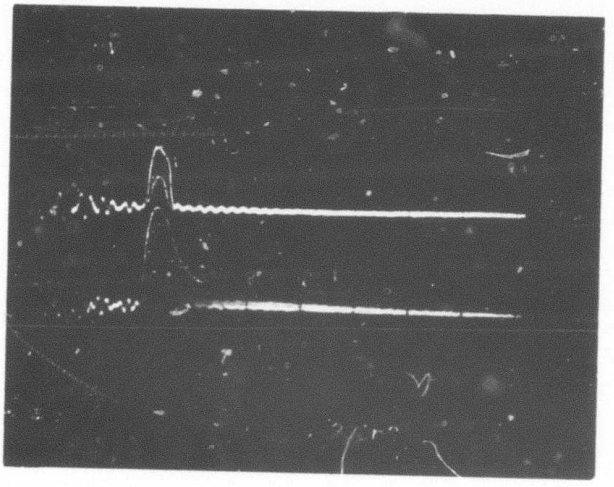
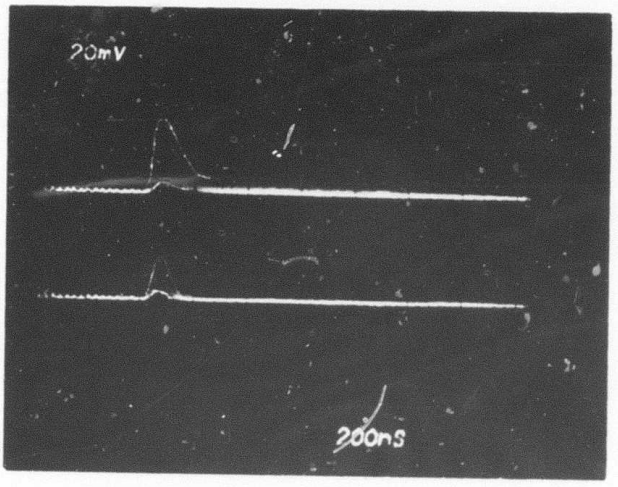


Figure 6: Transmitted laser pulse waveform when a CO_2 TEA laser produces air breakdown



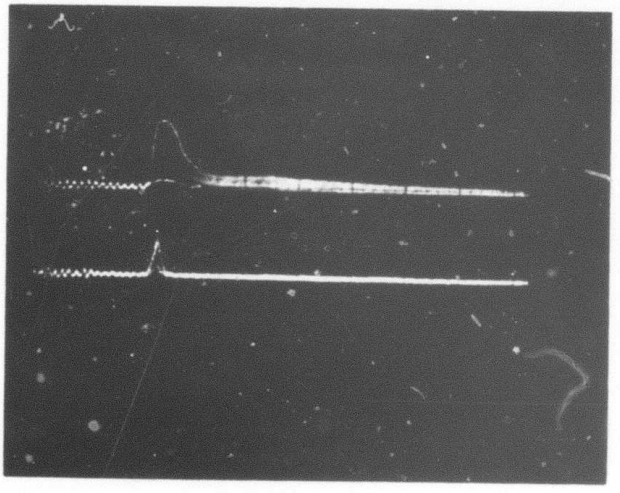


Figure 7: Transmitted laser pulse waveform when a CO_2 TEA laser produces damage in ZnSe (Sample No. ZRMB)
a. 3.82 cm lens focused on the sample's surface
b. 3.82 cm lens focused on the sample's bulk

Figure 8 shows the attenuation of the laser pulses produced when KCl is damaged. These data, and that for ZnSe shown in Figure 7, were taken at 8 mJ incident energy. This level is such that damage occurs on every pulse. We note that damage is produced very early in the gain switched leading part of the laser's output. This means that threshold measurements referring to temporally unresolved pulse waveforms may overestimate the material's damage resistance.[5]

The two ZnSe samples, Nos. ZRMB and ZRG-734, showed similar damage properties even though they differ by a factor of 2 in visible scattering in the bulk. This should not be too surprising since most of the visible scattering is caused by inclusions that are small when compared to the 10.6 μm laser wavelength. These small inclusions should not be heated by a 10.6 μm pulse as strongly as larger ones and so should not make a major contribution to the 10.6 μm damage process.[6] It is possible however, that 10.6 μm damage resistance and 10.6 μm scattering might be correlated.

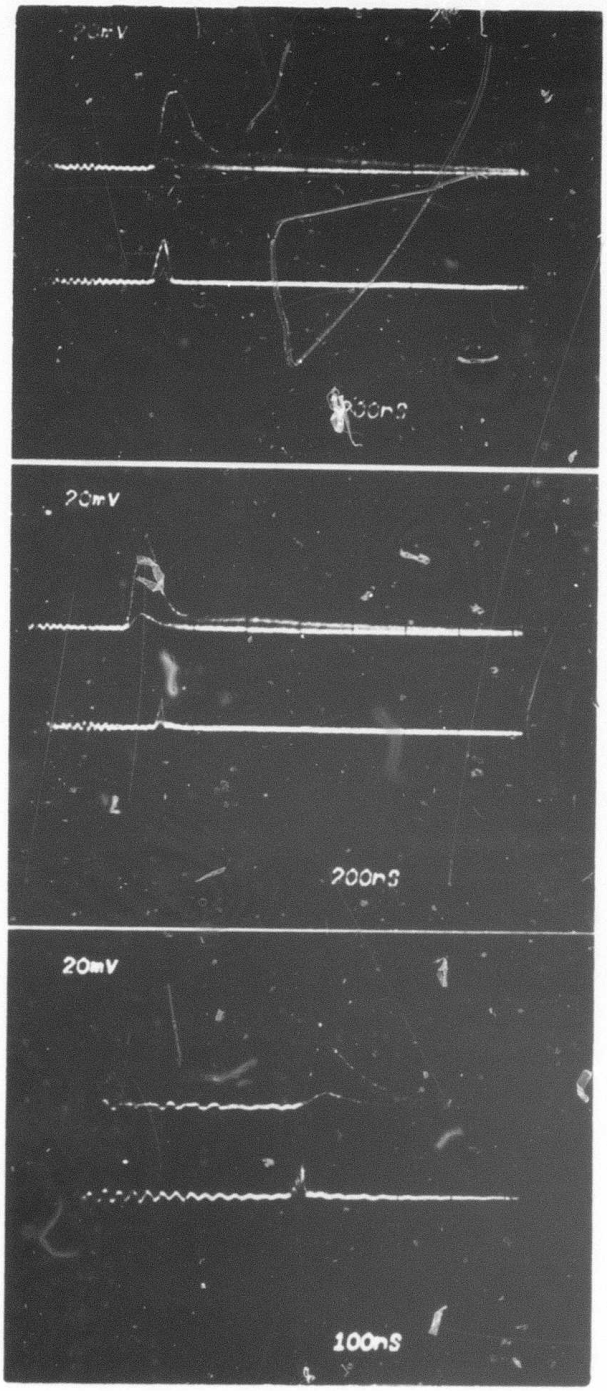


Figure 8: Transmitted laser pulse waveform when a CO_2 TEA laser produces damage in KCl (Sample No. KIC-4a)
a. 3.82 cm lens focused on the sample's surface
b. 3.82 cm lens focused in the sample's bulk
c. same as b but at faster sweep speed

REFERENCES

1. D. W. Fradin, M. Bass, D.P. Bua and L.H. Holway, Jr., "Visible and Infrared Laser-Induced Damage to Transparent Materials", Technical Report AFCRL-TR-74-0082 for Contract No. F19628-73-C-0127, January 1974.

2. This detector was loaned to us by V. Wang of the Hughes Research Laboratory.

3. M. J. Soileau and H. E. Bennett, "Testing the Surface Quality of Laser Materials" presented at the 1974 Laser Damage Symposium at Boulder, Colorado, May 1974.

4. D. W. Fradin and M. Bass, Applied Physics Letters 22, 157 (1973).

5. V. Wang, J.E. Rudisill, C.R. Guiliano, M. Braunstein and A. Braunstein, "Pulsed CO_2 Laser Damage in Windows, Reflectors and Coatings," presented at the 1974 Laser Damage Symposium, Boulder, Colorado, May 1974.

6. D. W. Fradin, "Laser Induced Damage in Solids" PhD Thesis, Harvard University, March 1973.

DISCUSSION

An apparatus to measure low absorption coefficients by calorimetry has been set up and is available for all materials to be investigated. Absorption at 10.6μm of semi-insulating GaAs grown from the melt shows the same spectral distribution and almost the same strength for seven different samples. This strongly suggests that the observed absorption coefficient $\alpha_{10.6} \approx 8 \times 10^{-3} cm^{-1}$ is the lowest that can be achieved in this material. We still have to see, however, whether material grown under radically different conditions does not have other properties. We have grown layers by chemical vapor transport but the program was discontinued before layers of good quality high resistivity material were obtained. Subsequently GaAs was grown by liquid-phase epitaxy from a gallium melt at 700-1000°C. Films of 0.65mm thick have been grown. This is thicker than has been reported anywhere for this type of growth; however, high-resistivity material has not yet been obtained.

Oxygen was removed from the gallium melt and from the gas phase by electrochemical pumping, and the result was monitored with an electrochemical gauge. Both the pump and the gauge are based on use of stabilized zirconia as a solid electrolyte.

The mechanical properties of various GaAs samples were studies; the active slip system was found to be {111} and $<1\bar{1}0>$; twinning proved not an active deformation mechanism. Doping with Si, making GaAs n-type, increased the yield strength above the value found in Zn-doped, p-type GaAs. Impurity hardening observed in GaAs-Si, could be attributed partly to interaction of glide dislocations with dislocation loops, partly to Si_{Ga}-V_{Ga} pairs. Anomalous streaks and spots in the electron diffraction pattern which were attributed to precipitates by other workers, were shown to be due to thermal diffuse scattering of electrons by phonons; similar effects were observed in CdTe.

Work on II-VI compounds was concentrated on CdTe and comprised work on hot-pressing and on the determination of the defect structure with the aid of optical and electrical measurements. Attempts were made to make dense polycrystalline CdTe samples by hot-pressing in the presence of liquid sintering aids such as Cd(ℓ), Te(ℓ) or $CdCl_2$(ℓ). The former two were ineffective due to lack of wetting. Dense samples were made by hot-pressing with addition

of $CdCl_2$, but not all the $CdCl_2$ was removed in the final stage so that removal by heating led to porous samples.

Combination of high-temperature Hall effect measurements and self diffusion measurements on pure and indium-doped CdTe with data on cooled crystals reported in the literature lead to a detailed defect model for pure and donor-doped CdTe. The residual infrared absorption in CdTe is found to be mainly due to free electronic carriers. Annealing studies show that high-resistivity material with $\alpha_{10.6\ \mu m} \approx 9 \times 10^{-4} cm^{-1}$ can be made by quenching of indium-doped CdTe after annealing at 700°C at $P_{Cd} = 5 \times 10^{-3}$ atm so that free carriers are removed. Thick samples cannot be quenched as effectively and therefore show a larger absorption, a cube of 10 x 10 x 10 mm showing $\alpha_{10.6\ \mu m} = 2 \times 10^{-2} cm^{-1}$ at the center. Crystals of CdTe doped with each of the elements Al, Ge, P were grown. Attempts to grow crystals doped with Cr were unsuccessful. Initial experiments with CdTe doped with germanium or phosphorus show that these dopants may lead to high resistivity material and may replace indium or chlorine as the dopants introduced to reduce the free carrier density. The absorption cross sections of electrons and holes at 10.6 μm were determined.

Precipitation of indium from CdTe was found to depend on the conditions of cooling, precipitation occurring if cadmium precipitated at the same time, but no precipitation of In occurring in the absence of Cd precipitation.

Local mode studies were started on ZnSe-Al and CdTe doped with Al, Al + Cu, Li, P. A λ^3 wavelength dependence of free electron absorption in n-type CdTe was determined. Dielectic constants were measured at 290°K; $\varepsilon_{GaAs} = 13.08$, $\varepsilon_{CdTe} = 11.00$ and $\varepsilon_{ZnSe} = 9.25$.

Alkali halide work led to the preparation of single crystals of KCl with a purity and an absorption coefficient at 10.6 μm equal to the best produced by others, with $\alpha_{10.6\ \mu m} = 10^{-4} cm^{-1}$. Introduction of 2×10^{-4} mol% KOH increased $\alpha_{10.6\ \mu m} \approx 2 \times 10^{-3} cm^{-1}$ remaining orders of magnitude larger than the expected value. It is believed that this is due to impurities, probably complexes of bromine and oxygen.

A method employing acoustic surface waves to probe absorption near the surface was developed, and a theory relating the observed parameters with the absorption was given. The method was tested on KCl and led to determination of a surface absorption coefficient of $10^{-2} cm^{-1}$. It is intended to increase the sensitivity by increasing the measuring frequency.

For laser damage sutdies a CO_2 TEA laser was built and tested, and used to study damage in ZnSe and KCl.

Theoretical work done during the contract period was concentrated in two areas: Diffraction theory of thermal lensing and the basic mechanisms of multi-phonon absorption. Of the latter there are two. One is based on the anharmonicity of intermolecular forces; the other is based on the non-linear dependence of electric dipole moments on lattice coordinates. A method is proposed to determine experimentally the ratio in which these two mechanisms contribute to the total effect. The thermal lensing problem was reviewed in the sections:

1. Diffraction Integral for Beams
2. Vector Corrections
3. Aberration Matrix for Thin Windows
4. Aberration Matrix for Cylindrical Anisotropy and Inhomogeneity (Thin Windows)
5. Diffraction Field for Cylindrical Anisotropy
6. Diffracted Beam Geometry for Specific Incident Polarization States
7. Relation to Notation of Bendow and Gianino
8. General Properties of Radia Dependence of Transmitted Intensity
9. Aberration Functions for a simple Window Model
10. Focal Intensity with No Birefringence for Simple Window Model
11. Influence of Birefringence on Focal Intensity for Simple Window Model
12. Influence of Birefringence on off-axis Intensity for Simple Window Model
13. Effect of Refocusing in Simple Window Model
14. Aberration Matrix for Non ideal Window Systems
15. Approximate Methods for Non ideal Systems I
16. Approximate Methods for Non ideal Systems II
17. Strategy for computing Aberration Matrix
18. Computation of the Aberration Matrix for cylindrical symmetry
19. Crystal Symmetries which lead to cylindrical symmetry in the plane stress approximation
20. Remarks on other orientations of crystalline Windows
21. Approximate computation of the Aberration Matrix for non-cylindrical symmetry

22. Diffraction Field for Acentric System: Thermal slewing
Section 1 through 10 appeared in QTR #6, Sections 11 and 12 in QTR #8
Section 13 in the present QTR #9 and Sections 14 through 22 will
be discussed in further reports.

PUBLICATIONS AND PRESENTATIONS

4.1 Publications

1. G.H. Narayanan and S.M. Copley, "Anomalous Diffraction Effects in GaAs Single Crystals", in Proceedings of the Third Conference on High Power Laser Window Materials, Carl Pitha, Ed., November 1973; Phys. Stat. Sol. (a) 23, 123 (1974).

2. V. Swaminathan and S.M. Copley, "The Temperature and Orientation Dependence of Plastic Deformation in GaAs Single Crystals", in Proceedings of the Third Conference on High Power Laser Window Materials, Carl Pitha, Ed., November 1973; submitted on August 19, 1974 to the Journal of the American Ceramic Society.

3. V. Swaminathan, G.H. Narayanan and S.M. Copley, "Comment on the Evidence of a Precipitate-Like Zone in As-Grown GaAs and Its Influence on Optical Absorptivity" submitted on August 19, 1974 to the Journal of Applied Physics.

4. V. Swaminathan and G.H. Narayanan, "Diffuse Streaks in Electron Diffraction Patterns from CdTe Single Crystals", submitted to the Journal of Applied Physics.

5. V. Swaminathan and S.M. Copley, "Impurity Hardening in GaAs Crystals", (In preparation).

6. S.S. Chern, H.R. Vydyanath and F.A. Kroger, "The Defect Structure of CdTe, Hall data", J. Solid State Chemistry; accepted for publication.

7. S.S. Chern and F.A. Kroger, "The Defect Structure of CdTe, Self Diffusion Data," J. Solid State Chemistry; accepted for publication.

8. S.S. Chern and F.A. Kroger, "Chemical Self Diffusion in CdTe", submitted to J. Solid State Chemistry; accepted for publication.

9. S.S. Chern and F.A. Kroger, " The Relative Magnitude of the Diffusion Constants of Cadmium Vacancies and Indium-Cadmium Vacancy Pairs in CdS and CdTe", Phys. Status Solidi (a) 25, 215-222 (1974).

10. H.R. Vydyanath and F.A. Kroger, "High-temperature Electron and Hole Mobilities in Pure and Doped CdS", J. Appl. Phys.; accepted for publication.

11. H.R. Vydyanath and F.A. Kroger, "The Defect Structure of Silver-doped CdS", J. Phys. Chem. Solids; accepted for publication.

12. H.R. Vydyanath and F.A. Kroger, "Self Diffusion of Cadmium in Slightly Impure CdS", J. Phys. Chem. Solids; accepted for publication.

4.1 Publications (Cont.)

13. C.P. Christensen, R. Joiner, S.T.K. Nieh and W.H. Steier, "Investigation of Infrared Loss Mechanisms in High Resistivity GaAs", J. Appl. Phys.,45, 4957 (1974).

14. J.H. Parks, D.A. Rockwell, T.S. Colbert, K.M. Lakin and D. Mih, "Acoustic Surface Wave Detection of Radioactive Absorption", Applied Physics Letters, Vol. 25, p. 537, (1974).

15. I. Strzalkowski, S. Joshi and C.R. Crowell, "Dielectric Constant and its Temperature Dependence for GaAs, CdTe and ZnSe".

4.2 Presentations

1. J. Marburger, S.M. Copley and J. Parks, "Progress Report, ARPA/USC Program", ARPA Laser Window Review, Washington D.C., April (1973).

2. V. Swaminathan and S.M. Copley, "Mechanical Behavior of Si-Doped GaAs Single Crystals", 1973 Fall Meeting, Basic Science Division, American Ceramic Society, Pittsburgh, Pa. (Sept. 23-26, 1973).

3. S.M. Copley and W.H. Steier, "Characterization of High Purity Melt-Grown GaAs Crystals", Third Conference on High Power Laser Window Materials, Hyannis, Mass., November 1973.

4. F.A. Kroger, S.S. Chern and H.R. Vydyanath, "The Defect Structure of CdTe and Its use as an IR Window Material", in Proc. Third Conference on High Power Laser Window Materials, Carl Pitha, H. Posen and A. Armington, Eds., Nov. (1973) AFCRL-TR-74-0085 (II) p. 437 (1974).

5. T. Colbert, D. Rockwell and J.H. Parks, "Alakali Halide Surface Properties Studied by Acoustic Probe Techniques", in Proc. Third Conf. High Power Laser Materials; Carl Pitha, H. Posen and A. Armington, Eds., p. 965; AFCRL-TR-74-0085 (III) 1974.

6. C.P. Christensen, R. Joiner, S.T.K. Nieh and W.H. Steier, "Investigation of Basic Infrared Loss Mechanisms in High-Resistivity GaAs", in Proc. Third Conf. on High Power Laser Window Materials; Carl Pitha, H. Posen and A. Armington, Eds., AFCRL-TR-74-0085 (I) p. 97, (1974).

7. R. Hellwarth and M. Mangir, "A Method of Measuring the Contribution of the Non-linear Dipole Moment to Multiphonon Absorption". in Proc. Third Conf. High Power Laser Materials; Carl Pitha, H. Posen and A. Armington, Eds., (I) p. 161 (1974).

8. M. Flannery and J. Marburger, "Birefringence Effects in Thermal Lensing", paper C.W., presented at the 8th International Quantum Electronics Conference, San Francisco, June 1974.

4.3 Reprints and Manuscripts

3. V. Swaminathan, G.H. Narayanan and S.M. Copley, "Comment on the Evidence of a Precipitate-Like Zone in As-Grown GaAs and Its Influence on Optical Absorptivity" submitted on August 19, 1974 to the Journal of Applied Physics.

4. V. Swaminathan and G.H. Narayanan, "Diffuse Streaks in Electron Diffraction Patterns from CdTe Single Crystals", submitted to the Journal of Applied Physics.

13. C.P. Christensen, R. Joiner, S.T.K. Nieh and W.H. Steier, "Investigation of Infrared Loss Mechanisms in High Resistivity GaAs", J. Appl. Phys., 45, 4957 (1974).

14. J.H. Parks, D.A. Rockwell, T.S. Colbert, K.M. Lakin and D. Mih, "Acoustic Surface Wave Detection of Radioactive Absorption", Applied Physics Letters, Vol. 25, p 537, (1974).